Tracers and Anthropogenic Carbon in the Tropical Atlantic Ocean and the Mediterranean Sea

Dissertation
zur Erlangung des Doktorgrades
der Mathematisch-Naturwissenschaftlichen Fakultät
der Christian-Albrechts-Universität
zu Kiel

vorgelegt von
Anke Schneider

Kiel
2011

Referent/in:	Prof. Dr. D. W. R. Wallace
Koreferent/in:	Prof. Dr. A. Körtzinger

Tag der mündlichen Prüfung:	17.06.2011
Zum Druck genehmigt:	17.06.2011

gez. Prof. Dr. rer. nat. Lutz Kipp
- Dekan -

Contents

Zusammenfassung **1**

Summary **3**

1 Scientific background **5**

1.1 Carbon dioxide (CO_2) 5

1.1.1 CO_2 in the atmosphere 5

1.1.2 CO_2 in the ocean 6

1.1.3 CO_2 flux 7

1.2 The carbonate system 8

1.2.1 Carbon species 9

1.2.2 Alkalinity 10

1.2.3 Calcium carbonate 11

1.3 Tracers in the ocean 12

1.4 Methods to estimate anthropogenic carbon (C_{ant}) 13

1.4.1 Overview 13

1.4.2 The transit time distribution method 15

1.5 Regional hydrography of the study regions 17

1.5.1 Mediterranean Sea 17

1.5.2 The eastern tropical Atlantic 19

2 Methodology **23**

2.1 Cruises 23

2.1.1 Meteor 51/2 23

2.1.2 Meteor 68/2 23

2.1.3 Maria S. Merian 10/1 24

2.1.4 Meteor 80/1 24

2.1.5 Meteor 80/2 24

2.2 Tracer measurements 25

2.2.1 Sampling 26

2.2.2 Measurements at sea 27

2.2.3 Measurements in the laboratory 28

2.2.4 Capillary column system - instrument A 29

2.2.5 Packed column system - instrument B 30

2.2.6 Detection 31

2.2.7 Standards and blanks 31

2.3 Data processing 32

2.3.1 General procedures 33

2.3.2 Statistical method for flame sealed ampoules 34

2.3.3 Secondary quality control and adjustments 37

3 Alkalinity of the Mediterranean Sea 39

4 High anthropogenic carbon content in the eastern Mediterranean 47

5 An evaluation of tracer measurements and anthropogenic carbon in the equatorial and the tropical North Atlantic 61

6 Conclusions and Outlook 83

Acknowledgements 85

Bibliography 87

Abbreviations 93

Zusammenfassung

Die vorliegende Doktorarbeit wurde im Rahmen eines Teilprojektes des europäischen Projektes CARBOOCEAN sowie des deutschen DFG Projektes 'Tracers in the tropical Atlantic' angefertigt. Ziel des CARBOOCEAN-Teilprojektes 'Carbon uptake and release at European regional scale' war die Erstellung eines geschlossenen Kohlenstoffbudgets für die Region West-Europa, wobei das Mittelmeer (zusammen mit der Nordsee) die Hauptrolle im marinen Teil spielt. Das 'Tracer' Projekt hatte zum Ziel, die Lücke an Tracermessungen im tropischen Atlantik zu füllen und den gespeicherten anthropogenen Kohlenstoff in den Auftriebsgebieten des tropischen Atlantik abzuschätzen. Zusätzlich dienen die Tracermessungen als Basis für Folgeuntersuchungen in dem Gebiet.

Anhand von Alkalinitätsmessungen und Messungen von gelösten inorganischen Kohlenstoff wurden Besonderheiten im Karbonatsystem des Mittelmeers erklärt. Es wurde gezeigt, dass die stark erhöhten Alkalinitätswerte nicht nur das Ergebnis von Verdunstungsprozessen im Becken sind, sondern dass auch Einträge durch Flüsse und durch das Schwarze Meer einen großen Teil beitragen. Durch Tiefenwasserbildung wird in bestimmten Regionen die erhöhte Alkalinität ins Beckeninnere transportiert und verlässt das Mittelmeer durch die Straße von Gibraltar. Auch gelöster inorganischer Kohlenstoff wird mit jährlich $38\,\mathrm{Tg\,C}$ in den Atlantik exportiert. Mittels der 'transit time distribution' Methode und des Tracer Dichlordifluormethan wurden die anthropogenen Kohlenstoffkonzentrationen ermittelt. Dabei zeigte sich, dass die gesamte Wassersäule des Mittelmeers von menschlichen Einflüssen geprägt, und der Gehalt an anthropogenem Kohlenstoff überraschend hoch ist. Ein Säuleninventar von bis zu $154\,\mathrm{mol\,m^{-2}}$ übersteigt die höchsten Werte im Nordatlantik. Das Gesamtinventar ist 3.5 mal größer als das globale Mittel. Im Gegensatz zu dem Export von gelöstem inorganischem Kohlenstoff, wird anthropogener Kohlenstoff durch die Straße von Gibraltar ins Mittelmeer eingebracht. Abschließend wurde postuliert, dass hohe Alkalinität im Oberflächenwasser in Kombination mit Tiefenwasserbildung verantwortlich für den erhöhten anthropogenen Kohlenstoffgehalt im Mittelmeer ist.

Mehrere Forschungsfahrten in den tropischen Atlantik zwischen 2006 und 2009 erbrachten fächendeckende Tracermessungen, die auch für zukünftige Forschungsarbeiten eine gute Grundlage darstellen. Eine wichtige Annahme in der Berechnung von anthropogenem Kohlenstoff mit dem 'transit time distribution' Ansatz ist die Stärke von Mischungsprozessen. In der 'transit time distribution' Methode wird diese Annahme durch den zentralen Parameter $^{\Delta}/_{\Gamma}$ widergespiegelt. Anhand der zwei gemessenen Tracer Dichlordifluormethan und Schwefelhexafluorid konnte das $^{\Delta}/_{\Gamma}$ Verhältnis für die oberen 1500 m des tropischen Atlantik bestimmt werden. Die Gesamtauswertung aller während der Forschungsfahrten gemessenen Tracerdaten ergab, dass das Alter der Wassermassen vom Äquator in Richtung Norden ansteigt und dass sich im Guinea Dome das älteste Wasser der Region befindet. Verglichen mit dem Gebiet nördlich von 5°N weist das äquatoriale Band zwischen 5°S and 5°N erhöhte anthropogene Kohlenstoffkonzentrationen auf. Das Gesamtinventar an anthropogenem Kohlenstoff ist am Äquator um etwa 35% größer, als in dem Gebiet gleicher Größe nördlich davon. Als Ursache dafür wird der Einfluss

von jüngeren Wassermassen in der Tiefe, die im Zusammenhang mit den äquatorialen zonalen Strömungsverhältnissen stehen, angenommen. Darüber hinaus konnte aus einem Vergleich von Tracerdaten aus dem selben Gebiet im Jahr 1999 mit den vorliegenden Messungen ein Wert für den Anstieg an anthropogenem Kohlenstoff in einem Zeitraum von etwa acht Jahren ermittelt werden.

Summary

This PhD thesis was part of a subproject of the European project CARBOOCEAN, as well as of the German DFG project 'Tracers in the tropical Atlantic'. The aim of the CARBOOCEAN subproject titled 'Carbon uptake and release at European regional scale' was the assessment of a closed carbon budget for Western Europe, for which the Mediterranean Sea (together with the North Sea) plays the major role in the marine compartment. The 'Tracer' project aimed at filling the gap of transient tracer data in the tropical Atlantic and at constraining the ocean sequestration of anthropogenic CO_2 in the upwelling regions of the tropical Atlantic. Further, the established tracer fields will serve as baseline for future studies.

Measurements of total alkalinity and dissolved inorganic carbon in the Mediterranean Sea were used to explain anomalies in the carbonate system of the basin. It was shown that the strongly elevated alkalinities are not only the result of concentration processes but also of enhanced inputs by rivers and the Black Sea. Through deep water formation these high alkalinities are transfered into the basin's interior and flow out into the Atlantic Ocean via the Strait of Gibraltar. Dissolved inorganic carbon is also exported to the Atlantic Ocean with a net flux of 38 $\mathrm{Tg\,C\,yr^{-1}}$. Using the transit time distribution method and the transient tracer CFC-12, the anthropogenic carbon concentrations in the Mediterranean Sea were estimated. The results show influence of human emissions in the entire water column and reveal surprisingly high anthropogenic carbon inventories. Column inventories with a maximum of 154 $\mathrm{mol\,m^{-2}}$ exceeded highest column inventories in the North Atlantic and the total inventory is higher by a factor of 3.5 than the global mean. In contrast to the export of dissolved inorganic carbon, a net anthropogenic CO_2 import into the Mediterranean Sea through the Strait of Gibraltar of 3.5 $\mathrm{Tg\,C\,yr^{-1}}$ exists. It was hypothesized that high alkalinities in surface waters combined with the existence of deep water formation areas are responsible for the elevated content of anthropogenic carbon in the Mediterranean Sea.

Several cruises from 2006 to 2009 to the tropical Atlantic Ocean yielded in a good coverage of transient tracer measurements (CFC-12 and SF_6) in the area and provide an excellent basis for future work. One crucial assumption to estimate anthropogenic carbon with the transit time distribution approach is the degree of water mass mixing, expressed in the Δ/Γ ratio as a central parameter of the transit time distribution method. With the help of the two tracers CFC-12 and SF_6, this value could be constrained for the upper 1500 m of the tropical Atlantic. The analysis of all tracer measurements obtained during the cruises revealed that water ages increase when moving north from the equator and the Guinea Dome was identified as an area with the oldest water masses in the area. Compared to the region north of 5°N, the equatorial belt (5°S - 5°N) showed elevated anthropogenic CO_2 concentrations. The total anthropogenic carbon inventory was about 35% higher at the equator than in an area of the same size north of it. This was in part attributed to the contribution of younger waters at depth, associated with with the strong zonal equatorial currents. Further, a comparison with data tracer data from 1999 allowed to estimate the anthropogenic carbon increase over a time period of about 8 years.

1 Scientific background

1.1 Carbon dioxide (CO_2)

1.1.1 CO_2 in the atmosphere

Although the atmosphere is the smallest carbon reservoir in the earth system it is important for the earth's heat budget, because CO_2 is such a strong greenhouse gas. The natural greenhouse effect describes the transformation of incoming solar energy into heat. The incoming shortwave solar radiation is absorbed by the earth's surface and emitted as longwave radiation. In the atmosphere this longwave radiation is absorbed by the greenhouse gases (mainly water, but also CO_2), transformed into kinetic energy and re-emitted or dissipated as thermal energy. Without this effect mean earth temperatures would be far below 0°C. In steady state the energy budget is balanced, which means that incoming radiation equals the outgoing radiation. With a change in greenhouse gases, like an increase in CO_2, more radiation is absorbed and thus the incoming energy exceeds its loss to outer space. As a consequence the temperatures rise until the balance is redressed.

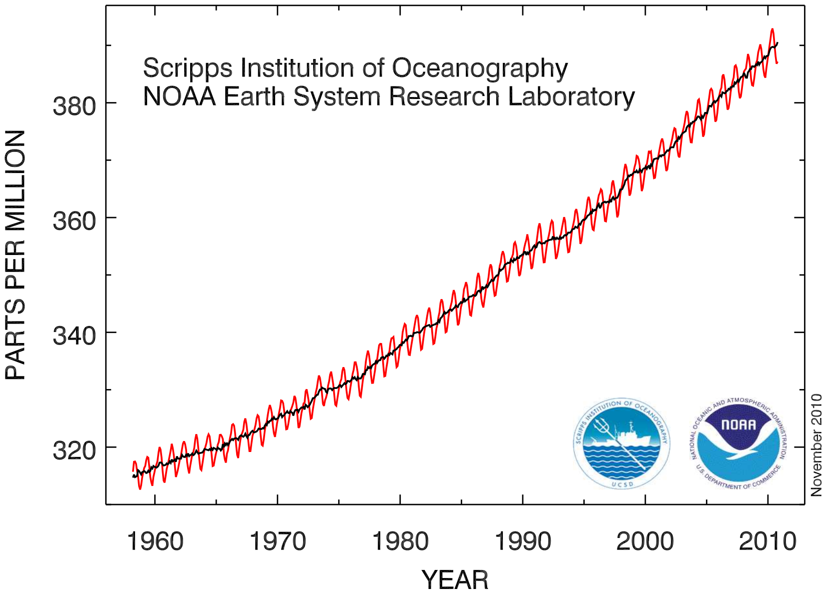

Figure 1.1: Monthly mean atmospheric carbon dioxide at Mauna Loa Observatory, Hawaii. [*Tans*, 2011].

Since 1958 atmospheric CO_2 concentrations have been measured accurately at the Mauna Loa Observatory in Hawaii (Fig. 1.1). These data constitute the longest record of direct CO_2

measurements in the atmosphere. They show a seasonal cycle, where in summer concentrations are lower due to increased plant uptake and in winter, when plant production declines but animals and microbes continue to respire, the concentrations are higher. Despite the seasonal oscillation a long-term increase in atmospheric CO_2 levels is evident. Responsible for these rising concentrations are additional man-made emissions through, mainly, fossil fuel burning as well as changes in land use pattern, primarily deforestation. With the help of air trapped in ice cores, the atmospheric record of CO_2 concentrations can be extended several hundred thousand years into the past [*Barnola et al.*, 1987; *Etheridge et al.*, 1996]. Glacial and interglacial cycles with CO_2 variations between 180 to 300 ppm were discovered in the past 400.000 years [*Petit et al.*, 1999] and the $p\mathrm{CO}_2$ increase over the last 100 years from a pre-industrial level of 280 ppm to about 390 ppm today stays exceptional. Such high values had even not occurred in the atmosphere since 23 million years [*Pearson and Palmer*, 2000]. However, the atmospheric growth has been smaller than estimates of the overall man-made CO_2 emissions, which suggests that the ocean and the terrestrial biosphere have taken up part of the additional CO_2.

1.1.2 $\mathbf{CO_2}$ in the ocean

Carbon enters the ocean through gas exchange via the air-sea interface, through river inputs, aeolian deposition and hydrothermal emissions. Carbon sinks are sedimentation and emissions back to the atmosphere. The predominant pool of carbon in the ocean is in the form of inorganic carbon. The inorganic carbon species carbonate and bicarbonate are the principal substances that account for the alkalinity in seawater (see section 1.2.2). CO_2 can be consumed during photosynthesis and therewith transfered to the much smaller organic carbon pool. During the oxidative destruction of organic matter CO_2 is again released back into the water. In the water column a rapid increase with depth of dissolved inorganic carbon and $p\mathrm{CO}_2$ to around 1000 m can be observed because most of the destruction of organic material takes place here. Below the maximum, C_T and $p\mathrm{CO}_2$ decrease with depth or stay rather constant. Their behavior at depth is influenced by mixing of water masses of different origin, by carbonate dissolution (at a certain depth ocean water gets undersaturated with respect to carbonates and these dissolve) and by 'rest-respiration' (a small amount of organic matter is not remineralized in the upper 1000 m and continues sinking through the water column where further respiration by bacteria takes place). The processes that lead to the transfer of carbon from the surface zone to the oceans interior are named the 'physical pump' and the 'biological pump' and are described in the following.

Two principal factors govern the ocean's capacity to hold CO_2:

1) The driving force for ocean-atmosphere CO_2 exchange is the difference between the $p\mathrm{CO}_2$ in surface water and the overlying air. When seawater is supersaturated with respect to CO_2, it tends to escape into the air and when the water is undersaturated, CO_2 uptake can occur. Combined with the thermohaline circulation this process is often referred to as the 'physical pump' (or 'solubility pump'). Two factors, in particular, influence the $p\mathrm{CO}_2$ in surface water. These are temperature and biological production. In warm water CO_2 is less soluble then in cold water and during phytoplankton blooms the utilization of CO_2 for photosynthesis leads to a drawdown of the gas into the water. The deep water formation in cold high-latitude waters effectively removes the CO_2 from the shallow surface layer and stores it in the larger reservoir of the deep ocean. Upwelling in contrast brings water with high CO_2 concentrations to the surface layer and leads to increased $p\mathrm{CO}_2$.

2) The 'biological pump' also removes carbon out of the mixed layer through sinking particles

but due to opposing effects on the atmospheric CO_2 it is separated into the 'organic carbon pump' and the 'alkalinity pump'. The biological production of organic matter in the surface ocean removes CO_2 from the atmosphere. In the deep water column the organic matter can either be remineralized by bacteria and therewith removed from interactions with the atmosphere for timescales of up to several hundred years, or the particles survive the water column and become buried in the sediment, which removes the carbon over much longer timescales. The biological formation of carbonates in the surface ocean on the other hand releases CO_2 to the atmosphere ($Ca^{2+} + 2HCO_3^- \rightarrow CaCO_3 + CO_2 + H_2O$) and decreases the alkalinity. On their way to the seafloor these carbonates can dissolve when surrounding waters are undersaturated with respect to e.g. $CaCO_3$ (see section 1.2), which leads to alkalinity increase, or otherwise they also become buried in the sediments. The two pumps are driven by the biological production of organic and particulate inorganic carbon in surface waters. The rate of biological productivity and the ratio between organic and inorganic carbon production depends on the availability of light and nutrients and on the mixed layer depth, the grazing pressure and the composition of the community. Phytoplankton with hard shells, like diatoms or coccolithophorids, are better protected against microbial attack and sink faster due to their ballast and therefore more likely reach the sediments.

1.1.3 CO_2 flux

The disequilibrium of the $p$$CO_2$ between atmosphere and surface water drives the flux of CO_2 across the air-sea interface. Sources and sinks change regionally and seasonally and over longer timescales. Regions of outgassing are located where upwelling brings cold and CO_2-enriched waters back to the surface at low latitudes. Generally warm equatorial waters are a source of CO_2. Regions of uptake are the cold high-latitude waters, where deep or intermediate water formation takes place, such as the North Atlantic. When atmospheric concentrations increase, the dissolved CO_2 in the ocean will also tend to increase to re-establish equilibrium. During the last decades a reasonable amount of data have become available to identify the source and sink characteristics of global surface ocean waters. The rapid accumulation of CO_2 in the atmosphere by human activity has led to an increased air to sea flux and increased surface $p$$CO_2$ in the oceans. *Takahashi et al.* [2009] summarized about 3 million $p$$CO_2$ measurements over the global oceans from 1970 - 2006 and constructed a climatological mean distribution for the surface water $p$$CO_2$. They estimated a mean $p$$CO_2$ increase in surface water of $1,5\ \mu\mathrm{atm\,yr^{-1}}$ and a total ocean uptake of $2(\pm 1)\ \mathrm{Pg\,C\,yr^{-1}}$, taking into account an estimated preindustrial steady-state source of $0.4\ \mathrm{Pg\,C\,yr^{-1}}$. This total uptake includes the anthropogenic CO_2 flux, which is the net change of natural oceanic CO_2 sources and sinks due to the man-made carbon dioxide increase in the atmosphere.

The anthropogenic CO_2 flux, however, has a very different distribution. The uptake mainly takes place in poorly ventilated water that is exposed to the modern atmosphere. Water in upwelling regions, such as the tropics, generally has a high $p$$CO_2$, due to respiration and is therewith a source of CO_2 to the atmosphere. But when such water is exposed to an atmosphere with elevated atmospheric CO_2 content, the outgassing is reduced over its preindustrial amount. This means, that more CO_2 stays dissolved in the ocean and, effectively, 'anthropogenic' CO_2 has been taken up. A second important factor for the uptake of anthropogenic CO_2 by the ocean, is the Revelle factor or buffer factor [*Revelle and Suess*, 1957]. A low Revelle factor implies, that for a given change in atmospheric CO_2, the anthropogenic CO_2 concentration in equilibrated surface water will be higher then in waters with a high Revelle factor. It is inversely proportional to the temperature, thus the ability to take up anthropogenic CO_2 is higher in warm waters. This is a direct response of the carbonate system to changing temperatures, since the buffer capacity decreases (fewer carbonate ions) with decreasing temperatures. The present day distribution of the Revelle factor is shown in figure 1.2 [*Sabine et al.*, 2004]. Highest values are found in the high latitudes and a minimum is obvious in the tropics and subtropics.

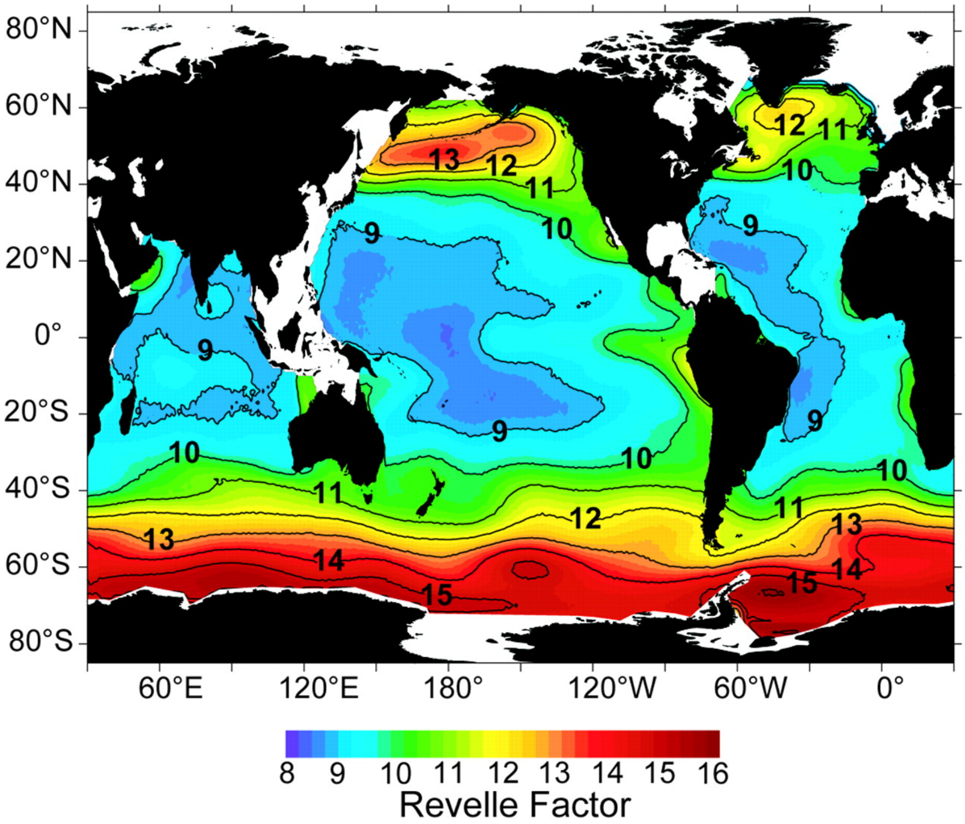

Figure 1.2: Map of the 1994 distribution of Revelle factor, averaged for the upper 50 m of the water column [*Sabine et al.*, 2004].

1.2 The carbonate system

The marine carbonate system is the primary buffer for acidity in the ocean and plays a key role in controlling the partial pressure of carbon dioxide ($p\mathrm{CO}_2$) in the atmosphere. The four measurable parameters involved in the carbonate system are pH (-log [H^+]), $p\mathrm{CO}_2$, total dissolved inorganic carbon (C_T) and total alkalinity (A_T). Any two of these can be used together with temperature (T) and pressure (P) and the dissociation constants of carbonic acid to calculate the remaining ones, as the different species are closely linked [*Pilson*, 1998]. Carbon dioxide (CO_2) in the atmosphere equilibrates with ocean surface waters via the air-sea interface. It reacts with water molecules to form bicarbonate and carbonate ions. CO_2 in the water column is consumed during photosynthesis and released during the oxidative destruction of organic matter. Calcium carbonate (CaCO_3) is a major sink for dissolved carbon in the long-term global carbon cycle. The release of CO_2 during remineralization at depth decreases the pH and makes the water more corrosive to CaCO_3. The dissolution of calcium carbonate in turn increases the alkalinity.

1.2.1 Carbon species

The ocean has a very large capacity to absorb atmospheric CO_2 and therewith mitigates the effect of increasing CO_2 concentrations in the atmosphere due to anthropogenic emissions. CO_2 from the atmosphere dissolves in ocean surface water. In equilibrium the atmospheric pCO$_2$ is related to the CO_2 in solution, CO_2(aq), via the Henry's law coefficient, K_H:

$$[\mathrm{CO_2}] = K_\mathrm{H} \cdot p\mathrm{CO_2}. \tag{1.1}$$

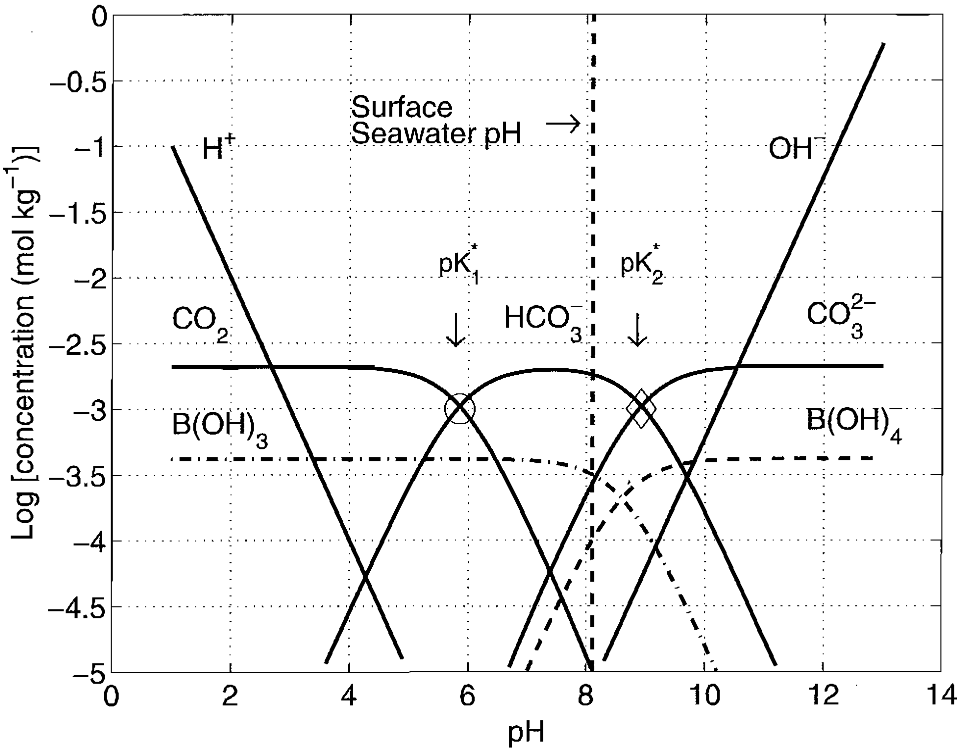

Figure 1.3: The relative proportions of the dominant species of the carbonate system at T = 25°C and S=35: Bjerrum plot (named after B. Bjerrum who invented the graphical representation of equilibrium relationships in 1914) [*Zeebe and Wolf-Gladrow*, 2001]. pK_1^* (pK_2^*) is the negative common logarithm of the first (second) dissociation constant of carbonic acid.

CO_2(aq) reacts with the water molecules and CO_3^{2-} to form carbonic acid (H_2CO_3) and then quickly dissociates to bicarbonate (HCO_3^-) and carbonate (CO_3^{2-}) (Eqn. 1.2, 1.3 and 1.4). The different carbon species in seawater react reversible and are in chemical equilibrium on time scales of minutes. The equilibria are temperature, pressure and salinity (S) dependent and are described by apparent equilibrium constants, K'. These have been determined experimentally in seawater as a function of temperature, salinity and pressure.

$$\mathrm{CO_2} + \mathrm{H_2O} \rightleftharpoons \mathrm{H_2CO_3} \qquad K'_{\mathrm{CO_2}} = \frac{[\mathrm{H_2CO_3}]}{[\mathrm{CO_2}]}, \tag{1.2}$$

$$\mathrm{H_2CO_3} \rightleftharpoons \mathrm{HCO_3^-} + \mathrm{H^+} \qquad K'_{\mathrm{H_2CO_3}} = \frac{[\mathrm{HCO_3^-}][\mathrm{H^+}]}{[\mathrm{H_2CO_3}]}, \tag{1.3}$$

$$HCO_3^- \rightleftharpoons CO_3^{2-} + H^+ \qquad K_2' = \frac{[CO_3^{2-}][H^+]}{[HCO_3^-]}, \tag{1.4}$$

where K_2' indicates the second dissociation constant of carbonic acid. Only a minor part of the dissolved inorganic carbon exists as H_2CO_3 and because $CO_2(aq)$ and H_2CO_3 are difficult to distinguish analytically, they are combined to:

$$H_2CO_3^* = CO_2(aq) + H_2CO_3. \tag{1.5}$$

Accordingly equation 1.2 and 1.3 can be combined to eliminate H_2CO_3:

$$H_2CO_3^* \rightleftharpoons HCO_3^- + H^+ \qquad K_1' = \frac{[HCO_3^-][H^+]}{[CO_2 \cdot]}, \tag{1.6}$$

where K_1' is the first dissociation constant of carbonic acid. The total concentration of dissolved inorganic carbon then becomes:

$$C_T = [H_2CO_3^*] + [HCO_3^-] + [CO_3^{2-}]. \tag{1.7}$$

In figure 1.3 the variation of the carbonate species concentrations is shown as a function of pH. In seawater, with a typical pH range of 7.8 - 8.4, the dominant species of the C_T is bicarbonate, followed by carbonate. Least abundant is $H_2CO_3^*$, which makes up less than 1% of the total dissolved carbon. The system tends to change the relative proportions of the different species in order to keep the pH constant. However, dissolution of additional CO_2 from the atmosphere leads to acidification and to a shift of the carbon species to more $H_2CO_3^*$ and less carbonate, whereas bicarbonate increases most strongly. The result is that the buffer capacity of seawater decreases, which means that the Revelle factor increases.

1.2.2 Alkalinity

The alkalinity refers to the ability of substances in seawater to react with hydrogen ions during titration with a strong acid. The main source of alkalinity for the ocean is the input by rivers. The main sink is sedimentation of carbonates. Substances that make up >99% of the alkalinity in seawater are HCO_3^-, CO_3^{2-} and $B(OH)_4^-$ (tetrahydroxyborate). Total alkalinity is defined as [*Dickson*, 1981]:

$$\begin{aligned} A_T = 2[CO_3^{2-}] + [HCO_3^-] + [B(OH)_4^-] + [OH^-] + [HPO_4^{2-}] + 2[PO_4^{3-}] \\ +[SiO(OH)_3^-] + [NH_3] + \cdots - [H^+] - [H_3PO_4]. \end{aligned} \tag{1.8}$$

The portion of the total alkalinity that is contributed by inorganic carbon species is denoted as the carbonate alkalinity. Usually it accounts for ~96% of the total alkalinity and thus the most important components of the total alkalinity are CO_3^{2-} and HCO_3^-. Only in deep waters nutrients contribute significantly to the total alkalinity.

In figure 1.4 the mean depth profiles of A_T compiled from the GLODAP dataset (Global Ocean Data Analysis Project) [*Key et al.*, 2004] are displayed for the major ocean basins. A gradual increase with depth is evident in all profiles, which is mainly attributable to carbonate dissolution. The formation and dissolution of calcium carbonate and to a smaller degree also the uptake and release of nitrate and phosphate through organisms contribute to the non-conservative behavior of alkalinity [*Wolf-Gladrow et al.*, 2007]. However, a linear relationship with salinity is often found in surface waters of smaller regions or subbasins, where primarily dilution and evaporation processes control alkalinity and no considerable primary production takes place.

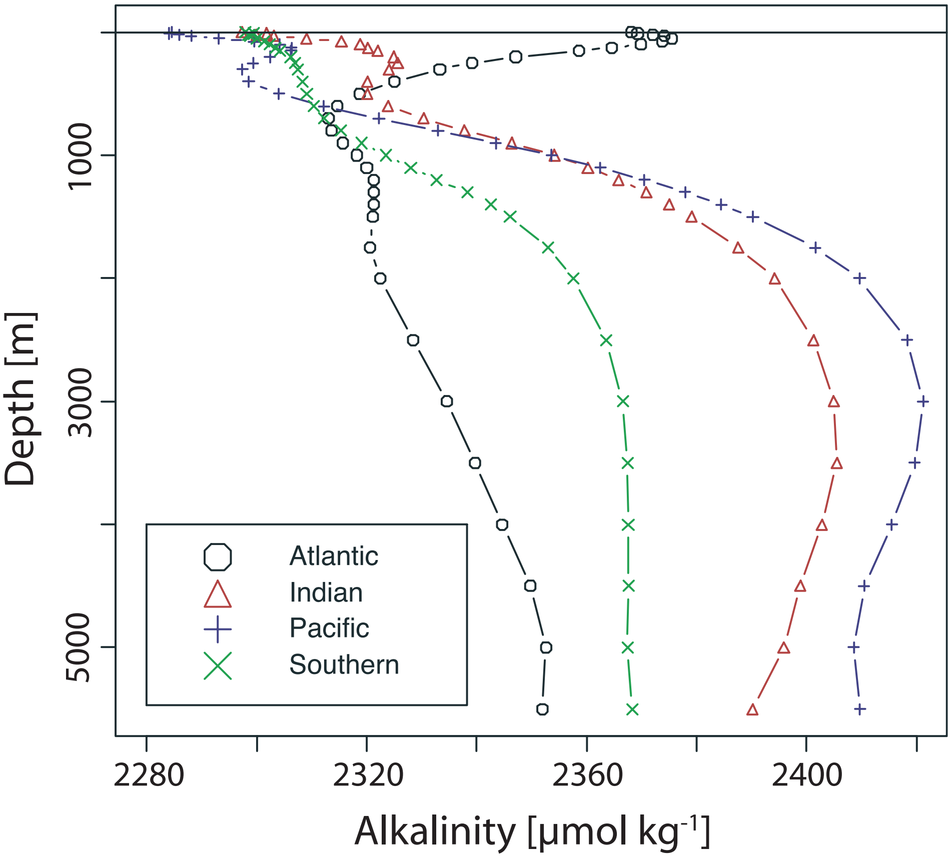

Figure 1.4: Average profiles of total alkalinity with the data from the Global Ocean Data Analysis Project (GLODAP) segregated by ocean [*Key et al.*, 2004].

1.2.3 Calcium carbonate

A result of biological activity in the surface ocean is the formation of calcareous shells that sink through the water column. This can be described chemically as:

$$Ca^{2+}(aq) + CO_3^{2-}(aq) \rightleftharpoons CaCO_3(s) \qquad K'_{sp} = [Ca^{2+}] \cdot [CO_3^{2-}] \tag{1.9}$$

The formation of solid calcium carbonate (by the consumption of carbonate ions) leads to a decrease in dissolved inorganic carbon and in alkalinity. As shown in equation 1.8, the effect on the alkalinity is twice as high as on the dissolved inorganic carbon. Calcium carbonate usually precipitates as one of 2 forms: aragonite or calcite, which have different solubility constants, K'_{sp}. Aragonite is more soluble and therefore less abundant in deep sea sediments than calcite. The saturation state (Ω) of seawater can be calculated as follows:

$$\Omega = \frac{[Ca^{2+}][CO_3^{2-}]}{K'_{sp}}, \tag{1.10}$$

where [Ca^{2+}] is the concentration of calcium ions, [CO_3^{2-}] the concentration of the carbonate ion and K'_{sp} is the apparent solubility constant of either aragonite or calcite. The calcium concentration is usually assumed to be proportional to salinity. An $\Omega > 1$ means supersaturation and $\Omega < 1$ means undersaturation and thus dissolution of $CaCO_3$. The upper ocean is supersaturated with respect to both forms of $CaCO_3$, but inorganic precipitation does not generally occur. The saturation horizon $\Omega = 1$ is the depth below which water becomes undersaturated for $CaCO_3$ and the 'lysocline' marks the depth below which carbonates decrease rapidly in the sediments. The main reason for this is that with increasing pressure and decreasing temperature at depth the solubility of $CaCO_3$ in the water column increases. The increasing pressure has also an effect on the dissociation constants of carbonic acid and causes a decrease in pH and thus a decrease of CO_3^{2-} concentration. Respiration of organic matter further decreases the pH and CO_3^{2-} concentration at depth, and the combined effects lead to the dissolution of $CaCO_3$. For example the saturation depth of calcite in the North Atlantic is >4000 m and in the North Pacific it is <1000 m [*Doney et al.*, 2009].

1.3 Tracers in the ocean

Many processes in the ocean cannot be directly quantified. Either analytical methods do not exist or are not sensitive enough to measure specific parameters, or direct measurements are inadequate because regional and temporal variability, in which the processes occur, cannot be addressed. Mixing and transport of water masses, biogeochemical processes or the uptake of anthropogenic CO_2 are some examples. So called 'tracers' can give insights into such processes and help to quantify them. Common tracers used in the ocean are temperature, salinity, dissolved oxygen, artificial and natural radionuclides, isotopes and man-made substances like the chlorofluorocarbons (CFCs) and sulfur hexafluoride (SF_6). Conservative tracers have no sources or sinks in the ocean (T, S, CFCs, SF_6) and are distinguished from the non-conservative tracers that are involved in biogeochemical cycles (O_2) or are subject to radioactive decay (radionuclides). Depending on the choice of tracers different signals in the ocean can be identified resulting from mixing and transport and from biogeochemical processes. For example, on the basis of natural radiocarbon measurements the residence time of water in the deep sea has been estimated to be ~1000 years and oxygen isotopes in carbonates were used to identify past climate conditions [*Chester*, 2003].

Anthropogenic carbon (C_{ant}) cannot be directly measured. In the atmosphere the anthropogenic fraction can be determined by subtracting the known preindustrial CO_2 value from the total measured CO_2 concentration. To quantify the C_{ant} inventory of the ocean, one option is to use gaseous tracers like dichlorodifluoromethane (CFC-12) and SF_6. CFC-12 has no natural sources. It has been first synthesized in 1928 and used as aerosol spray propellant and refrigerant since then. Concentration in the atmosphere started to increase exponentially. In the stratosphere CFC-12 depletes the ozone layer and after the discovery of the ozone whole in the mid 1980s, its usage has been regulated. In the year 1989 several countries signed the Montreal Protocol to stop the production of CFC-12 and consequently concentrations in the atmosphere increased with a slower rate and now started to decrease (Fig. 1.5). SF_6 neither has natural sources. It has been produced since the 1950s and is used mainly in the electricity sector as gaseous insulator and in the magnesium industry to prevent oxidation of molten magnesium. SF_6 has an extremely high global warming potential (GWP) of 22.800 over a time scale of 100 years [*Forster et al.*, 2007]. The GWP describes the contribution of a given mass of greenhouse gas to global warming over a specific time interval relative to the same mass of CO_2, which by

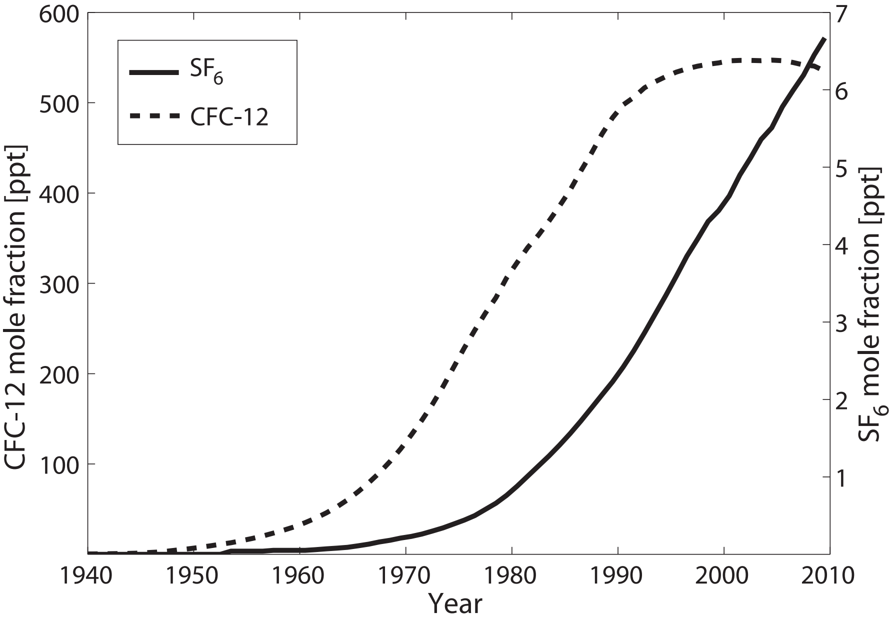

Figure 1.5: CFC-12 and SF_6 mixing ratios in the northern hemisphere. Data are taken from *Bullister* [2010]

convention has a GWP of 1. However, the overall contribution to global warming is rather low as the mixing ratio of SF_6 is only about 7 ppt in the year 2010 compared to a mixing ratio of 390 ppm for CO_2. Thus no major restrictions for the SF_6 production have been released in the past and atmospheric concentration continue to increase linearly (Fig. 1.5). Like CO_2, both tracers enter the ocean via the air-sea interface in dependency of the atmospheric concentration and their water solubility. In contrast to CO_2, CFC-12 and SF_6 are inert in the water column and can therefore be used to estimate the waters age (see section 1.4.2).

1.4 Methods to estimate anthropogenic carbon (C_{ant})

1.4.1 Overview

Anthropogenic carbon accounts for only a small fraction of the carbon reservoir in the ocean. By direct measurements it cannot be distinguished from the vast natural background but several methods have been developed to determine the ocean's C_{ant} inventory. The first estimates of C_{ant} used back-calculation techniques based on measurements of inorganic carbon, developed independently by *Brewer* [1978] and *Chen and Millero* [1979]. This approach did not find general acceptance [*Shiller*, 1981; *Broecker et al.*, 1995] but was reintroduced by the concept of the 'quasi-conservative' tracer ΔC^* *Gruber et al.* [1996]. Further variations of this approach and specific regional adjustments have been proposed since then [e.g., *Goyet et al.*, 1999; *Perez et al.*, 2002; *Lo Monaco et al.*, 2005; *Touratier and Goyet*, 2004; *Touratier et al.*, 2007] and have been reviewed by e.g. *Wallace* [1995] and *Friis* [2006].

The ΔC^* method corrects the measured C_{T} for all changes that have occurred since the water parcel lost contact with the atmosphere, which results in the preformed carbon (C_{T}^0). The changes are due to biological production and respiration (C_{bio}) and to calcium carbonate dissolution (C_{carb}):

$$C_{\mathrm{T}}^{0} = C_{\mathrm{T}} - C_{\mathrm{bio}} - C_{\mathrm{carb}} \tag{1.11}$$

The biological fraction is assessed via the apparent oxygen utilisation (AOU) because C and $\mathrm{O_2}$ are combined via a constant stoichiometric ratio ($R_{\mathrm{C:O_2}}$):

$$C_{\mathrm{bio}} = R_{\mathrm{C:O_2}} \cdot (\mathrm{O_2} - \mathrm{O_2^{sat}}) \tag{1.12}$$

The carbonate dissolution process is assessed via the change in total alkalinity (A_{T}). As described earlier, total alkalinity is not only affected by the change in carbonate and bicarbonate ion concentration but also by the change in hydrogen ion concentration (see equation 1.8). During oxidative decomposition of organic matter, hydrogen ions and nutrients are released and the change in hydrogen ion concentration is assumed to be proportional to the change in nitrate concentration, which in turn is proportional to the change in $\mathrm{O_2}$ through a constant ratio ($R_{\mathrm{N:O_2}}$). Thus:

$$C_{\mathrm{carb}} = \frac{1}{2} \cdot (A_{\mathrm{T}} - A_{\mathrm{T}}^{0} + R_{\mathrm{N:O_2}} \cdot (\mathrm{O_2} - \mathrm{O_2}^{sat})). \tag{1.13}$$

The preformed alkalinity (A_{T}^{0}) can be estimated by a (multiple) linear regression with salinity [*Brewer*, 1978; *Chen and Millero*, 1979; *Gruber et al.*, 1996].

Assuming 100% $\mathrm{CO_2}$ saturation of surface water, the preindustrial preformed carbon concentration $C_{\mathrm{T}}^{0/280}$ can be determined with the preindustrial $p\mathrm{CO_2}$ of 280 ppm and the preformed alkalinity. The anthropogenic fraction of C_{T} can be estimated as:

$$C_{\mathrm{ant}} = C_{\mathrm{T}} - C_{\mathrm{T}}^{0/280} - C_{\mathrm{bio}} - C_{\mathrm{carb}}. \tag{1.14}$$

A alternative method to estimate the excess carbon in the ocean is the 'time-series multiparameter analysis' introduced by *Wallace* [1995]. It is based upon repeat surveys of the carbon system parameters to determine the change in C_{T} over time, e.g. during the World Ocean Circulation Experiment (WOCE). Assumptions for this method show some similarities with those of the back-calculation techniques. The natural relationships between carbon and the alkalinity, oxygen and nutrient contents are assumed to stay constant, whereas the uptake of the excess $\mathrm{CO_2}$ changes the C_{T} content of seawater in a way, which is assumed to be independent of these natural correlations. Through multiple linear regressions (MLR) between C_{T} and predictors such as T, S, $\mathrm{O_2}$, A_{T} and nutrients measured on the same water sample, an empirical predictive equation for C_{T} is established. This equation refers to one survey at a particular time, which is termed the 'baseline survey'. Applying the predictive equation to subsequent (or previous) surveys and comparing the residuals of observed minus predicted C_{T}, should result in an increase of the residuals in case an uptake of anthropogenic $\mathrm{CO_2}$ has taken place. Integration over the residual changes could give an estimate for the inventory change during the period between the surveys. In order to eliminate the natural variability of C_{T}, *Friis et al.* [2005] extended the MLR to the so called extended multiple linear regression (eMLR). The authors developed two predictive equations for two time-separated surveys and subtracted the two predictive equations from each other. The residual equation can then be used to estimate C_{ant} with either of the two datasets.

A further approach uses the $^{13}\mathrm{C}/^{12}\mathrm{C}$ isotopic anomaly to quantify the anthropogenic carbon inventory [*Quay et al.*, 1992; *Körtzinger et al.*, 2003]. The $\mathrm{CO_2}$ released during fossil fuel burning has a smaller $^{13}\mathrm{C}/^{12}\mathrm{C}$ ratio than the atmosphere. This is due to fractionation during photosynthesis as terrestrial plants preferentially fix the lighter carbon isotope ^{12}C. The extensive use of fossil fuel has lead to an overall decrease of the ^{13}C/^{12}C ratio in the atmosphere, which in turn is exchanged with the surface ocean. The constructed mass balance for the anomaly contained terms that presented large uncertainties so that its application is limited.

An almost completely different category of observational methods to estimate C_{ant} is based on measurements of anthropogenic tracers such as the bomb-derived carbon (^{14}C), CFCs and SF$_6$. With the help of the atmospheric time histories of these compounds and the analytical investigation of their concentrations in the ocean, conclusions can be drawn about the water mass ages and, by inference, the C_{ant} content. It should be mentioned that *Friis* [2006] showed that the ΔC^* technique is similar to a tracer technique. An extensive description of the transit time distribution (TTD) method based on CFC-12 and SF$_6$ measurements is given in the next section 1.4.2.

1.4.2 The transit time distribution method

As described in section 1.3, the tracers CFC-12 and SF$_6$ are supposed to be stable in ocean waters and thus their concentrations can be converted into ages. This age is the time elapsed between the year when the water left the mixed layer, which is assumed to be in equilibrium with the atmosphere mixing ratios, and the year when the subsurface tracer was measured [*Haine and Richards*, 1995]. A further assumption for this classical age calculation is the uniform origin of the sampled water parcel, which does not hold true in reality. The transit time distribution (TTD) method instead assumes that a water parcel consists of waters with varying time histories. So instead of a single age, each water parcel has an age or transit time distribution (Fig. 1.6). The TTD method has been developed for atmospheric transport by *Hall and Plumb* [1994] and its application to oceanic transport followed [e.g., *Beining and Roether*, 1996; *Delhez et al.*, 1999; *Deleersnijder et al.*, 2001; *Haine and Hall*, 2002]. It assumes steady-state water transport.

The shape described by the TTD can be approximated by an 'inverse Gaussian function' ($G(t)$) with two free parameters that have to be estimated:

$$G(t) = \sqrt{\frac{\Gamma^3}{4\pi\Delta^2 t^3}} \cdot exp\left(\frac{-\Gamma\,(t-\Gamma)^2}{4\Delta^2 t}\right), \tag{1.15}$$

where Γ is the mean transit time ('mean age') and Δ defines the width of the TTD. The $^{\Delta}/_{\Gamma}$ ratio is a measure for mixing. The higher the ratio the stronger the mixing. Knowledge of this ratio leaves only one remaining free parameter, the mean age Γ. For ocean interior waters a constant $^{\Delta}/_{\Gamma}$ ratio of 1 has shown to be reasonable [*Waugh et al.*, 2004].

Further, the interior concentration $c(r,t)$ of any tracer at location r and time t can be determined by [*Hall and Plumb*, 1994]:

$$c(r,t) = \int_0^\infty c_0(t-t') \cdot G(r,t')dt', \tag{1.16}$$

where t' is the integration variable, representing all the apparent ages in the water parcel (from 0 to ∞ years). $G(r,t')$ is the TTD presented in equation 1.15 at location r, giving the appropriate fraction for each water age t', and $c_0(t-t')$ is the surface water tracer concentration in the year $t-t'$ to be multiplied by this fraction. The surface tracer concentration is assumed to be in equilibrium with the atmosphere. Given an interior tracer concentration and a $^{\Delta}/_{\Gamma}$ ratio, the mean age of the water sample can now be constrained with equation 1.15 and 1.16.

The application of the TTD method to estimate the anthropogenic CO_2 of a water parcel considers C_{ant} as inert passive tracer, that fully equilibrates at the air-sea interface. According to equation 1.16 each interior C_{ant} concentration is related to the concentration history in surface waters ($C_{\mathrm{ant},0}$) as:

$$C_{\mathrm{ant}}(t) = \int_0^\infty C_{\mathrm{ant},0}(t - t') \cdot G(t')dt', \tag{1.17}$$

where t is the sampling year. The mean ages and the corresponding TTDs are determined using tracer measurements (e.g. CFC-12). The local variable r can be left out because for each discrete water sample a new TTD is determined. With the help of the atmospheric history of anthropogenic CO_2 and an empirical relation between surface salinity and alkalinity, the historical C_{ant} concentrations in surface waters can be calculated, assuming that alkalinity has not changed since preindustrial times. A last assumption of the TTD method is a constant air-sea CO_2 disequilibrium over time, whilst it can change in space.

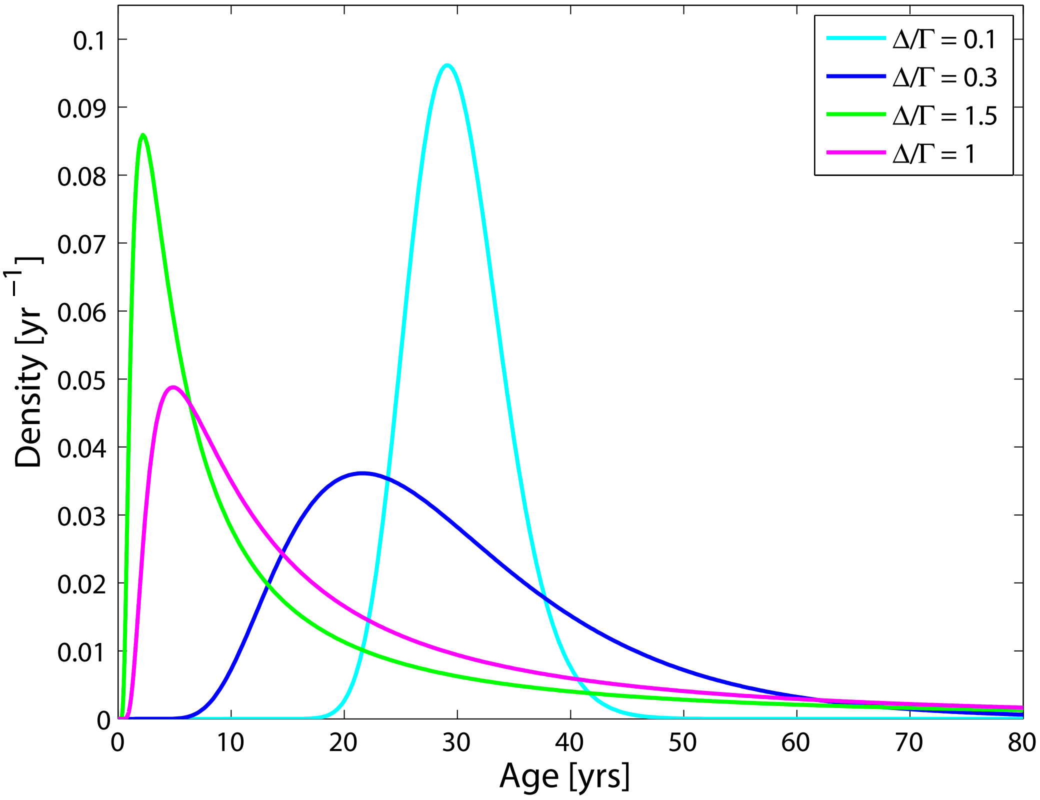

Figure 1.6: Transit time distributions (TTDs) for different $^{\Delta}/_{\Gamma}$ ratios.

The uncertainty in the $^{\Delta}/_{\Gamma}$ ratio can be reduced with the help of a second tracer (e.g. SF_6). This is be done by initially calculating the mean age with the first tracer (CFC-12) and then, the concentration of the second tracer (SF_6) is calculated using that mean age and the same $^{\Delta}/_{\Gamma}$ ratio. If the calculated SF_6 concentration matches the measured SF_6 concentration, the assumed $^{\Delta}/_{\Gamma}$ ratio is accurate or otherwise, the $^{\Delta}/_{\Gamma}$ ratio is varied in order for the two tracer mean ages to match.

1.5 Regional hydrography of the study regions

Water samples taken on cruises to the tropical North Atlantic and to the Mediterranean Sea are the basis for this work. Both regions are thought to be important in terms of C_{ant} uptake from the atmosphere and/or its removal from the mixed layer for general reasons already described in this chapter and specific reasons summarized here: The Mediterranean Sea has a relatively low Revelle factor and contains deep water formation areas where C_{ant} can be transferred to depth. Furthermore it is a small scale ocean were processes can be studied more easily and the findings can potentially be related to larger scales processes in the world ocean. The tropical North Atlantic is an area with one of the lowest Revelle factors and additionally it contains upwelling regions with high capacity to take up C_{ant}. In the following, these two oceanic regimes are described in detail.

1.5.1 Mediterranean Sea

The Mediterranean Sea is known as a 'concentration basin' with an anti-estuarine thermohaline circulation, which is the result of a negative freshwater balance [*Bethoux et al.*, 1999]. Evaporation over the basin exceeds the gain of water through precipitation and river inputs. The only connection of the Mediterranean to the ocean is via the narrow Strait of Gibraltar where low salinity Atlantic Water (AW) flows in at the surface and high-salinity water, mainly Levantine Intermediate Water (LIW) flows out at a deeper layer. The classical circulation pattern is schematically described by an open thermohaline cell with two closed secondary cells [*Lascaratos et al.*, 1999] (Fig. 1.7).

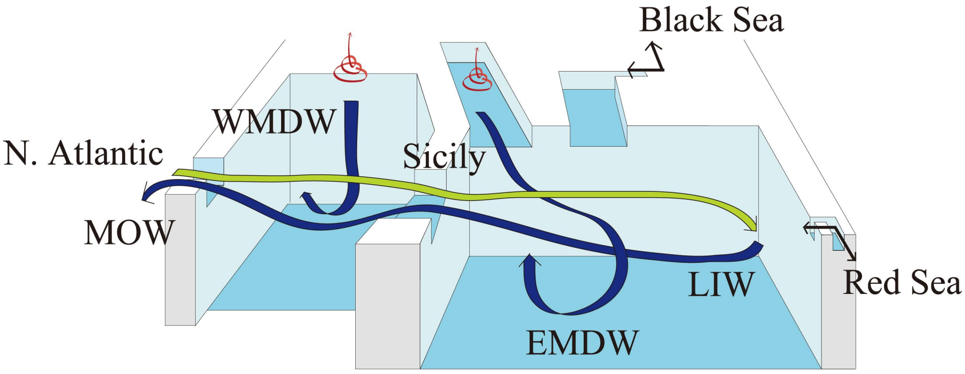

Figure 1.7: A schematic of the thermohaline circulation in the Mediterranean Sea. The green line indicate the inflowing surface water from the Atlantic. The blue lines indicate the Levantine Intermediate Water (LIW) spreading at intermediate depths and leaving the Mediterranean Sea as Mediterranean Overflow Water (MOW), and the Western and the Eastern Mediterranean Deep Waters (WMDW and EMDW), respectively. The red curls in the deep water formation areas indicate heat loss due to either cooling or wind. The figure is taken from *Lee et al.* [2011].

The principal cell pictures the transformation of the eastward flowing AW, which by then is named modified Atlantic Water (MAW), to LIW. On its way to the Levantine basin (the most eastern part of the Mediterranean) the relatively cool and low-salinity MAW ($T \approx 13°$C; $S \approx 36$) is exposed to high temperatures which lead to warming and evaporation. In the Levantine basin surface waters can reach temperatures of over 26°C and salinities of more than 39. In the Rhodes cyclone cold winds during the winter months cool these high salinity surface waters and they become dense enough to sink and mix with underlying water [*Ovchinnikov*, 1984]. Subduction rates vary between 0.6 and 1.3 Sv (1 Sv $= 1 \cdot 10^6$ m^3 s^{-1}) depending on the interannual variability of atmospheric forcing [*Stratford and Williams*, 1997; *Lascaratos et al.*, 1999]. At intermediate depths (200 - 500 m) this water mass flows back in westward direction. The renewal timescale for LIW is about 10 - 20 years [*Stratford and Williams*, 1997]. The two secondary cells describe the transformation of surface and intermediate water into Western Mediterranean Deep Water (WMDW) and Eastern Mediterranean Deep Water (EMDW). The WMDW is formed in the Gulf of Lyon. Due to the existence of a cyclonic gyre in this area, upwelling takes place and denser intermediate water comes close to the surface [*Gascard*, 1978]. Preconditioned by this process the stability of the water column is effectively reduced in winter by excess cooling and evaporation due to strong continental cold and dry winds (Mistral) [*Gascard*, 1978]. The vertical extension of convection is ~2000 m, approximately the full water depth in this area [*Lascaratos et al.*, 1999] and the newly formed very dense deep water spreads southwards. In a similar way the EMDW is formed in the southern part of the Adriatic Sea where strong preconditioning takes place also through a permanent cyclonic gyre. *Pollak* [1951] found a small contribution of dense water formation in the northern part of the Adriatic Sea where shallow shelf water experiences cooling and evaporation in winter during the Bora events and moves to the southern Adriatic Sea. Together with the inflowing LIW it seems to be a part of the deep convection happening in this area. This mixed and very dense water sinks to the bottom and flows through the Strait of Otranto to the deepest parts of the Ionian Sea and then into the Levantine Sea. In both basins temperature and salinity of the deep waters are very homogeneous (13.3°C; 38.66) [*Schlitzer et al.*, 1991].

Anthropogenic tracers, such as CFCs and tritium ($t_{1/2} = 12.43$ yr), can be used to obtain information on the ages of water masses on decadal to interdecadal timescales and thus they are rather suitable for the Mediterranean Sea. Overturning times of the deep water are estimated to be 70 - 120 years for the eastern basin [*Roether et al.*, 1996; *Stratford et al.*, 1998] and 40 years for the western basin [*Stratford et al.*, 1998]. With a new model approach *Steinfeldt* [2004] tried to reflect the circulation of the EMDW, assuming steady state. Using age spectra (distribution of transit times) instead of single water ages he calculated a mean spreading velocity of 0.4 cm s^{-1} for the EMDW with a single source in the Adriatic Sea. Successively the deep water flushes the Northern and Central Ionian and the Levantine basins in 1.5, 4.5 and about 20 years respectively. For the upwelling of old deep water in the Levantine, *Steinfeldt* [2004] estimated a velocity of about 35 m yr^{-1}.

However, recently the 'classical thermohaline circulation' of the Mediterranean Sea has started to change from a single deep water source in the Eastern Mediterranean basin to a two source system. During past decades the Aegean Sea did not contribute substantially to the formation of EMDW but was forming an intermediate water mass spreading out in the Ionian Sea between about 500 and 1200 m depth [*Schlitzer et al.*, 1991], thus having properties intermediate between LIW and EMDW. Meanwhile the circulation has entered a new state where 20% of the deep and bottom water of the Eastern Mediterranean Sea has been replaced by a rather salty and warm overflow from the Aegean Sea [*Roether et al.*, 1996]. Development of this new state seems to have started after the year 1987, when deepwater salinities were still rather homogeneous whereas in 1995 elevated salinities had been observed in the deep waters of Crete [*Roether et al.*, 1996]. Further evidence for the intrusion was given by increased CFC-12 amounts in the same area that indicates 'younger', more recently downwelled water. The initial reason for the ongoing deep inflow of Aegean water to the Ionian Sea was an increase in density of the Cretan Sea [*Roether et al.*, 1996], which in turn might have been a consequence of a change in the heat and freshwater balance for the period 1988 - 1995 (high evaporation and cooling [*Josey et al.*, 1997], reduced precipitation [*Theocharis et al.*, 1999]) or of a redistribution of salinity within the eastern Mediterranean [*Roether et al.*, 1996]. Recently it has been proposed that the change in deep water formation is connected to the so called Bimodal Oscillating System (BiOS), which is a feedback mechanism between the Adriatic and the Ionian [*Civitarese et al.*, 2010]. The authors assume that, on a decadal time scale, the circulation of the North Ionian Gyre changes from cyclonic to anticyclonic and vice versa, which in turn influences the location of the EMDW formation. A comparison of the current two deep water sources of the Eastern Mediterranean shows that the Aegean inflow rate of ~1 Sv [*Roether et al.*, 1996] exceeds three times the inflow from the Adrian Sea (~0.3 Sv) [*Schlitzer et al.*, 1991; *Roether and Schlitzer*, 1991]. As a consequence, all major water masses in the Eastern Mediterranean have been affected [*Klein et al.*, 1999]. The additional great amount of dense water flowing into the eastern basin has led to an uplift of deep water and thereby influenced the circulation at intermediate depth and changed the nutrient distribution in the upper water column [*Klein et al.*, 1999].

1.5.2 The eastern tropical Atlantic

The hydrography in the tropical region of the Atlantic Ocean is complex. It is mainly affected by the trade winds resulting in seasonal equatorial upwelling, coastal upwelling and a multitude of zonal currents. The southeast and the northeast trade winds lead to a westward surface current, the Equatorial Current. About 3° north and south of the equator the Coriolis force begins to have an effect and diverts the currents towards the south and the north, respectively (Ekman transport). The divergence of surface water causes upwelling, associated with lower temperatures at the equator. The so called cold tongue develops when the trade winds are strongest. This is the case in northern summer, when the Intertropical Convergence Zone (ITCZ) reaches its northernmost position. The ITCZ is a roughly zonally oriented band of atmospheric convection, forming the border between the southeast and the northeast trade winds. It is positioned in the area of the highest sea surface temperature (SST), which moves northward in boreal summer and southward in boreal winter, and is associated with enhanced cloud formation and rain. Influenced by the continents the SST in the tropical Atlantic Ocean is always higher in the northern hemisphere, thus the ITCZ always stays north of the equator. Variations reach from 6°N off Africa in February to 15°N in August [*Molinari et al.*, 1986]. Migration of the ITCZ also influences the strength and position of the currents. Main difference of the season where the ITCZ is at its northernmost position is the existence of the North Equatorial Counter Current (NECC) (Fig. 1.8). It develops because the low-wind region within the ITCZ displays a barrier for the northeastward surface water drift and the pressure gradient drags the water eastward.

The Subtropical Cells (STCs) describe the shallow overturning circulation of the poleward flowing upwelled water back to the equator at maximum depths of 500 m (Schott et al 2004). The currents included in the STCs are shown in figure 1.8. At the surface the water diverges off the equator and when it reaches the Subtropical Gyres, it eventually subducts. Due to the anticyclonic flow, the Subtropical Gyres are known to be extensive subduction areas, represented with the blue shading in figure 1.8. The North Equatorial Current (NEC) and the South Equatorial Current (SEC) are part of the winddriven Subtropical Gyres, when they leave the African coast. In the southern hemisphere the SEC transports the subducted STC waters westward and then equatorward with the North Brazilian Under Current (NBUC). The NBUC is part of the Meridional Overturning Circulation (MOC) with northward flow of warm water and has its maximum speed at ~250 m depth. When it is complemented by the shallower inflow of SEC and gets deflected by the Brazilian coast, it becomes the surface-intensified North Brazilian Current (NBC) [*Schott et al.*, 2004]. A second part of the NBUC continues south along the south American coast as Brazil Current. The NBC overshoots the equator [*Johns et al.*, 1998; *Schott et al.*, 1998] and follows the Brazilian coast at which most of it is lost into the eastward flowing Equatorial Under Current (EUC), the North Equatorial Under Current (NEUC) and the NECC [*Schott et al.*, 2004], where the water slowly upwells. The STC in the northern hemisphere is weaker because it is not supported by cross-equatorial transport of water by the MOC. According to the southern hemisphere, the subducted northern STC water is carried westward with the NEC. A weak current, called the Guiana Undercurrent, flows southward along the South American continent and picks up water from the NEC and carries it equatorward to supply the NECC and the EUC [*Schott et al.*, 2004, 1998].

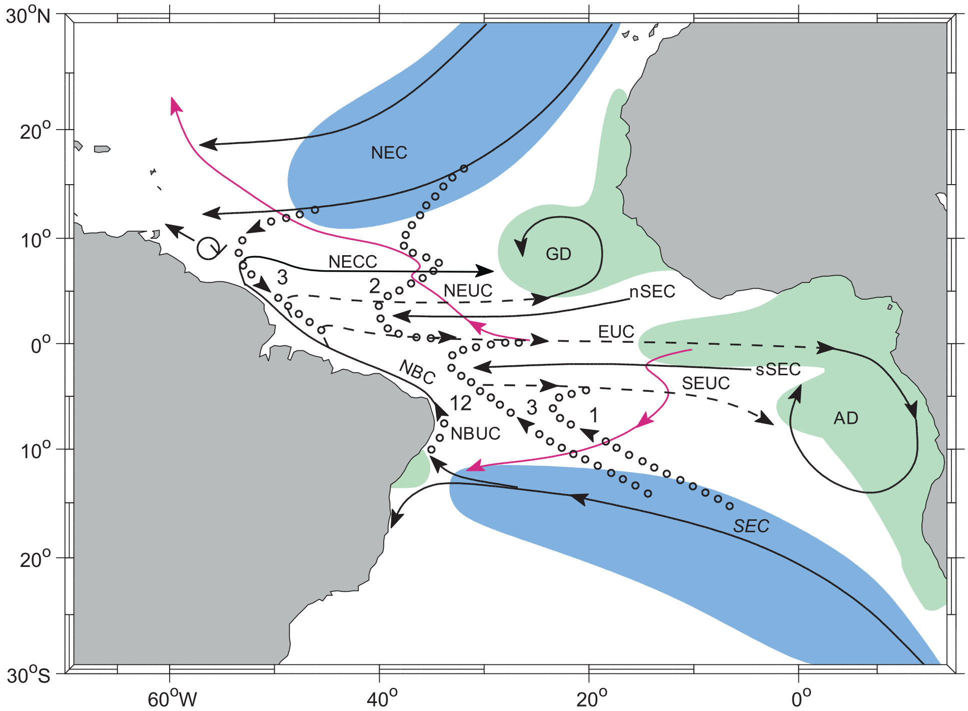

Figure 1.8: Schematic representation of the Atlantic Subtropical Cell (STC) circulation with subduction (blue) and upwelling (green) zones that participate in the STCs. Currents and upwelling areas are named as follows: NEC and SEC = North and South Equatorial Current, NECC = North Equatorial Coutercurrent, EUC = Equatorial Undercurrent, NEUC and SEUC = North and South Equatorial Undercurrent, NBC and NBUC = North Brazil Current and Undercurrent, GD and AD = Guinea and Angola domes. Interior equatorward thermocline pathways are dotted and transport estimates are marked for interior and western boundary pathways. Surface poleward pathways for the central basin (from drifter tracks, after *Grodsky and Carton* [2002]) are marked by thin, magenta lines. The figure is taken from *Schott et al.* [2004].

In addition to the currents along the Brazilian coast, the STCs are closed by weak interior equatorward thermocline pathways indicated with dots in figure 1.8. In the northern hemisphere the interior water flow partly gets distracted to the east by the NECC and the NEUC before reaching the equator. This also contributes to the weakness of the northern STC.

A shadow zone south and southeast of the northern Subtropical Gyre is not ventilated from the north [*Luyten and Stommel*, 1986]. Instead the area between the NEC and the NECC is governed by a cyclonic circulation, which leads to the permanent, quasi-stationary Guinea dome [*Siedler et al.*, 1992]. The Angola dome is the corresponding gyre in the southern hemisphere. Off-equatorial upwelling happens in both hemispheres along the coast and in the two cyclonic domes. The Guinea dome stretches across an area of 700 - 1000 km in diameter where a thermocline and pycnocline displacement of ~30 - 80 m in the upper 350 m takes place [*Siedler et al.*, 1992]. Some of the central water circulation (100 - 500 m) described above provides water for the Guinea and the Angola domes, especially the NEUC and the SEUC (Fig. 1.8) and due to their not negligible Ekman upwelling, the domes might play a considerable role for the STC circulation [*Schott et al.*, 2004].

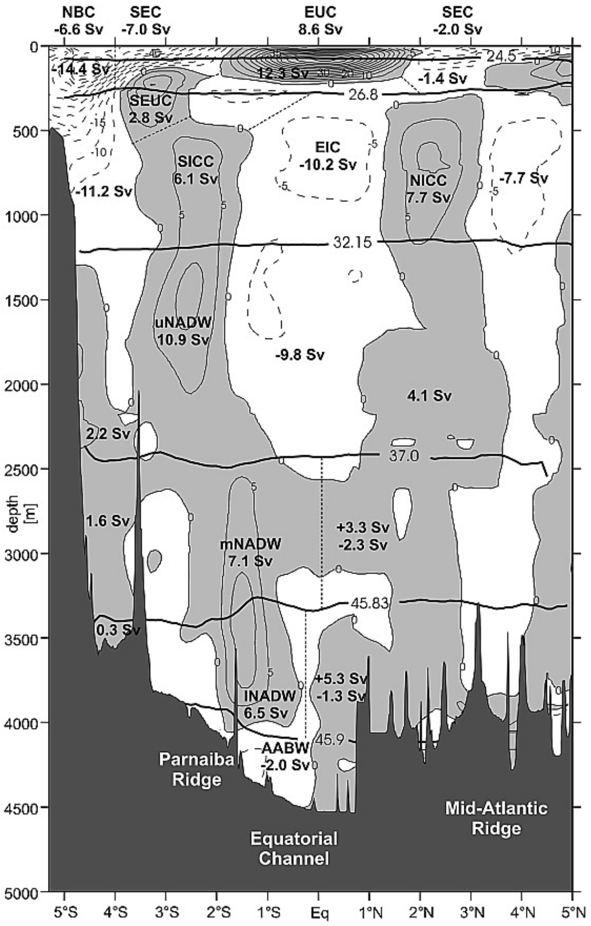

Figure 1.9: Mean zonal current distribution across 35°W, with transports (in Sv = $10^6 m^3 s^{-1}$) of the different current branches marked. The intermediate and deep currents are named as follows: SICC and NICC = South and North Intermediate Counterurrent, EIC = Equatorial Intermediate Current, uNADW, mNADW and lNADW = upper, middle and lower North Atlantic Deep Water, AABW = Antarctic Bottom Water. The figure is taken from *Schott et al.* [2003].

In figure 1.9 a meridional section at 35°W reveals the main zonal currents in the water column of the equatorial region. They are influenced by intermediate and deep waters from the southern and the northern hemispheres. The Antarctic Intermediate Water (AAIW) originates from a surface region in the Antarctic Ocean and slowly flows along the South American coast. It is found at depths between 600 and 1000 m. The high oxygen concentrations of the AAIW after subduction decrease on its way north and turn into low oxygen content north of 21°S [*Stramma and Schott*, 1999]. This is a consequence of the eastward advection of a large amount of AAIW with the South Intermediate Countercurrent (SICC) and the following transport around the Subtropical Gyre ending with the westward return within the southern SEC. The oxygen is heavily reduced by consumption during that circulation [*Stramma and Schott*, 1999]. As the AAIW is picked up at the lower boundary of the NBC it also participates in the STC circulation.

Another important water mass at depth in the Atlantic Ocean is the cold limb of the MOC, which consists mainly of the North Atlantic Deep Water (NADW). With the Deep Western Boundary Current (DWBC) the NADW is transported from the North Atlantic into the southern hemisphere. The upper NADW has increased CFC content centered at 1600 - 1800 m and is also named upper Labrador Sea Water (upper LSW) [*Rhein et al.*, 1995; *Rhein and Stramma*, 2005]. A CFC maximum is also found in the lower NADW at depths around 3700 - 4000 m [*Rhein and Stramma*, 2005]. Before crossing the equator, small part of the NADW recirculates in the Guiana Basin [e.g., *Friedrichs et al.*, 1994] and south of the equator the NADW mainly continues southward with the DWBC. Part of the upper LSW flows into eastward direction just south of the equator, thus reaches the eastern basin [*Rhein et al.*, 1995; *Andrié*, 1996]. According to CFC data in the equatorial Atlantic, the upper LSW seems to be captured in the region and circulates within westward equatorial and eastward off-equatorial deep jets [*Andrié et al.*, 2002]. The upper LSW does not directly take part in the STC circulation but upwells slowly in the equatorial region.

2 Methodology

The data for this thesis arise from five research cruises. The first part of the methodology section lists these cruises and shortly describes the sampling and analysis procedures of the corresponding parameters. In table 2.1 the relevant analysis and error information of all tracer measurements performed by the Chemical Oceanography department at IFM-GEOMAR (Leibniz Institute of Marine Science, Kiel, Germany) are summarized. Subsequently, instrument and methodology details are given for the CFC-12 and SF_6 measurements that were performed as part of the PhD work. Finally, the approach to estimate anthropogenic CO_2 is explained.

2.1 Cruises

2.1.1 Meteor 51/2

During the Meteor cruise in October/November 2001 (M51/2) to the Mediterranean Sea CFC-12 samples were measured onboard with a technique described by *Bulsiewicz et al.* [1998]. There were no duplicates analysed. The error for the CFC-12 measurements was estimated at $\pm 2\,\%$ or ± 0.02 pmol kg^{-1}, whichever is greater.

Samples for A_T and C_T were taken in 500-mL Duran glass bottles and fixed with 100 μL $HgCl_2$. Using a potentiometric titration method [*Mintrop et al.*, 2000] for A_T and a coulometric titration method [*Johnson et al.*, 1993] for C_T, the samples were analysed in the laboratory. Precision was 4.2 μmol kg^{-1} and 1.5 μmol kg^{-1}, respectively (95 % confidence interval). Accuracy was assessed with measurements of Certified Reference Material (CRM, supplied by Andrew Dickson, Scripps Institution of Oceanography (SIO), La Jolla, CA, USA) and yielded a mean offset of -0.82 ± 2.85 μmol L^{-1} for A_T and of $+0.62\pm1.01$ μmol L^{-1} for C_T (95 % confidence interval, n = 41). Both parameters were corrected for these mean offsets.

Oxygen samples were taken after the tracer samples and analysed at sea using the Carpenter-Winkler titration procedure [*Carpenter*, 1965] and a Radiometer automatic titrator (TTT80), equipped with a dual platinum electrode, in the dead-stop end point mode. Precision was 0.3 %. Duplicate samples for nutrient analysis were collected in 15-mL acid washed plastic vials and immediately frozen. They were determined in the laboratory using a segmented flow Technicon AutoAnalyser II (AA-II) system with the methods described by *Krom et al.* [1991] and *Kress and Herut* [2001]. The precision for nitrate and phosphate is 0.02 and 0.003 μmol L^{-1}, respectively. The limit of detection (2 times the standard deviation of the blank) for the procedures is 0.075 μmol L^{-1} for nitrate and 0.008 μmol L^{-1} for phosphate.

2.1.2 Meteor 68/2

During the Meteor cruise in June/July 2006 (M68/2) from Brazil to the Cape Verde Islands CFC-12 samples were taken in glass syringes and analysed with a purge and trap system similar to the one described by *Bullister and Weiss* [1988], in the following referred to as PT1. Precision was ±1.4 % (95 % confidence interval, n = 190) and a blank of 0.003 $\mathrm{pmol\,kg^{-1}}$ was removed from all samples. SF_6 samples were flame sealed and measured back in the laboratory on a packed column system (instruments B) with the methods described in sections 2.2.3 and 2.2.5. No duplicate samples were taken.

2.1.3 Maria S. Merian 10/1

During the Maria S. Merian cruise in November/December 2008 (MSM10/1) to the Guinea Dome region, SF_6 was measured onboard with the capillary column system (instrument A). The used methods are described in sections 2.2.2 and 2.2.4. Unfortunately, only one duplicate sample was measured which revealed a precision of ±2.2 %. Due to co-elution problems CFC-12 could not be quantified on the same instrument but was measured on the parallel running instruments PT1 and PT2 (both similar to the system described by *Bullister and Weiss* [1988]). The cross-system precision for these measurements is 10.8 $\mathrm{fmol\,kg^{-1}}$ or 1.9 %, whichever is greater (duplicates: n = 541).

2.1.4 Meteor 80/1

During the Meteor cruise in October/November 2009 (M80/1), CFC-12 and SF_6 samples were taken on a 23°W section in the equatorial Atlantic. Due to initial problems the first half of the samples taken was flame sealed and measured back in the laboratory. The remainder of the samples was measured onboard.

Onboard measurements

Samples were analysed on instrument B using the methods described in sections 2.2.2 and 2.2.5. At the end of the cruise problems with the trap were encountered and SF_6 could not be quantified anymore. Precision for CFC-12 was 0.05 $\mathrm{pmol\,kg^{-1}}$ or 6 %, whichever is greater (duplicates: n = 4). For SF_6 precision could not be determined because the duplicates were measured, after the problems with the trap had appeared.

Laboratory measurements

The sealed ampoules were analysed on instrument B with the methods described in sections 2.2.3 and 2.2.5. The scatter in the SF_6 measurements unfortunately turned out to be too large and the results are discarded. The CFC-12 samples also show considerable scatter but seem usable. The large scatter in both parameters and also the fact that tracer concentrations greater than zero were found in deep samples suggest that probably contamination with air occurred during the process of flame sealing. On account of this, a blank of 40 fmol (average excess concentrations from depths where values close to zero are expected) was subtracted from the CFC-12 measurements. No duplicates had been flame sealed.

2.1.5 Meteor 80/2

During the Meteor cruise in November/December 2009 (M80/2) to the Guinea Dome region, CFC-12 was measured on the instruments PT1 and B. As mentioned before PT1 is similar to the system described by *Bullister and Weiss* [1988]. Samples measured on this instrument were taken in 250 mL glass syringes and a volume of 100 mL was analysed. SF_6 was sampled and measured together with CFC-12 on instrument B. The methods are described in sections 2.2.2

Table 2.1: Analytical details and corrections of all tracer measurements analysed by the Chemical Oceanography department at IFM-GEOMAR

Cruise	Tracer	System	Analysis	Systematic errors[a] [fmol kg^{-1}]	Precision [fmol kg^{-1}] / [%] (n)	Std. adjustment[b] [%]
M68/2	SF_6	B	shore-based	-	- (0)	87
	CFC-12	PT1	onboard	-3	- / ±1.4 (190)	-
MSM10/1	SF_6	A	onboard	-0.05	- / ±2.2 (1)	83
	CFC-12	PT1/2	onboard	-	±10.8 / ±1.9 (541)	-
M80/1	SF_6	B	onboard	-0.08	- (0)	88
	CFC-12	B	shore-based	-42.3	- (0)	-
	CFC-12	B	onboard	-	±50 / ±6 (4)	109
M80/2	SF_6	B	onboard	-	±0.05 / ±10 (13)	90
	CFC-12	PT1	onboard	-	±6 / ±1 (46)	-
	CFC-12	B	onboard	-	±40 / ±3.8 (13)	109

---

[a] measured blanks (section 2.3.1) and analytical errors (section 2.3.2 and 2.3.3) combined

[b] inconsistencies between sample and standard measurements required adjustments described in section 2.3.3

and 2.2.5. Precision for CFC-12 is 6 fmol kg^{-1} or 1 %, whichever is greater (PT1; duplicates: n = 46) and 0.04 pmol L^{-1} or 3.8 % (B; duplicates: n = 13). Precision for SF_6 is 0.05 fmol L^{-1} or 10 % (B; duplicates: n = 13).

2.2 Tracer measurements

For analysing the water samples, different purge and trap systems followed by gas chromatography are used (see the analysis procedures for the different cruises in section 2.1). Here only system A and B are described in detail. For details of the other systems see *Bulsiewicz et al.* [1998] and *Bullister and Weiss* [1988].

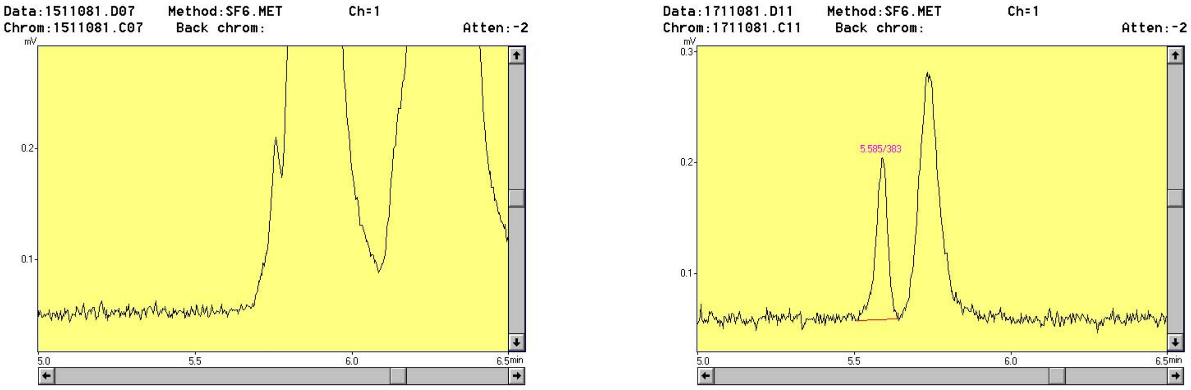

(a)

(b)

Figure 2.1: Chromatograms of a 300 m sample during the MSM10/1 cruise measured with the capillary column system. a) The co-elution between SF_6 (retention time 5.75 min) and CFC-12 (retention time 6.25 min) makes it impossible to quantify the SF_6 peak. b) After adjusting the precolumn flushing times, the co-elution could be separated from the SF_6 peak (retention time 5.6 min) but therefore the CFC-12 had to be cut off.

In a purge tower the water is purged with clean nitrogen to strip out all gases. To concentrate the compounds, the gases are trapped cryogenically on a small-volume trap. For cooling, liquid nitrogen is used. The trap is filled with a compound-specific material for better adsorption. For desorption, the trap is heated and the carrier gas is transferred to the chromatographic columns. Heating is achieved by applying a voltage on the steel trap. The resulting electrical current quickly heats the highly resistant material. Temperatures are controlled by a thermocouple attached to the trap. During the cooling phases the temperature has to be regulated manually by changing the level of liquid nitrogen below the trap. The heating process is automated by a temperature regulator. In the precolumn the group of compounds of interest is separated from other volatile compounds present in sea water. In the main column further separation of the compounds is achieved. The signals get detected and can be quantified with the computer.

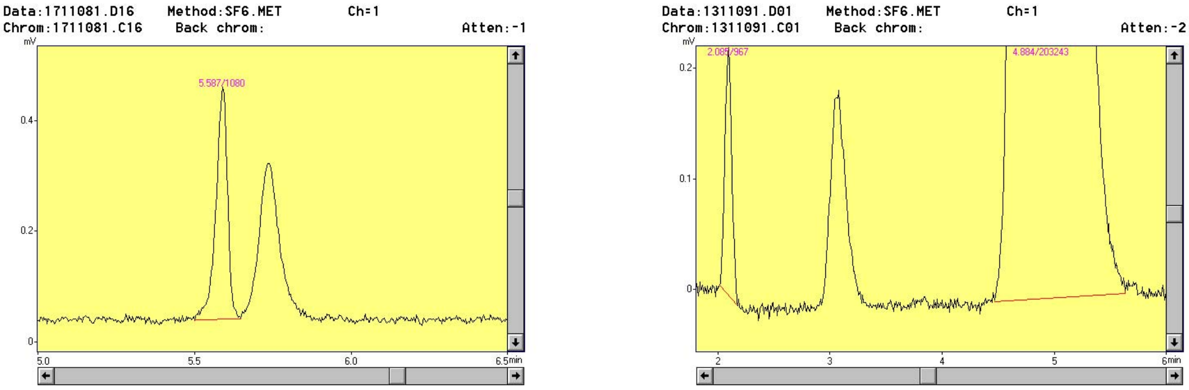

(a) (b)

Figure 2.2: Chromatograms of surface water samples measured a) with the capillary column system during the MSM10/1 cruise and b) with the packed column system during the M80/1 cruise.

During the PhD work two different instrument setups were used. The first one contains packed and capillary columns and two traps in order to increase sensitivity for SF_6. Unfortunately, problems like co-elution of unknown substances, breaks in the capillary columns and long retention times were encountered. Furthermore, the precision was poor (see section 2.3.1) and the expected sensitivity was not achieved. During the MSMS10/1 cruise a co-elution between SF_6 and CFC-12 was encountered on this instrument (Fig. 2.1(a)). Attempts to separate the co-elution from the SF_6 peak resulted in the loss of the CFC-12 peak and only SF_6 could be measured (Fig. 2.1(b)). Thereupon the instrument was altered to a simplified system which runs with one trap and exclusively with packed columns. Figure 2.2 compares the chromatograms of surface water samples measured with the two different systems. The sensitivity for SF_6 is similar but due to the described problems in the capillary column system, CFC-12 could not be measured.

2.2.1 Sampling

Water samples were taken from 10-L Niskin bottles into 330-mL glass ampoules. The ampoules are equipped with a removable stainless steel inlet tube with a nozzle, which fits into the stop cock of the Niskin bottle. The inlet tube reaches down to the bottom of the ampoule and at the top of the ampoule there is a stainless steel overflow tube. Thus, the ampoule gets filled from the bottom to the top. The ampoules are rinsed twice their volume until the overflow tube is capped. While filling the ampoule air bubbles have to be removed from the steel tubings and the glass walls. After sampling, the ampoules are stored in ice water to prevent outgassing and formation of bubbles due to decreasing gas solubility with increasing temperature.

2.2.2 Measurements at sea

The setup of the purge system used on board is shown in figure 2.3. To improve the stripping efficiency the water sample is heated for 15 to 20 minutes in a water bath to about 35°C and then the water inlet of the ampoule is connected to the purgetower.

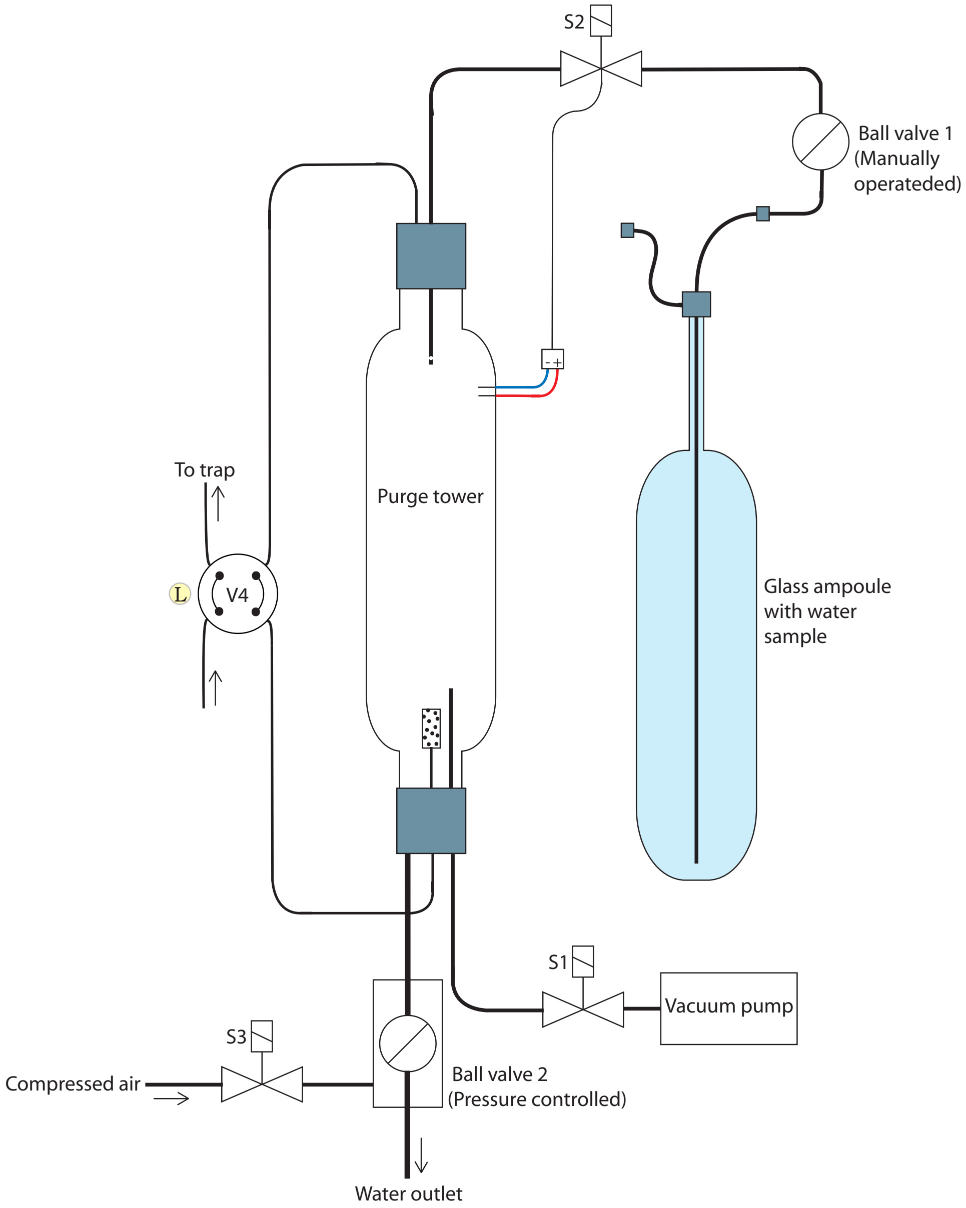
S2
Ball valve 1
(Manually
operateded)
- +
To trap
Purge tower
L
V4
Glass ampoule
with water
sample
S1
Vacuum pump
S3
Compressed air
Ball valve 2
(Pressure controlled)
Water outlet

Figure 2.3: Purge system used on board. V stands for 'valve', S for 'solinoid valve' and L for the 'load' position of a valve.

The purgetower gets evacuated by manually opening and then closing again the solenoid valve S1. After manually opening ball valve 1 the program for the subsequent, automated analysis is started. (Ball valve 1 has been added because the solenoid valve S2 started to leak slightly after the first runs with sea water.) When S2 is opened, the water is drawn from the ampoule into the purgetower. Due to the strong vacuum and the pin holes to the side of the inlet strainer, the water sprays against and runs down the glass wall of the purgetower. Thereby, most of the dissolved volatile gases in the water already pass into the gas phase. In the upper part of the purgetower the ends of two wires are placed to the inside tower wall - one above the other with a gap of about 1 cm in between. When the sea water reaches the second wire an electrical circuit is closed due to the conductivity of saltwater and S2 is shut. The purgetower has now been filled with the water sample leaving a small headspace. Now valve V4 is switched to the 'inject' position and the water sample is purged for 10 minutes with clean nitrogen and trapped cryogenically. The trapping process and the subsequent procedures are described in sections 2.2.4 and 2.2.5, respectively. To avoid contamination by air from inside the tubings before flushing or by water from the previous sample, first of all the tower and the tubings are flushed with a small volume of the water sample and then evacuated again. When the purging and trapping is completed S3 activates the pressure controlled ball valve 2 and the water is drained from the purgetower. Prior to each cruise the volume of the purgetower has been calibrated in the laboratory by filling and draining it several times and weighing the water. With the salinity and the temperature the volume has been calculated for all repetitions. The average of these volumes is used to determine the sample masses on board with the respective salinities and temperatures.

2.2.3 Measurements in the laboratory

Water samples for later analysis in the laboratory have to be processed in a different way. After taking the water sample, it is flame sealed. To do so, the ampoule outlet is connected to a low nitrogen flow, while the end of the inlet tube has been carefully positioned in the upper 3 cm of the ampoule body, whereby the water is displaced with a nitrogen headspace. The inlet tube is now positioned in the upper part of the ampoules neck and with a continuing nitrogen flow the neck gets flame sealed with a gas torch. With this method samples can be stored several months.

The setup of the purge system used in the laboratory is shown in figure 2.4. Ampoules are heated in a hot bath over night to about 65°C. Due to decreasing solubility with increasing temperature, most of the dissolved volatile gases in the water sample should now be found in the headspace, which reduces the purge time. The ampoule then is placed and tightened in the cracker. In order to remove the air from the cracker it is flushed for six minutes with clean nitrogen, by switching V4 to the 'inject' position. To increase the flow rate and thus to decrease the flushing time, the ball valve is open during the first four minutes . After flushing the cracker it is again isolated from the system by switching V4 to 'load'. With the outside handle on the cracker the ampoule can now be cracked open and then the purge tube is inserted manually. The ten minutes purging and trapping starts with switching V4 again to the 'inject' position.

After desorption from the trap and detection of the signal, in the case of CFC-12 the entire process would have to be repeated several times on the same water sample to achieve 100 % purge efficiency. As each purge is very time intensive (approx. half hour) a statistical method that only requires two purges has been developed instead and is applied. This method is described in section 2.3.2. After measuring a sample the cracked ampoule is weighed. Thereafter, the sea water is drained from the ampoule, which is then rinsed with distilled water and dried.

The dry weight subtracted from the filled ampoule weight gives the water sample mass.

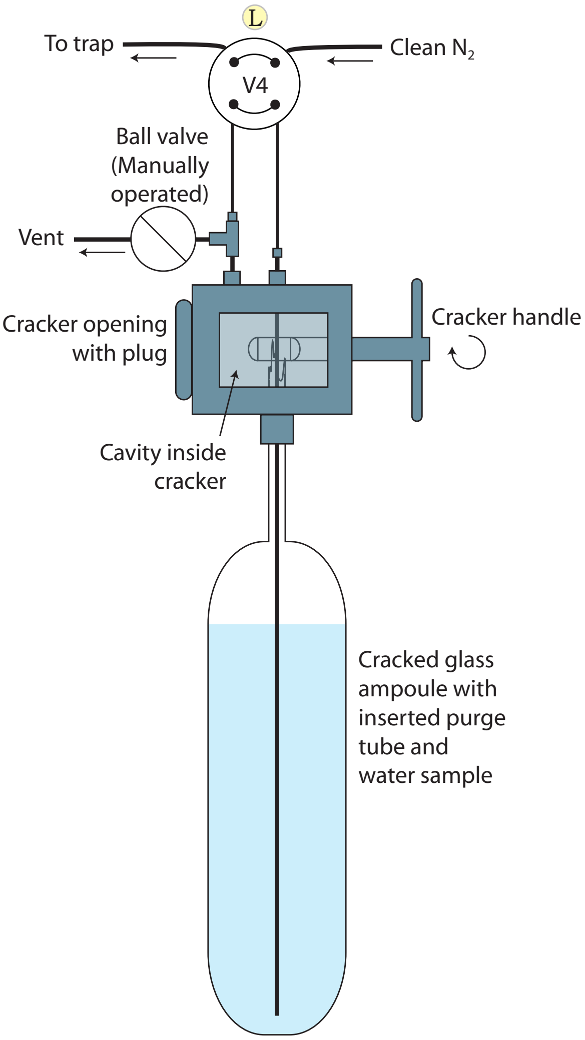
L
To trap
Clean N$_2$
V4
Ball valve (Manually operated)
Vent
Cracker opening with plug
Cracker handle
Cavity inside cracker
Cracked glass ampoule with inserted purge tube and water sample

Figure 2.4: Purge system used in the laboratory. L stands for the 'load' position of a valve.

2.2.4 Capillary column system - instrument A

Figure 2.5 shows the setup for instrument A (capillary column system). During the purging process the gas is trapped at $-100°$C on a 1 m, $1/16''$ stainless steel trap filled with Haysep D, which retains low molecular weight compounds, especially halogen and sulfur groups. V6, V4 and V7 are on the 'inject' position. Before reaching trap 1 the gas passes a nafion dryer and 15 cm of magnesium perchlorate, in order to dry the purge gas. After ten minutes of purging with clean nitrogen at a flow rate of 120 mL min^{-1} trap 1 is isolated by switching V7 to the 'load' position and heated up to 100°C. When the temperature is reached V6 is switched to 'load' and V7 and V8 to 'inject'. Trap 1 is backflushed and the gas passes the precolumn with 8 mL min^{-1} and is trapped on trap 2. The precolumn is a $1/8''$ stainless steel tubing packed with 50 cm Porasil C and 50 cm molecular sieve 5Å. It is located in the GC oven which is held at 35°C. Porasil C preseparates the volatile compounds according to size and the molecular sieve retains the molecules smaller than SF_6. Trap 2 is a 5 cm $1/32''$ stainless steel tubing filled with Carboxene 1000, which provides good performance for low boiling compounds. It is held at −70°C. After 1:50 min SF_6 has passed the precolumn and has been trapped quantitatively on trap 2. V6 is switched to 'inject' and V8 to 'load'. The precolumn gets backflushed. T2 is heated to 150°C for one minute and the desorbed gases flow through the main column and to the detector. The main column is a combination of two capillary columns arranged in series. The first on is a 75 m DB 624 (medium polarity, 0.53 mm inner diameter, 3 μm film thickness). The second one is a 30 m RT-molecular sieve 5Å (0.53 mm inner diameter, 50 μm film thickness).

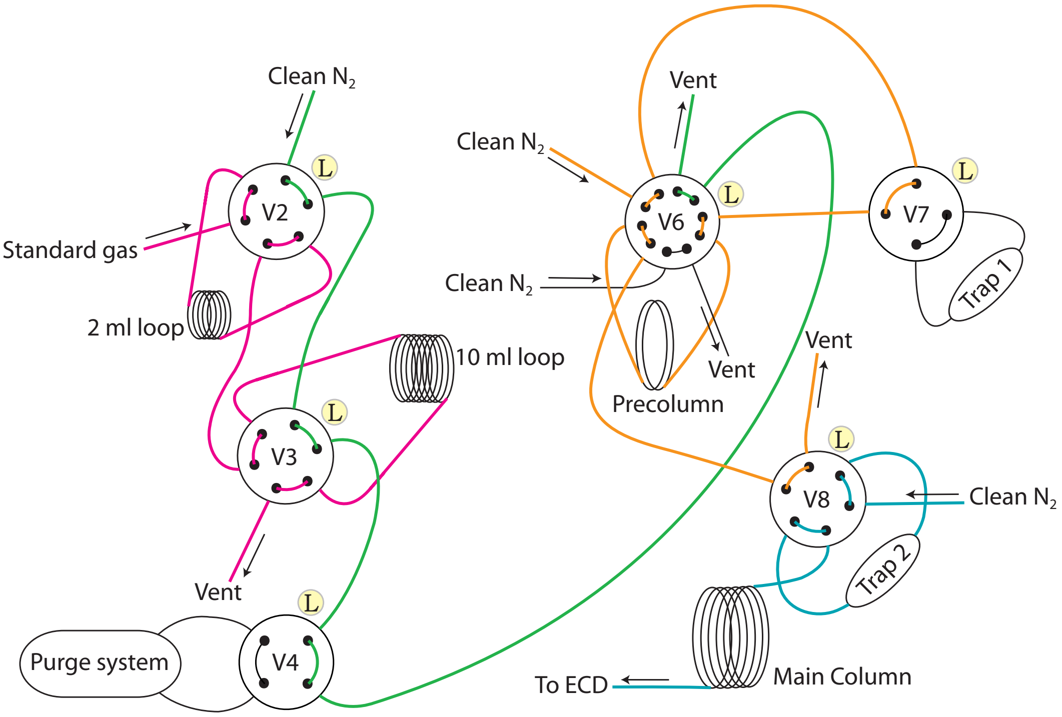

Figure 2.5: Setup of instrument A using capillary columns. V stands for 'valve' and L for the 'load' position of a valve.

2.2.5 Packed column system - instrument B

In figure 2.6 the setup for the simplified instrument B using only packed columns and one single trap is illustrated. The water sample is purged for ten minutes with a flow rate of about 80 mL min^{-1}. After passing the nafion dryer and 15 cm of magnesium perchlorate the gas is trapped on a 70 cm 1/16″ stainless steel trap filled with Haysep D. V6 and V4 are on 'inject' position and V7 on 'load'. The trap is isolated by switching V6, heated to 130°C and then brought in-line with the precolumn and the main column by switching V7 to the 'inject' position. The trap is backflushed and with a flow rate of 15 mL min^{-1} SF_6 and CFC-12 have passed the 30 cm 1/8″ precolumn filled with Porasil C after about 1:20 min. V7 is switched to 'load' and V6 to 'inject'. The compounds are separated on the main column while the precolumn is backflushed. Both are located in the oven at 60°C. The main column is a two meter 1/8″ tubing packed with 180 cm Carbograph and 20 cm molecular sieve 5Å. Due to a bulk contamination peak after the CFC-12 peak, the oven temperature is increased to 90°C for 10 min after each sample, to condition the column.

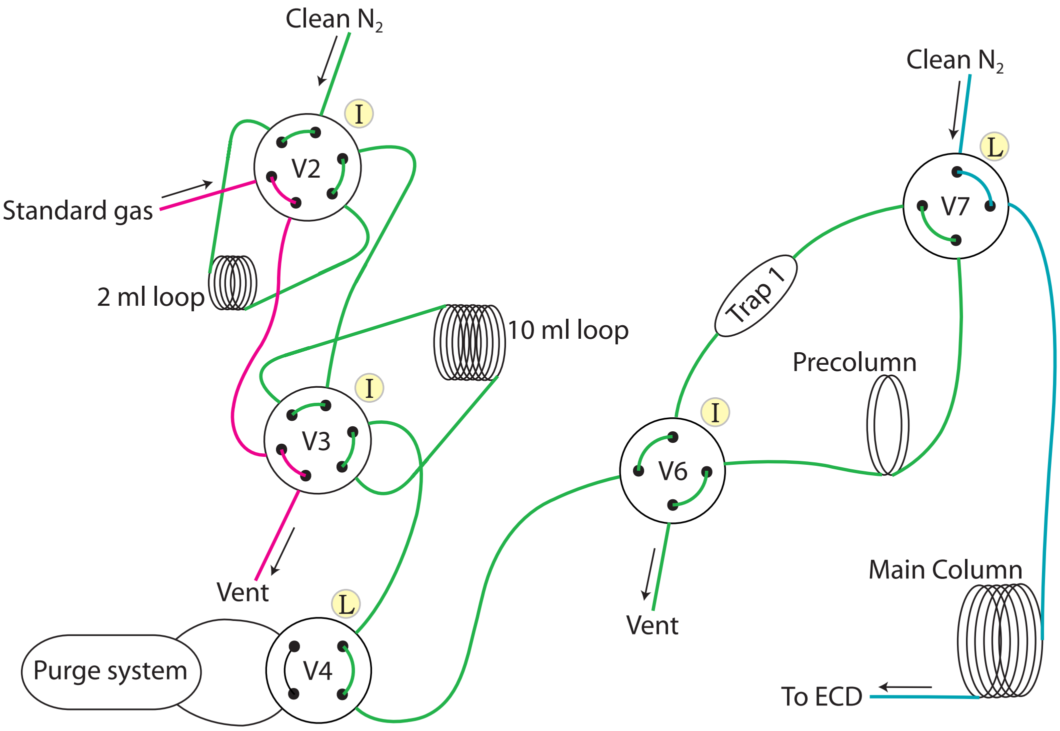

Figure 2.6: Setup of instrument B using only packed columns. V stands for 'valve', L for the 'load' position of a valve and I for the 'inject' position of a valve.

2.2.6 Detection

For detecting the compounds coming off the gas chromatographic columns, an Electron Capture Detector (ECD) is used. This detector is very sensitive to halogenated compounds. It is made of an ionization chamber with a cathode and an anode. The chamber has an inlet and an outlet for the carrier gas. The cathode is a metal foil coated with the radioactive isotope ^{63}Ni. ^{63}Ni is a beta emitter. In the β-decay primary electrons are formed which collide with the nitrogen molecules of the carrier gas. Positively charged N_2-molecules are formed and free secondary electrons. By applying voltage these free electrons move to the anode and lead to an electrical current - the baseline. If the gas flow carries a substance with high electronegativity, such as chlorine or fluorine, part of the free electrons are captured, which leads to a reduced current. This reduction of current presents the detector signal and is interpreted as a peak in the chromatogram.

2.2.7 Standards and blanks

The standard gas is calibrated using a second standard with known SF_6 and CFC-12 concentrations. Standard loops of 2 mL and 10 mL are used to calibrate the system. (The exact volumes of the standard loops were calibrated with a third standard loop of known volume.) For standard measurements either V2 or V3 or both are switched to the 'load' position (Fig. 2.5 and 2.6), depending what volume of standard gas needs to be measured. One or both loops are thereby filled with standard gas. To avoid temperature and associated gas volume changes in the loops, they are constantly heated to a temperature of about 43°C. When V2 and/or V3 together with V6 are switched back to 'inject', the standard is trapped. In order to measure varying standard volumes, the process of filling the standard loops and trapping can be repeated several times until the critical time limit for breakthrough on the trap is reached. The maximum standard volume for a calibration curve was set in order to cover the maximum water concentrations. Generally this was twice the 10 mL loop. When trapping is completed, the desorption process follows as described in sections 2.2.4 and 2.2.5, respectively.

System blanks are performed by running a standard measurement but instead of standard gas clean nitrogen is used. To test the sampling process and the purgetower on board, sample blanks are run with deep water samples (~3000 m), where no CFC-12 nor SF_6 are expected. Sample blanks in the laboratory are achieved by processing and analysing an ampoule without cracking.

During the ship measurements a standard curve is performed every day. Additionally, one selective standard volume is run 1 - 3 times together with a blank before and after each station. Sample blanks are measured at the beginning of a cruise. Since the analysis of one ampoule in the laboratory is a matter of about one hour, the two hours standard curves are only run weekly. The selective standard volume together with either a system blank or a sample blank is measured once in the morning and in the evening and three times at noon. In figure 2.7 the chromatogram of a standard run is shown.

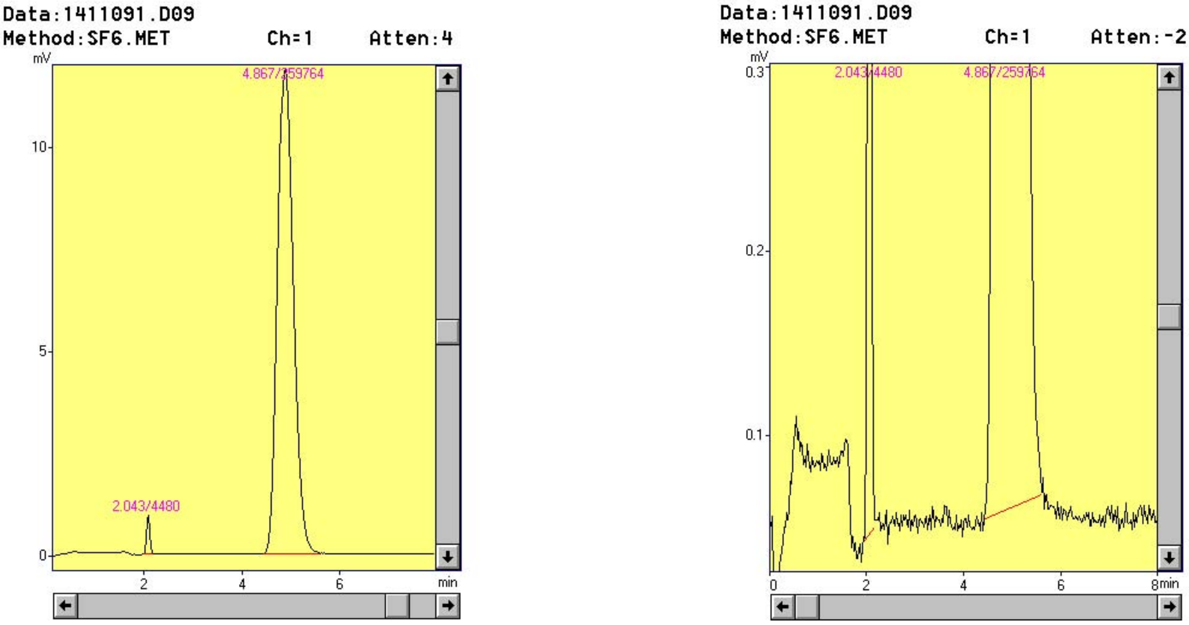

(a) (b)

Figure 2.7: Chromatogram of a standard sample measured with the packed column system. a) is an overview and b) shows the chromatogram in high resolution.

2.3 Data processing

After the analysis of the water samples, the achieved chromatograms have to be processed in several steps to receive the appropriate tracer concentrations of the sample. These procedures are described in section 2.3.1. The measurements made in the laboratory require an additional procedure described in section 2.3.2. In a primary quality control outliers are flagged. In a secondary quality control possible discrepancies in the data are identified. An explanation for these discrepancies is searched and if possible, the data are adjusted. In section 2.3.3 the identified problems of all datasets and the applied troubleshooting and adjustments are described.

2.3.1 General procedures

All peaks in the chromatograms are manually reintegrated and the peak areas of the system blanks (if existent) are subtracted from the peak areas of the standard and the water measurements, whereas the sample blanks are subtracted only from the water measurements. When a constant blank is present, its mean value is subtracted. When an occasional blank appears, it is subtracted from measurements during that period. In table 2.1 only the constant errors are considered. With the known tracer mixing ratio in the standard (M), the loop temperature (T), the atmospheric pressure (P), the ideal gas constant (R) and the exact volume of the standard loop (V), the injected moles of standard (n) for each run can be determined using the ideal gas law:

$$n = \frac{PV}{RT} \cdot M. \tag{2.1}$$

The peak area now equates to a number of moles (n). With the standard curve measurements a function that describes the dependency of n to the peak area is determined (Fig. 2.8). For SF_6 this dependency is almost linear. For high CFC-12 concentrations the detector sensitivity decreases and the standard curve flattens slightly. To calculate the tracer concentration of a water sample in pmol kg^{-1} this function and the mass of the measured sample is needed. Thus the peak area is a measure of concentration.

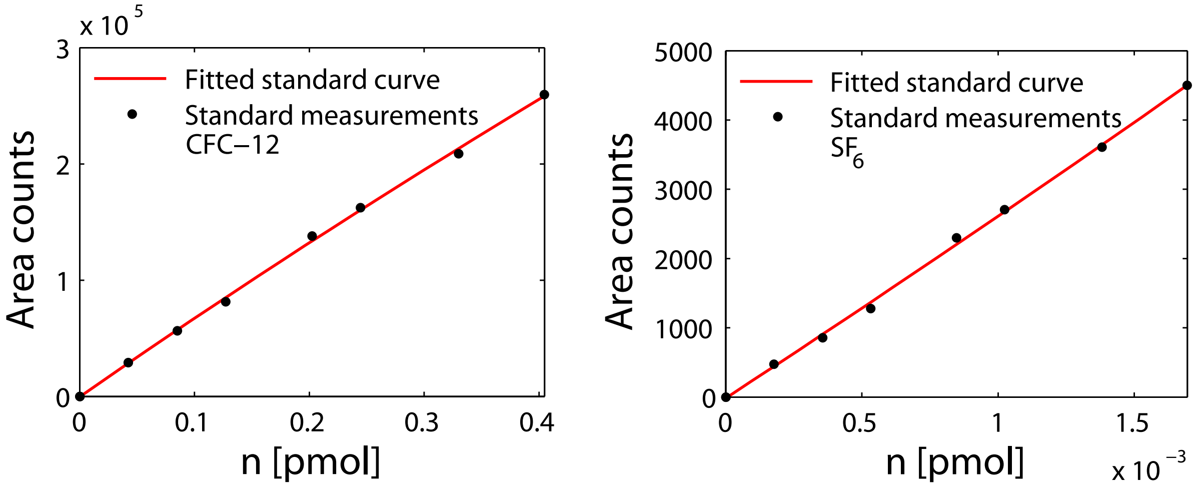

(a)

(b)

Figure 2.8: Standard curve measurements for CFC-12 and SF_6.

The daily performed single standard runs are used to determine the drift of the system (Fig. 2.9). To do so, one measurement is defined as reference and all other measurements reflect the relative divergence from that point. In practice each standard curve is defined as a reference point and the single standard measurements referring to that curve are used to calculate the relative drift, which is then used to correct all water measurements referring to that same curve. The double and triple standard measurements are used to determine the precision of the system. Only when the standard deviation is small relative to the drift variations (Fig. 2.9), the drift correction as described above is performed. Otherwise a mean response factor is applied. For example, the standard measurements during MSM10/1 on the capillary column system show high variability (Fig. 2.10). This was one reason to change this system to one with packed columns, which are less susceptible. The origin of the system drift remains unclear. It could neither be attributed to changes in temperature nor in atmospheric pressure (Fig. 2.9).

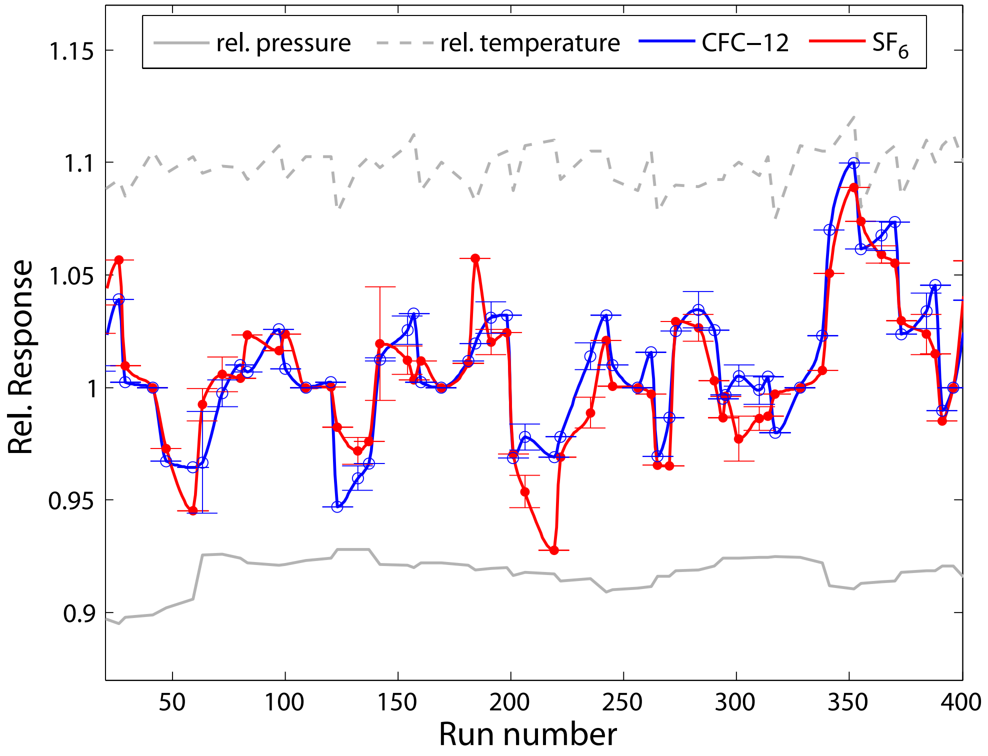

Figure 2.9: Drift correction for the instrument B. Where the circles and the crosses coincide, a standard curve has been measured and new reference points were set for both compounds. Error bars show the standard deviation of double or triple standard measurements. The dashed gray line is the relative temperature of the standard loops and the solid gray line is the relative atmospheric pressure.

2.3.2 Statistical method for flame sealed ampoules

The detected tracer concentration of the first purge after cracking an ampoule is dominated by gases in the headspace. About 80 - 90 % of CFC-12 and nearly 100 % of SF_6 have gone into the gas phase because of heating. CFC-12 is less volatile than SF_6, thus one purge is not enough to strip out all of the remaining CFC-12 dissolved in the water. The detected concentrations of the subsequent purges decrease exponentially (Fig. 2.11(a)). In order to avoid multiple purges for each water sample a method is developed to quantify CFC-12 with only two purges. As basis Henry's law is used:

$$A_1 = A_0 \cdot e^{-\left(\frac{H \cdot V_g}{V_w}\right)}, \tag{2.2}$$

where A_0 is the initial tracer concentration in the water sample, A_1 is the concentration remaining in the water after the first purge, H is the temperature dependent Henry's constant, V_g the purge gas volume and V_w the water volume.

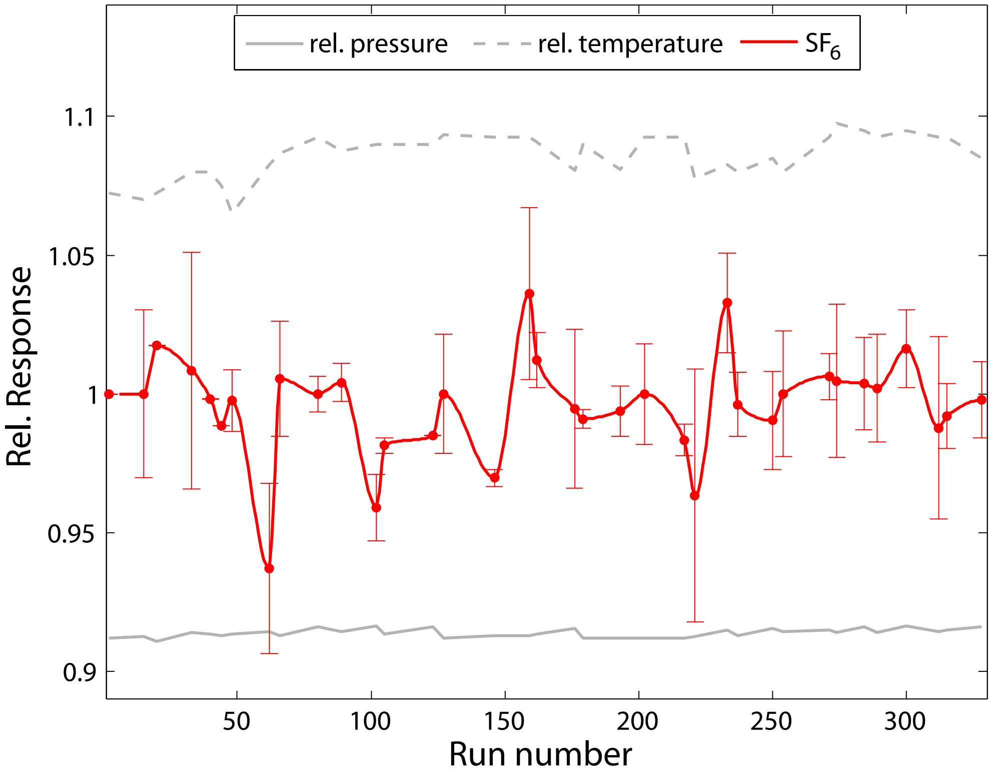

Figure 2.10: Drift correction for the instrument A. Error bars show the standard deviation of double or triple standard measurements. The dashed gray line is the relative temperature of the standard loops and the solid gray line is the relative atmospheric pressure.

As mentioned before, our first purge is dominated by the gases in the headspace and therefore equation 2.2 only applies to the following purges. We adapt the equation to:

$$A_2 = A_1 \cdot e^{-\left(\frac{H \cdot V_g}{V_w}\right)}, \tag{2.3}$$

where A_2 is the concentration remaining in the water after the second purge. We replace A_2 by $A_1 - P_2$, where P_2 is the detected concentration of the second purge (i.e. the tracer amount purged out of the sample during the second purge). Since we are interested in the remains after the first purge, we solve the equation for A_1. Thus:

$$A_1 = \frac{-P_2}{e^{-\left(\frac{H \cdot V_g}{V_w}\right)}} - 1. \tag{2.4}$$

With the detected concentration of the first purge (P_1) the initial concentration can then be determined:

$$A_0 = A_1 + P_1. \tag{2.5}$$

To verify this theoretical approach, 10 samples are purged several times until the water is depleted with respect to CFC-12 (4 - 7 times). To cover possible differences in the purge behavior depending on concentration, samples with a broad range of CFC-12 concentrations (surface, intermediate and deep samples) are used. The sum of all purges of one sample gives the initial tracer concentration (A_0) and $A_1 = P_2 + P_3 + \cdots + P_n$.

Applying equation 2.4 to the 'test-samples' to calculate A_1 results in too low values compared to the measured results. The error for A_1 is about 50 % and for A_0 about 7 %. The reason for this is that Henry's law assumes 100 % equilibrium between the water and the purge gas and this assumption does not hold true for the system setup. The size of the purge gas bubbles and the limited time they are passing through the water are unsuitable to achieve equilibrium. In order to reduce this error, the exponential function 2.3 is fitted to the measured values by adding a factor (F) smaller then one to the Henry's constant:

$$A_2 = A_1 \cdot e^{-\left(\frac{F \cdot H \cdot V_g}{V_w}\right)}, \tag{2.6}$$

which quasi decreases the speed of the gas exchange (Fig. 2.11(b)). With this correction the errors decreased substantially.

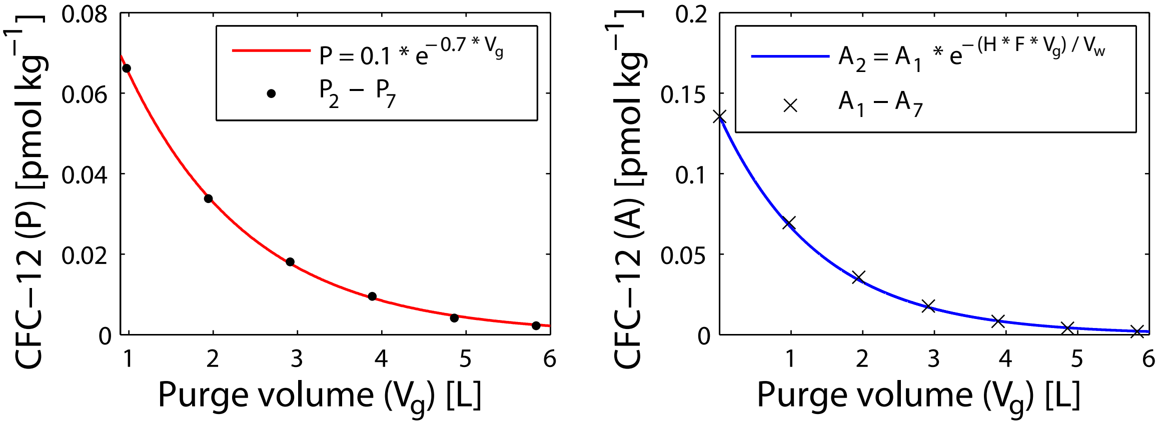

(a) (b)

Figure 2.11: a) Decreasing CFC-12 concentrations through multiple purges. b) Henry's law fitted to the multiple-purge samples from the M80/1 cruise using equation 2.6 with $F = 0.0058$, which means that only 0.6 % equilibrium is reached during the purging.

The laboratory measurements were performed in two sets. In the first one, samples from M68/2 were analysed and in the second one, samples from M80/1. For both sets 'multiple-purge test samples' to fit the theoretical decay curve were measured. For M68/2 samples, the best guess for F in equation 2.6 was 0.0078 and for M80/1 it was 0.0058. After applying the factor and calculating A_0, errors were overall less than 1 % for the M68/2 samples. Similar uncertainties emerged for the M80/1 cruise except for samples with low tracer concentrations, suggesting a blank problem. After subtracting a small blank of 0.0018 pmol kg^{-1} from all measurements, the results were much better and we got an error of less than ±1.5 %. We suspect that the contamination originates from air entering the system during the cracking process, which means that also the SF_6 measurements got contaminated. To determine the mean SF_6 blank, the atmospheric ratio of CFC-12 to SF_6 (~78.7) was taken and applied to the CFC-12 blank. Resultant a SF_6 blank of $2.3 \cdot 10^{-5}$ pmol kg^{-1} was obtained. Both blanks are substracted from all water sample measurements.

2.3.3 Secondary quality control and adjustments

Calculation of the surface water saturation (upper 20 m) with respect to atmospheric tracer mixing ratios revealed unusual values for several cruises. Accordingly, CFC-12 concentrations during M80/1 and M80/2 measured on instrument B were too low, with saturations of 90 - 93 %. The CFC-12 samples measured parallel on instrument PT1 during M80/2 showed 'normal' surface water saturation around 100 % and thus helped to adjust the suspect samples. It has to be tested whether the problem can be attributed to an inaccurate standard concentration or to contamination with e.g. grease. Meanwhile a factor of 1.09 has been applied to all CFC-12 concentrations measured on instrument B during M80/1 and M80/2. Surprisingly, the flame sealed ampoules of M80/1 measured post-cruise did not show the same trend. Applying the factor of 1.09 to these measurements results in supersaturation of the surface samples ($>$ 110 %) and therefore does not seem reasonable. The SF_6 saturation in the upper 20 m was uncommonly high for all cruises, which implies that our standard concentration had been determined inaccurate. This has to be verified by a new standard calibration. By then the SF_6 data are corrected by adjusting the surface water saturation to 100 %. The standard corrections in % for both, CFC-12 and SF_6 are shown in table 2.1.

Plotting the CFC-12/SF_6 ratios against the CFC-12 concentrations and comparing them to the expected curve demonstrated an additional small error in the SF_6 concentrations of two cruises. Following a value of 0.05 fmol kg^{-1} for MSM10/1 and of 0.08 fmol kg^{-1} for M80/1 (onboard) was subtracted from the SF_6 concentrations respectively.

3 Alkalinity of the Mediterranean Sea

A. Schneider, D.W.R. Wallace and A. Körtzinger (2007), *Geophysical Research Letters*, 34 (15), doi: 10.1029/2006GL028842.

Contribution: Anke Schneider performed the calculations, evaluated the data and wrote the paper. Douglas W.R. Wallace and Arne Körtzinger assisted with input to the manuscipt and revision.

GEOPHYSICAL RESEARCH LETTERS, VOL. 34, L15608, doi:10.1029/2006GL028842, 2007

Alkalinity of the Mediterranean Sea

Anke Schneider,[1] Douglas W. R. Wallace,[1] and Arne Körtzinger[1]

Received 27 November 2006; revised 16 May 2007; accepted 7 June 2007; published 11 August 2007.

[1] Total alkalinity (A_T) was measured during the Meteor 51/2 cruise, crossing the Mediterranean Sea from west to east. A_T concentrations were high (~2600 μmol kg^{-1}) and alkalinity-salinity-correlations had negative intercepts. These results are explained by evaporation coupled with high freshwater A_T inputs into coastal areas. Salinity adjustment of A_T revealed excess alkalinity throughout the water column compared to mid-basin surface waters. Since Mediterranean waters are supersaturated with respect to calcite and aragonite, the excess alkalinity likely reflects alkalinity inputs to coastal areas close to regions of deep and intermediate water formation. An alkalinity budget shows that main alkalinity inputs come from the Black Sea and from rivers, whereas the Strait of Gibraltar is a net sink. The major sink appears to be carbonate sedimentation. The basin-average net calcification rate and $CaCO_3$ sedimentation was estimated to be 0.38 mol m^{-2} yr^{-1}. The estimated residence time of A_T is ~160 yr.

Citation: Schneider, A., D. W. R. Wallace, and A. Körtzinger (2007), Alkalinity of the Mediterranean Sea, *Geophys. Res. Lett.*, *34*, L15608, doi:10.1029/2006GL028842.

1. Introduction

[2] The Mediterranean Sea is a semi-enclosed basin, connected to the Atlantic Ocean via the Strait of Gibraltar. The inflowing low-nutrient Atlantic water is responsible for its generally oligotrophic and relatively well oxygenated character. Due to insolation and resulting evaporation on the one hand and little precipitation and river discharge on the other, the Mediterranean Sea has a negative freshwater balance resulting in an anti-estuarine thermohaline circulation. The classical circulation is schematically described as an open thermohaline cell with two deep-reaching closed secondary cells [*Lascaratos et al.*, 1999]. The principal cell pictures the transformation of inflowing Atlantic Water (AW) at the surface to outflowing Levantine Intermediate Water (LIW): on its way eastwards, the AW becomes warmer and saltier, forming Modified Atlantic Water (MAW). In winter chilly winds cool the surface waters in the Levantine basin making them dense enough to sink and mix with underlying water [*Ovchinnikov*, 1984]. At intermediate depths the now called LIW flows back to the west. The two secondary cells describe the development of Eastern and Western Mediterranean Deep Waters, once again driven by strong evaporation and cooling of surface waters in the Adriatic and the Gulf of Lyon, respectively [*Gascard*, 1978; *Pollak*, 1951]. In 1988, with the development of a new deep water component originating in the Aegean Sea, the 'classical circulation' changed from a single deep water source in the Eastern Mediterranean to a two source system [*Roether et al.*, 1996]. Since then a major portion of the former bottom water in the Eastern Mediterranean has been uplifted and replaced by this very dense Aegean water [*Klein et al.*, 1999].

[3] Due to the sparseness of measurements, especially in the eastern basin, little is known about the carbonate system of the Mediterranean Sea. Published data for total alkalinity (A_T) are spatially and temporally limited [*Copin-Montégut*, 1993; *Copin-Montégut and Bégovic*, 2002; *Millero et al.*, 1979] and make it difficult to draw a coherent picture of the alkalinity distribution. Here we present a new, broad and reliable dataset for A_T which covers primarily the eastern basin (Figure 1) and allows a reasonable estimate of the alkalinity budget.

2. Materials and Methods

[4] Measurements of salinity, temperature and oxygen were made at 42 stations along the cruise track of R/V Meteor cruise 51/2 (M51/2, 18 October – 11 November 2001, Malaga – La Valetta), crossing the Mediterranean Sea from west to east. Measurements of A_T and total dissolved inorganic carbon (DIC) were made at 14 stations using potentiometric titration [*Mintrop et al.*, 2000] and coulometric titration [*Johnson et al.*, 1993] methods, respectively. Water samples were taken from Niskin bottles in 500 mL Duran glass bottles and poisoned with 100 μL of saturated aqueous solution of mercuric chloride for later shore-based analysis. The results of the DIC measurements will be presented elsewhere. (Data are available from the database CDIAC, http://cdiac.ornl.gov).

[5] The accuracy of the A_T determination was assessed by regular measurements of Certified Reference Material (CRM, supplied by Andrew Dickson, Scripps Institution of Oceanography (SIO), La Jolla, CA, USA). The A_T concentration of each CRM batch is certified by shore-based potentiometric titration [*Dickson*, 1998; *Dickson et al.*, 2003]. A_T measurements on CRMs from 2 batches (batch # 48 and 52) yielded a mean offset between our measurements and the certified values of -0.82 ± 2.85 μmol kg^{-1} (95% confidence interval, $n = 41$). Measured A_T concentrations were therefore adjusted to the certified values by correction for this mean offset. Precision of the A_T measurements was 4.2 μmol kg^{-1} (95% confidence interval), determined from duplicate samples ($n = 15$).

[6] The degree of saturation (Ω) for calcite and for aragonite was calculated from A_T and DIC with the software program CO2SYS [*Lewis and Wallace*, 1995], using the carbonic acid dissociation constants (K_1 and K_2) from *Mehrbach et al.* [1973] as refitted by *Dickson and Millero*

---

[1] Forschungsbereich Marine Biogeochemie, Leibniz-Institut für Meereswissenschaften, IFM-GEOMAR, Kiel, Germany.

Copyright 2007 by the American Geophysical Union.
0094-8276/07/2006GL028842$05.00

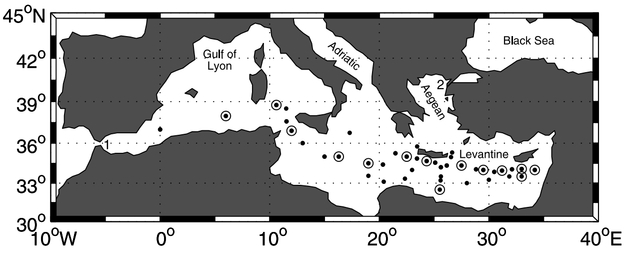

Figure 1. Station plot of the Meteor 51/2 cruise in October/November 2001. Encircled dots indicate stations where alkalinity and DIC measurements were made. 1: Strait of Gibraltar; 2: Dardanelles.

[1987] and the dissociation constant for HSO_4^- from *Dickson* [1990].

3. Results and Discussion

3.1. Alkalinity Distribution

[7] Figure 2a shows the relatively homogeneous distribution of A_T throughout the water column (salinity-adjusted alkalinities shown in Figure 2b are described later). Concentrations are high, reflecting the high salinity of the Mediterranean Sea and are typically ~2600 μmol kg^{-1}. Two exceptions are 1) the MAW with lower salinities and accordingly lower A_T, and 2) the western basin with alkalinities around 2580 μmol kg^{-1}, which also can be attributed to slightly lower salinity.

[8] Figure 3a displays the linear relationships between A_T and salinity (S). In surface waters (depth < 25 m) A_T shows the following correlation with S:

$$A_T = 73.7(\pm 3.0) \cdot S - 285.7(\pm 114.94)\ \mu\text{mol kg}^{-1}$$
$$\left(n = 15, r^2 = 0.98, \sigma_y = 8.20\right). \tag{1}$$

[9] Although previous authors have reported negative intercepts of the A_T-S relationship in the Mediterranean A_T-S regression, no explanation has been given for this unusual feature. The negative intercept can be explained by exceptional circumstances in the Mediterranean, namely: high evaporation and high alkalinity of freshwaters entering the basin by rivers and the Black Sea. These processes are represented by vectors in Figure 3b. Starting point for our considerations is the inflow of Atlantic water from the west (A), which is low in both A_T and S. Disregarding other effects, evaporation would drive a steady increase in S and A_T during the surface waters' movement towards the east. The corresponding theoretical evaporation line (evap) on the A_T-S diagram would run through the origin (S = 0; A_T = 0). The second major influence on Mediterranean water alkalinity is A_T addition by rivers and by the Black Sea: both carry very high alkalinities (between 2000 μmol kg^{-1} and 6500 μmol kg^{-1}) at low or zero salinity. These inputs occur in coastal areas and in the eastern basin, respectively, where surface S and A_T tend to be highest due to the cumulative effects of evaporation. Hence on the A_T-S diagram the influence of coastal alkalinity inputs occurs towards the high-salinity-end of the evaporation line, e.g. at the hypothetical point B with a maximum salinity of 40 on Figure 3b. Accordingly, mixing between high salinity surface water (B) and river or Black Sea water, with their respective endmembers, shifts the characteristics of surface waters towards lower S and higher A_T, i.e. in the direction of the arrows for "riv" and "bs". As a result, the mixture of Mediterranean surface water does not follow a pure evaporative line on an A_T-S diagram but reflects this admixture of high-A_T, low-S endmembers. Consequently, in Figure 3b the mixing lines "riv", "bs" and "evap" picture the boundaries between which our data points should fall and one can observe that most measured samples do lie between these boundaries. Towards lower salinities (i.e. in the western basin) the surface A_T-S relationship of our samples matches the evaporation line rather well, and no clear influence of the high A_T endmembers can be observed. In contrast, at salinities greater than 38, i.e. in the eastern basin and in marginal seas, this effect starts to appear and the deviations from the evaporation line increase with increasing salinity.

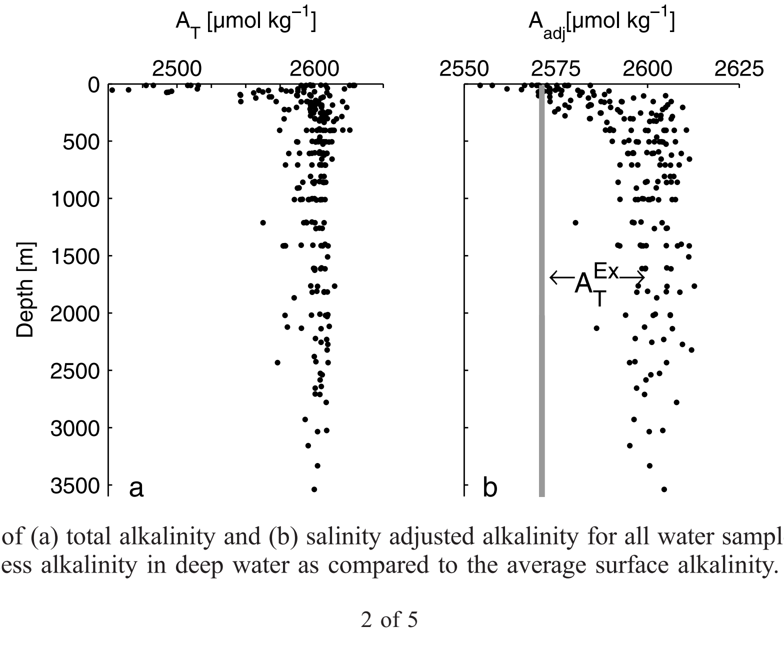

Figure 2. Scatter plot of (a) total alkalinity and (b) salinity adjusted alkalinity for all water samples taken during M51/2. A_T^{Ex} represents the excess alkalinity in deep water as compared to the average surface alkalinity.

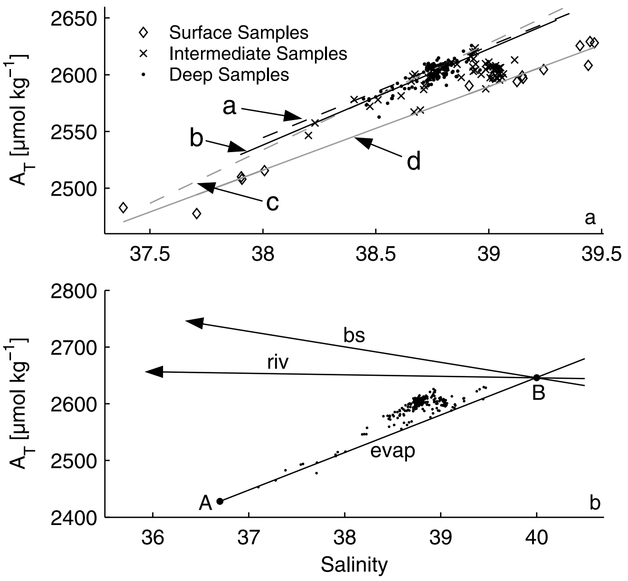

Figure 3. (a) A_T-S-correlation of samples from all stations. Surface samples reach from 0-25 m, intermediate depth samples from 100-400 m and deep samples are below 400 m. The grey line (d) shows the surface regression and the black line (b) the deep regression of the samples. The dashed lines (a and c) show the correlations between alkalinity and salinity at the Dyfamed Site (grey (c) = surface regression, black (a) = deep regression) reported by *Copin-Montégut and Bégovic* [2002]. Linear equations are displayed in the text. (b) Demonstration of evaporation and mixing processes in the Mediterranean Sea as described in the text. Atlantic water (A) evaporates (evap) and high salinity water (B) mixes with riverine (riv) and Black Sea (bs) water. All samples from M51/2 plot well within the A_T-S diagram (black datapoints).

Hence the observed A_T-S relationship in the Mediterranean is steeper than the evaporation line and yields a negative intercept. It is worthwhile to reiterate that this intercept is not representative of any endmember component but a consequence of the presence of high-A_T, low-S influence in the central basin.

[10] The correlation found for deep waters (depth > 400 m) is:

$$A_T = 84.7(\pm 4.89) \cdot S - 682.1(\pm 189.37)\,\mu\text{mol kg}^{-1} \qquad (2)$$
$$\left(n = 152, r^2 = 0.67, \sigma_y = 5.54\right),$$

which suggests an enhanced influence of high alkalinity coastal waters in the deep basins. Within the error bars the deep water relationship (Equation (2)) is in agreement with the relationship observed by *Copin-Montégut and Bégovic* [2002] at the Dyfamed Site in the NW Mediterranean Sea below 500 m (A_T = 80.62 · S − 518.96 μmol kg^{-1}). In contrast, the surface water regression line of *Copin-Montégut and Bégovic* [2002] (A_T = 93.996 · S − 1038.1 μmol kg^{-1}) differs from ours (Equation (1)). The reason for the less steep slope and the less negative intercept of our correlation (Equation (1)) likely reflects the different sampling locations. The Dyfamed Site is located in the north-western Mediterranean Sea (43°25′N, 07°52′E) and likely more coastally-influenced than most of our stations. In coastal regions, alkalinity inputs from rivers (e.g. the nearby Rhone River with a mean alkalinity of 2885 μmol kg^{-1}, Table 1) and potentially from the sediments cause the steeper slope of the regression line.

[11] In order to compensate for salinity-driven variations, A_T was adjusted to a reference salinity (S_{ref} = 38.75) which is the mean surface salinity of our samples. The adjusted alkalinity (A_{adj}, Figure 2b) was calculated according to *Friis et al.* [2003]: $A_{adj} = [(A_T - A_T^{S=0})/S] \cdot S_{ref} + A_T^{S=0}$. This equation includes the non-zero intercept ($A_T^{S=0}$ = −286 μmol kg^{-1}) resulting from our surface A_T-S relationship (Equation (1)). Excess alkalinity (A_T^{Ex}) is defined as the difference between a given sample's alkalinity (adjusted to S_{ref} = 38.75) and the surface ocean reference alkalinity of 2571.2 μmol kg^{-1} (mean alkalinity in the upper 25 m at the mean salinity of 38.75). Overall we find positive values for A_T^{Ex} throughout the sub-surface, which means that, independent of salinity variations, the entire water column is enriched in alkalinity relative to the upper 25 m. The highest excess values were found in the eastern basin. At around 27°E, surface properties extend down to about 300 m depth, which could be the result of the anticyclonic Iera Petra Gyre in this region. This feature was also observed in other parameters (e.g. temperature and oxygen).

[12] A surface-to-depth increase of A_T^{Ex} would be expected, if calcifying organisms removed alkalinity from the photic zone and dissolution of calcium carbonate added alkalinity at depth. However, within the Mediterranean A_T^{Ex} remains constant below ~300 m at about 30 μmol kg^{-1} (Figure 2b). Furthermore, calculation of calcite and aragonite saturation states reveals that Mediterranean waters are strongly supersaturated ($\Omega > 1$) with respect to both minerals throughout the entire water column (Figure 4). Hence dissolution of calcium carbonates is not favoured thermodynamically. The degree of saturation for calcite lies

Table 1. Discharge and Mean A_T of Six Main Rivers Discharging Into the Mediterranean[a]

River	Discharge km^3 yr^{-1}	Reference	Mean A_T μmol L^{-1}	Reference
Rhone	49.5	GEMSWATER, 2002[b]	2885	GEMSWATER, 2002[b]
Po	46.7	GEMSWATER, 2002[b]	2918	GEMSWATER, 2002[b]
Nile	30.0	GEMSWATER, 2002[b]	2213	GEMSWATER, 2002[b]
Ebro	17.4	GEMSWATER, 2002[b]	2148	GEMSWATER, 2002[b]
Tiber	7.2	Vorosmarty et al., 1998[c]	6600	*Copin-Montégut* [1993]
Adige	7.2	Vorosmarty et al., 1998[c]	2100	*Copin-Montégut* [1993]

[a] Total discharge of these six rivers is 158 km^3 yr^{-1} (nearly one third of the overall river discharge into the Mediterranean Sea) and the mean discharge-weighted A_T is 2820 μmol L^{-1}.

[b] GEMSWATER 2002: Water quality data tables for 82 major river basins, 2006, from www.gemswater.org/atlas-gwq/intro.e.html.

[c] Vorosmarty et al., 1998: Global River Discharge Database (RivDIS) V. 1.1, 2006, from http://www-eosdis.ornl.gov.

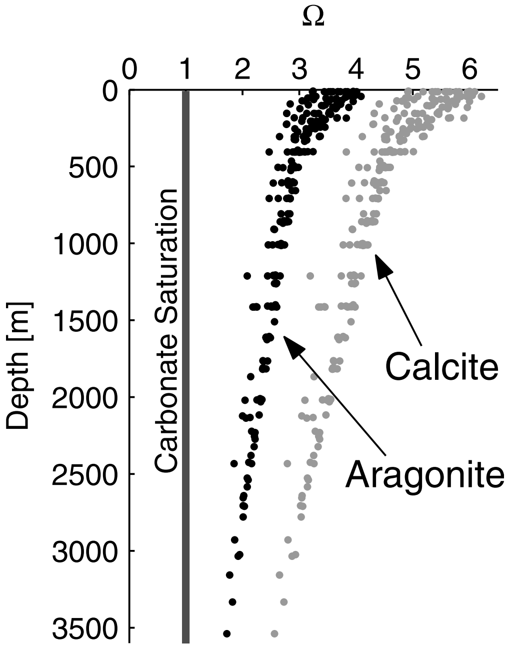

Figure 4. Vertical profiles of the saturation state (Ω) of calcite and aragonite in the Mediterranean Sea.

between 5 and 6 at the surface and ~2.5 at 3500 m depth. For aragonite it ranges between 3 and 4 at the surface and ~1.5 at depth. Similar observations have been reported previously for the western, the central and the eastern basins [*Millero et al.*, 1979, and references therein].

[13] We hypothesise that the inflow of high alkalinity water from rivers as well as from the Black Sea contributes to both the observed A_T^{Ex} and the high saturation state of deep waters, with the high alkalinity arising from weathering of limestone in adjacent areas. Deep water formation in marginal seas appear to rapidly transport coastal alkalinity anomalies directly into the deep basins where they show up as A_T^{Ex}, thereby effectively bypassing the surface waters of the central Mediterranean (to which A_T^{Ex} is referenced). As our stations were located mainly in the mid-basin, our surface water samples were heavily influenced by the inflowing AW with lower alkalinity. A_T measurements from coastal and marginal seas, and especially in the areas of deep water formation, are needed to test this hypothesis. In the absence of such data, it cannot be ruled out that dissolution of readily soluble high magnesium carbonates and other carbonate particles within the water column above the saturation horizon might also contribute to deep water excess alkalinity. Anyway, little is known about these processes and because of the high saturation state throughout the water column in the Mediterranean Sea, carbonate dissolution seems unlikely and is not further considered here.

3.2. Alkalinity Budget

[14] We compiled an alkalinity budget in order to quantify sources and sinks as well as the turnover time of A_T in the Mediterranean Sea. The Mediterranean Sea alkalinity is controlled by water exchange with the Atlantic and the Black Sea, as well as by riverine inputs, and sedimentation of calcium carbonate. With the exception of the sedimentary sink, all net fluxes can be calculated from published estimates of the volumes of inflowing and outflowing water and measurements or estimates of their corresponding alkalinity concentrations (Table 2). Local alkalinity values were estimated from salinity data and an appropriate regional A_T-S regression correlation. The alkalinity of water leaving the Mediterranean towards the Black Sea was estimated from the A_T-S correlation of the surface waters presented in this paper (Equation (1)). A_T entering the Mediterranean through the Dardanelles from the Marmara Sea was estimated from A_T concentrations of water leaving the Black Sea [*Hiscock and Millero*, 2006, Figure 6] and consideration of the subsequent salt and alkalinity divergence within the Marmara Sea [*Besiktepe et al.*, 1994]. The alkalinity of water leaving the Mediterranean Sea through the Strait of Gibraltar was estimated using an A_T-S correlation obtained from our measurements in the western LIW. The mean alkalinity of the inflowing Atlantic water was determined via a relationship published by *Lee et al.* [2006] of A_T with salinity and temperature for the North Atlantic. Finally a mean river alkalinity was estimated from the discharge-weighted alkalinities of six main rivers discharging into the Mediterranean (Table 1). The estimated values of the mean alkalinities in Table 2 have uncertainties and our estimates require verification through direct measurements.

[15] All fluxes at the interfaces of the Mediterranean Sea are listed in Table 2. Main contributors of A_T are the Black Sea and rivers, whereas the Strait of Gibraltar is a net sink for alkalinity. Compared to the findings of *Copin-Montégut* [1993] who estimated a net alkalinity flux of $2.43 \cdot 10^{12}$ mol yr^{-1} into the Atlantic, we obtained a much lower export ($0.8 \cdot 10^{12}$ mol yr^{-1}), which accounts for only about one third of the net A_T inputs. If we assume Mediterranean Sea alkalinity to be in steady state, long term net inputs of alkalinity must equal long term sinks, for which

Table 2. Water, Salinity, and Alkalinity Exchange of the Mediterranean Sea With the Atlantic, the Black Sea, and Rivers[a]

	In/Out	Water Volume, km^3 yr^{-1}	Mean Salinity	Mean A_T, μmol L^{-1}	Salt-Flux, kg yr^{-1} $\cdot$ 10^{13}	A_T−Flux, mol yr^{-1} $\cdot$ 10^{12}	
Atlantic Ocean	in	22706[b]	36.1[b]	2436	+82.0	+55.3	net flux −0.8
	out	21444[b]	38.2[b]	2617	−81.9	−56.1	
Black Sea	in	1218[c]	29.3[c]	2967	+3.6	+3.6	net flux +1.2
	out	918[c]	38.9[c]	2643	−3.6	−2.4	
Rivers	in	513[d]	0	2820	0	+1.5	net flux +1.5

[a] Here "in" refers to water flowing into the Mediterranean and "out" to water escaping the basin. Mean A_T values were estimated as described in the text.

[b] *Bryden et al.* [1994].

[c] *Besiktepe et al.* [1994].

[d] *Tixeront* [1969].

only sedimentation appears to be a reasonable candidate. Under this assumption, the alkalinity loss via carbonate sedimentation amounts to $\sim 1.9 \cdot 10^{12}$ mol yr^{-1}. When distributed equally across the Mediterranean basin (surface area of $2.5 \cdot 10^{12}$ m^2 [*Menard and Smith*, 1966]) this alkalinity loss corresponds to a surface ocean calcification rate of 0.38 mol m^{-2} yr^{-1} (neglecting water column carbonate dissolution). Recently published data for the carbonate flux in the NW Mediterranean [*Martin et al.*, 2006] are consistent with this estimate: For example, whereas sediment traps in the Palamós submarine canyon showed very high carbonate fluxes close to the coast (up to 40 mol m^{-2} yr^{-1}), the values decreased with increasing distance from the coast. The farthest-offshore mooring (depth = 1300 m) showed a mean annual flux of 0.40 mol m^{-2} yr^{-1}, which corresponds to our estimate.

[16] An A_T inventory of the Mediterranean Sea was estimated by integrating the mean depth profile of alkalinity over the average basin depth of 1500 m [*Menard and Smith*, 1966] and by scaling the resulting column inventory to the surface area of the entire basin. With a calculated A_T inventory of $9.7 \cdot 10^{15}$ mol, the residence time (τ) of alkalinity in the basin is $\sim$160 yr. For comparison, we determined a salt inventory ($2.42 \cdot 10^{17}$ kg) and a residence time for salt ($\tau \cong 280$ yr) in the same manner as for alkalinity. As expected, the residence time for salinity is longer than that of A_T.

[17] **Acknowledgments.** We thank the crew of R/V Meteor for their assistance, Peter Streu and Tobias Steinhoff for collection and measurement of the samples. Thanks also to Birgit Klein for helpful discussions and to Wolfgang Roether, the Chief Scientist of the cruise. Funding for this work was provided by the CarboOcean IP of the European Commission (grant 511176-2) and by the Deutsche Forschungsgemeinschaft (DFG).

References

Besiktepe, S. T., H. I. Sur, E. Ozsoy, M. A. Latif, T. Oguz, and U. Unluata (1994), The circulation and hydrography of the Marmara Sea, *Prog. Oceanogr.*, *34*(4), 285–334.

Bryden, H. L., J. Candela, and T. H. Kinder (1994), Exchange through the Strait of Gibraltar, *Prog. Oceanogr.*, *33*(3), 201–248.

Copin-Montégut, C. (1993), Alkalinity and carbon budgets in the Mediterranean Sea, *Global. Biogeochem. Cycles*, *7*(4), 915–925.

Copin-Montégut, C., and M. Bégovic (2002), Distributions of carbonate properties and oxygen along the water column (0–2000 m) in the central part of the NW Mediterranean Sea (Dyfamed site), *Deep Sea Res., Part II*, *49*(11), 2049–2066.

Dickson, A. G. (1990), Standard potential of the reaction - AgCl(s) + 1/2 H2(g) = Ag(s) + HCl(aq) and the standard acidity constant of the ion HSO_4^- in synthetic sea-water from 273.15 K to 318.15 K, *J. Chem. Thermodyn.*, *22*(2), 113–127.

Dickson, A. G. (1998), Reference material for oceanic carbon dioxide measurements, *CDIAC Commun.*, *25*, 1, 16.

Dickson, A. G., and F. J. Millero (1987), Comparison of the equilibrium-constants for dissociation of carbonic-acid in seawater, *Deep Sea Res., Part I*, *34*(10), 1733–1743.

Dickson, A. G., J. D. Afghan, and G. C. Anderson (2003), Reference materials for oceanic CO_2 analysis: A method for the certification of total alkalinity, *Mar. Chem.*, *80*(2–3), 185–197.

Friis, K., A. Körtzinger, and D. W. R. Wallace (2003), The salinity normalization of marine inorganic carbon chemistry data, *Geophys. Res. Lett.*, *30*(2), 1085, doi:10.1029/2002GL015898.

Gascard, J. C. (1978), Mediterranean deep-water formation baroclinic instability and oceanic eddies, *Oceanol. Acta*, *1*(3), 315–330.

Hiscock, W. T., and F. J. Millero (2006), Alkalinity of the anoxic waters in the western Black Sea, *Deep Sea Res., Part II*, *53*(17–19), 1787–1801.

Johnson, K. M., K. D. Wills, D. B. Butler, W. K. Johnson, and C. S. Wong (1993), Coulometric total CO_2 analysis for marine studies, *Mar. Chem.*, *44*(2–4), 167–187.

Klein, B., et al. (1999), The large deep water transient in the eastern Mediterranean, *Deep Sea Res., Part I*, *46*(3), 371–414.

Lascaratos, A., W. Roether, K. Nittis, and B. Klein (1999), Recent changes in deep water formation and spreading in the eastern Mediterranean Sea: A review, *Prog. Oceanogr.*, *44*(1–3), 5–36.

Lee, K., L. T. Tong, F. J. Millero, C. L. Sabine, A. G. Dickson, C. Goyet, G.-H. Park, R. Wanninkhof, R. A. Feely, and R. M. Key (2006), Global relationships of total alkalinity with salinity and temperature in surface waters of the world's oceans, *Geophys. Res. Lett.*, *33*, L19605, doi:10.1029/2006GL027207.

Lewis, E., and D. W. R. Wallace (1998), Program developed for CO_2 System Calculations, *ORNL/CDIAC-105*, http://cdiac.ornl.gov/oceans/co2rprt.html, Carbon Dioxide Inf. Anal. Cent., Oak Ridge Natl. Lab., U.S. Dep. of Energy, Oak Ridge, Tenn.

Martin, J., A. Palanques, and P. Puig (2006), Composition and variability of downward particulate matter fluxes in the Palamos submarine canyon (NW Mediterranean), *J. Mar. Syst.*, *60*(1–2), 75–97.

Mehrbach, C., C. Culberso, J. E. Hawley, and R. Pytkowic (1973), Measurement of apparent dissociation-constants of carbonic-acid in seawater at atmospheric-pressure, *Limnol. Oceanogr.*, *18*(6), 897–907.

Menard, H. W., and S. M. Smith (1966), Hypsometry of ocean basin provinces, *J. Geophys. Res.*, *71*(18), 4305–4325.

Millero, F. J., J. Morse, and C. T. Chen (1979), Carbonate system in the western Mediterranean Sea, *Deep Sea Res., Part I*, *26*(12), 1395–1404.

Mintrop, L., F. F. Perez, M. Gonzalez-Davila, M. J. Santana-Casiano, and A. Körtzinger (2000), Alkalinity determination by potentiometry: Intercalibration using three different methods, *Cienc. Mar.*, *26*(1), 23–37.

Ovchinnikov, I. M. (1984), Intermediate water formation in the Mediterranean Sea, *Oceanology*, *24*(2), 217–225.

Pollak, M. J. (1951), The sources of the deep water of the eastern Mediterranean Sea, *J. Mar. Res.*, *10*(1), 128–151.

Roether, W., et al. (1996), Recent changes in eastern Mediterranean deep waters, *Science*, *271*(5247), 333–335.

Tixeront, J. (1969), Le bilan hydrologique de la mer Noire et de la mer Méditerranée, *Bull. Int. Assoc. Sci. Hydrol.*, *14*(4), 61–69.

A. Körtzinger, A. Schneider, and D. W. R. Wallace, Forschungsbereich Marine Biogeochemie, Leibniz-Institut für Meereswissenschaften, IFM-GEOMAR, Düsternbrooker Weg 20, D-24105 Kiel, Germany. (aschneider@ifm-geomar.de)

4 High anthropogenic carbon content in the eastern Mediterranean

A. Schneider, T. Tanhua, A. Körtzinger and D.W.R. Wallace (2010), *Journal of Geophysical Research – Oceans*, 115 (C12), doi: 10.1029/2010JC006171.

Contribution: Anke Schneider performed the calculations, evaluated the data and wrote the paper. Douglas W.R. Wallace and Arne Körtzinger assisted with input to the manuscipt and revision. Toste Tanhua assisted with the TTD calculations and with input to the manuscipt.

JOURNAL OF GEOPHYSICAL RESEARCH, VOL. 115, C12050, doi:10.1029/2010JC006171, 2010

High anthropogenic carbon content in the eastern Mediterranean

A. Schneider,[1] T. Tanhua,[1] A. Körtzinger,[1] and D. W. R. Wallace[1]

Received 15 February 2010; revised 24 August 2010; accepted 20 September 2010; published 21 December 2010.

[1] This work presents data of dichlorodifluoromethane (CFC-12), dissolved inorganic carbon and total alkalinity from a cruise to the Mediterranean Sea during October–November 2001, with the main focus on the CFC-12 data and on the eastern basin. Using the transit time distribution method, the anthropogenic carbon concentrations in the basin were estimated. Results were cross-checked with a back-calculation technique. The entire water column of the Mediterranean Sea contains anthropogenic CO_2, with minimum concentrations of 20.5 μmol kg^{-1} (error range: 16.9–27.1 μmol kg^{-1}) in the most eastern part of the basin at intermediate depths, where the waters' mean age is >130 yr. Column inventories of up to 154 mol m^{-2} (132–179 mol m^{-2}) are found and a total inventory of 1.7 Pg (1.3–2.1 Pg) of anthropogenic carbon in the Mediterranean Sea was estimated. There is a net flux of 38 Tg yr^{-1} (30–47 Tg yr^{-1}) of dissolved inorganic carbon through the Strait of Gibraltar into the Atlantic Ocean and an opposite net flux of 3.5 Tg yr^{-1} (−1.8–9.2 Tg yr^{-1}) of anthropogenic carbon into the Mediterranean Sea.

Citation: Schneider, A., T. Tanhua, A. Körtzinger, and D. W. R. Wallace (2010), High anthropogenic carbon content in the eastern Mediterranean, *J. Geophys. Res.*, *115*, C12050, doi:10.1029/2010JC006171.

1. Introduction

[2] The carbon dioxide (CO_2) concentration in the atmosphere has increased from 280 parts per million (ppm) in the preindustrial time period to a present-day value of ~390 ppm. This represents only a fraction of the anthropogenic CO_2 emissions and several attempts have been made to quantify the increase of oceanic carbon inventories. As anthropogenic carbon (C_{ant}) cannot be distinguished directly by measurements from the natural background of dissolved inorganic carbon (C_T), several empirical methods to estimate its concentration have been developed and improved over the past few decades [e.g., *Brewer*, 1978; *Chen and Millero*, 1979; *Wallace*, 1995; *Gruber et al.*, 1996; *Waugh et al.*, 2004; *Touratier and Goyet*, 2004; *Friis et al.*, 2005]. There are significant differences in quantity and distribution of C_{ant} estimated using these different methods [*Tanhua et al.*, 2007; *Alvarez et al.*, 2009; *Vazquez-Rodriguez et al.*, 2009], but generally a consistent picture has emerged. For example, highest C_{ant} column inventories are found in the North Atlantic and estimates for the total C_{ant} inventory in the global oceans in 1994 are 118 ± 19 Pg C, using the ocean tracer-based ΔC^* back-calculation method [*Sabine et al.*, 2004] and 146 Pg C, based on the transit time distribution (TTD) approach [*Waugh et al.*, 2006]. The net CO_2 emissions from 1750–1994 have been estimated to be 283 ± 19 Pg C [*Bindoff et al.*, 2007], thus the two estimates of C_{ant} in the ocean correspond to 42% and 52%, respectively.

[3] The Mediterranean Sea is a marginal sea that has a considerable influence on the circulation in the Atlantic Ocean [*Reid*, 1979; *O'Neil Baringer and Price*, 1997; *Serra and Ambar*, 2002] and which has been suggested to play a relevant role in the drawdown of anthropogenic carbon [*Álvarez et al.*, 2005; *Aït-Ameur and Goyet*, 2006]. It is a semi-enclosed basin connected only to the Atlantic Ocean via the Strait of Gibraltar. The Strait of Sicily, with a water depth of 300–400 m separates the eastern Mediterranean from the western Mediterranean and limits the water exchange between the two basins. The biogeochemistry of, particularly, its eastern basin is strongly influenced by the Black Sea as well as by rivers. The main circulation pattern in the Mediterranean Sea is as follows: Atlantic surface water flows from the Strait of Gibraltar eastward, becoming warmer and saltier. In the Levantine basin, the surface water becomes dense enough in winter to subduct and form the Levantine Intermediate Water (LIW). This returns westwards at depths between 200 and 500 m and leaves the Mediterranean Sea through the Strait of Gibraltar [*Ovchinnikov*, 1984]. In the western and the eastern basins deep water formation takes place in the Gulf of Lyon and the Adriatic Sea, respectively, when cold winds cool the high salinity surface waters [*Gascard*, 1978; *Pollak*, 1951]. The Western and Eastern Mediterranean Deep Waters (WMDW and EMDW) flow near the bottom into the two main basins where they slowly upwell and mix with overlying water. The deep water renewal time has been estimated to be 20–40 years in the western basin [*Stratford et al.*, 1998] and about 100 years in the eastern basin [*Roether et al.*, 1996; *Stratford and Williams*, 1997; *Stratford et al.*, 1998]. After 1989 a new deep water source in the Aegean Sea contributed to form the EMDW and probably increased the upwelling rate greatly [*Roether et al.*,

---

[1] Leibniz-Institut für Meereswissenschaften an der Universität Kiel (IFM-GEOMAR), Kiel, Germany.

Copyright 2010 by the American Geophysical Union.
0148-0227/10/2010JC006171

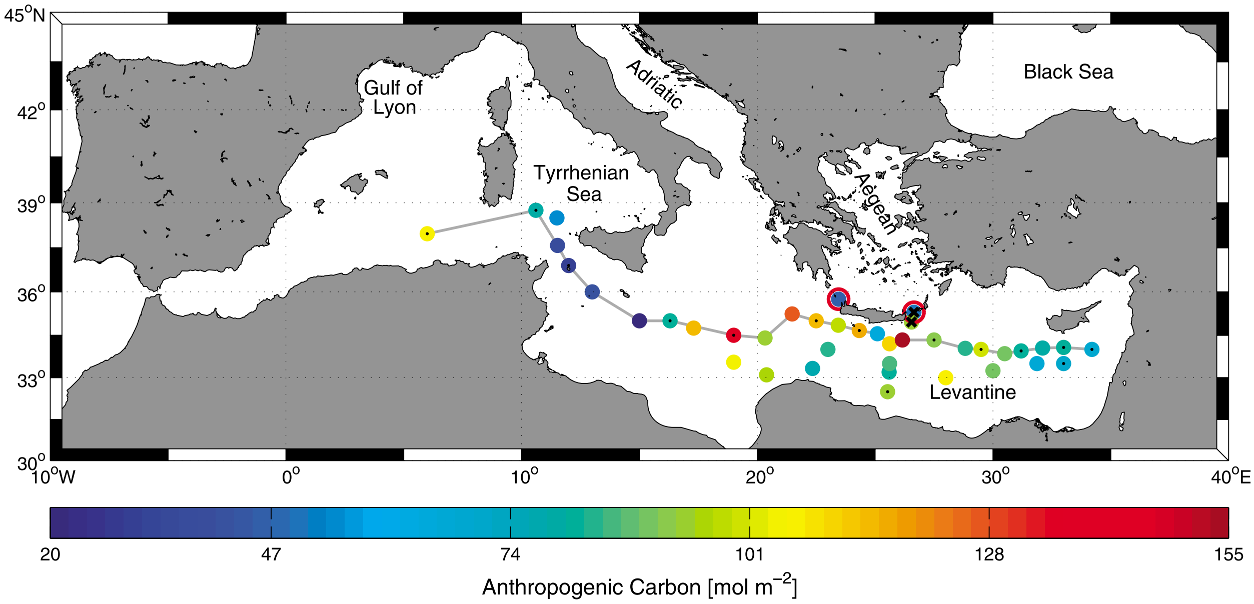

Figure 1. Station plot of the Meteor 51/2 cruise in October/November 2001. Colored dots are the integrated C_{ant} column inventories of all stations in mol m^{-2}. The gray line connects the stations used to create the section plots in Figure 2. The red encircled dots indicate the two stations on the Aegean shelf, which were used to calculate the C_{ant} inventory for the Aegean and the Adriatic Seas. Stations 533 and 534, highlighted with black crosses, are the two stations compared in Figure 3. All stations, where C_T and A_T were measured, are indicated with black dots.

1996]. *Stratford et al.* [1998] suspected a renewal timescale of 30–40 years for recent decades.

[4] Relatively little effort has been made to quantify the C_{ant} content of marginal seas and coastal areas, perhaps because the area of these regions has been considered to be insignificant in terms of C_{ant} uptake compared to the global oceans. In both of the previously mentioned estimates of the global C_{ant} inventory neither data from the Arctic Ocean nor from marginal seas were used. Therefore, in order to obtain a global inventory, an estimate of 12 Pg C for all such regions combined was added by the authors. Since then, the C_{ant} inventory of the Arctic Ocean has been estimated to be 2.1–2.8 Pg C (for the year 1994) by *Tanhua et al.* [2009] which is about 50% less than that estimated by *Sabine et al.* [2004]. Data to assess C_{ant} inventories in marginal seas remain scarce. Until recently there has also been relatively little attention paid to the Mediterranean Sea in terms of its carbon chemistry and, especially in the eastern basin, few reliable data are available. Here we present measurements of C_T and dichlorodifluoromethane (CFC-12), which allow us to estimate the C_{ant} concentrations and inventories and so refine the estimate of the global inventory.

2. Methods

2.1. Water Samples

[5] Between 18 October and 11 November 2001 cruise M51/2 of the R/V Meteor crossed the Mediterranean Sea from west to east. Measurements of salinity, temperature, and oxygen were made at 42 stations along the cruise track. Tracer observations included CFC-11, CFC-12, CFC-113 (SIO 1998 scale), helium isotopes, and tritium at 40 stations. Water for the CFC analysis was sampled first from the 10-L Niskin bottles to prevent contamination by air and was analyzed directly on board using a gas chromatographic technique described by *Bulsiewicz et al.* [1998]. Data are available from the database CDIAC (http://cdiac.ornl.gov). Here only the CFC-12 depth profiles are examined. The error for the CFC-12 measurements is ±2% or ±0.02 pmol kg^{-1}, whichever is greater. In the following, the CFC-12 data are expressed as "equivalent mixing ratios," which are more descriptive in comparison with temporally varying atmospheric mixing ratios. The equivalent mixing ratio of CFC-12 (in ppt) is obtained by:

$$\text{Equivalent mixing ratio} = \frac{c}{F(T,S) \times [P_{\text{atm}} - P_{\text{H}_2\text{O}}(T,S)]},$$

where c is the CFC-12 concentration in pmol kg^{-1}, $F(T, S)$ is the temperature- and salinity-dependent solubility function in mol kg^{-1} atm^{-1} [*Warner and Weiss*, 1985], P_{atm} is the mean atmospheric pressure in atm, and $P_{H_2O}(T, S)$ is the temperature- and salinity-dependent partial pressure of water vapor [*Weiss and Price*, 1980].

[6] Measurements of total alkalinity (A_T) and C_T were made at 14 stations (Figure 1). Results from alkalinity measurements have been presented by *Schneider et al.* [2007]. Accuracy assessment based on measurements of Certified Reference Material [CRM, supplied by Andrew Dickson, Scripps Institution of Oceanography (SIO), La Jolla, CA, USA] yielded a mean offset of -0.82 ± 2.85 μmol kg^{-1} for A_T and in $+0.62 \pm 1.01$ μmol kg^{-1} for C_T (95% confidence interval, $n = 41$). Both parameters have been corrected for this mean offset. Precision of the A_T and C_T measurements was 4.2 and 1.5 μmol kg^{-1}, respectively (95% confidence

interval), as determined from duplicate samples (n = 15 and n = 14).

2.2. Transit Time Distribution

[7] In order to estimate anthropogenic CO$_2$ concentrations, the transit time distribution (TTD) method was applied using the transient tracer CFC-12. The TTD method is based on the idea that each water parcel is composed of different source waters with varying time histories. Each water sample has an age- or transit time distribution. For historical surface water concentrations of CFC-12 the atmospheric time history of *Walker et al.* [2000] was used together with a time-dependent saturation estimated by *Tanhua et al.* [2008]. The latter allows for nonequilibrium surface water concentrations by assuming that the near-surface saturation of CFC-12 was 86% before the year 1989, when the atmospheric growth rate exceeded 15 ppt yr^{-1}, and that it has increased since then, in inverse proportion to its atmospheric growth rate. Since 1999 the saturation is supposed to be 100%. The interior concentration $c(r, t)$ of the tracer at location r and time t is then given by [*Hall and Plumb*, 1994]:

$$c(r,t) = \int_0^\infty c_0(t-t')G(r,t')dt',$$

where t' is the integration variable, representing all the apparent ages in the water parcel (from 0 to ∞ years). $G(r, t')$ is the TTD at location r, giving the appropriate fraction for each water age t' and c_0 $(t - t')$ is the surface water tracer concentration in the year $t - t'$ to be multiplied with this fraction. For steady transport the TTD at each interior location can be approximated by an inverse Gaussian function [*Waugh et al.*, 2004], that is:

$$G(t') = \sqrt{\frac{\Gamma^3}{4\pi\Delta^2 t'^3}} \times \exp\left[\frac{-\Gamma(t'-\Gamma)^2}{4\Delta^2 t'}\right],$$

where Γ is the mean transit time ("mean age") and Δ defines the width of the TTD. The Δ/Γ ratio is a measure for mixing. The larger the ratio the stronger the mixing. Here $\Delta/\Gamma = 1$ is assumed, which has been shown to be reasonable for ocean interior waters [*Waugh et al.*, 2004] but has not yet been tested for its applicability to the Mediterranean Sea. Given an interior CFC-12 concentration (or age) and the above approximations, the mean age of the water sample can be constrained. Further, with the help of the atmospheric history of anthropogenic CO$_2$ and an alkalinity-salinity (A_T-S) correlation for this specific area [$A_T = 73.7(\pm 3.0) \times S - 285.7 (\pm 114.9)$ μmol kg^{-1}] [*Schneider et al.*, 2007] the anthropogenic carbon concentration was determined as follows:

$$C_{\mathrm{ant}}(t) = \int_0^\infty C_{\mathrm{ant},0}(t-t')G(t')dt',$$

where t is the sampling year. The local variable r can be left out because for each discrete water sample a new TTD is determined.

3. Results

[8] The main focus of this work lies on the eastern basin as only a few stations were sampled in other regions of the Mediterranean Sea. These few data may not be fully representative for the whole basin but all available data have been used in the interpretation, in order to obtain a first estimate of the anthropogenic CO$_2$ inventory of the Mediterranean Sea. A detailed error analysis, including consideration of uncertainties associated with incomplete sample coverage, is provided in section 4.

3.1. Carbon and Tracers

[9] The Mediterranean Sea is known as a basin where remineralization and evaporation dominate. The lowest C_T concentration (2150 μmol kg^{-1}) is found in the upper 100 m with the inflowing Atlantic water and increases toward the east in part due to evaporation (Figure 2). With increasing depth, addition of respiratory CO$_2$ also leads to high C_T concentrations. Below 500 m, in the eastern basin C_T stays rather constant at about 2305 μmol kg^{-1}. In the deep western basin concentrations are slightly higher (up to 2330 μmol kg^{-1}). Estimates found in the literature for the C_T concentration in the inflowing Atlantic water through the Strait of Gibraltar are about 2100 μmol kg^{-1} and for the outflowing Mediterranean water 2300 μmol kg^{-1} [*Copin-Montégut*, 1993; *Santana-Casiano et al.*, 2002; *Aït-Ameur and Goyet*, 2006]. The C_T data presented here are consistent with these values.

[10] Waters in the Mediterranean Sea circulate relatively fast. Residence times in the entire basin have been estimated from a water balance to be ~150 yr (using data of the water volume of the Mediterranean Sea [*Menard and Smith*, 1966] and water inputs from the Atlantic Ocean [*Bryden et al.*, 1994], the Black Sea [*Besiktepe et al.*, 1994], rivers [*Tixeront*, 1969], and precipitation [*Tixeront*, 1969]). It is therefore not surprising that the entire water column in the Mediterranean Sea is found to contain detectable levels of the anthropogenic tracer CFC-12 (Figure 2). CFC-12 in the atmosphere has increased from 0 ppt in the 1930s to a maximum of almost 550 ppt in 2001. Since then concentrations have slowly decreased. With no, or little, atmospheric CFC-12 change per year, the near-surface water and the atmosphere are expected to be close to equilibrium and similar mixing ratios should be found in both phases. Accordingly, the presented CFC-12 data in the surface water from the year 2001 show contemporary high levels of more than 500 ppt, decreasing rapidly with depth to around 200 ppt at 500 m. The lowest concentrations are found between 800 and 1500 m with a value of 71 ppt in the easternmost part of the basin. Below 1500 m the CFC-12 mixing ratios increase again up to 220 ppt near the bottom. This reflects the rapid deep water formation in the marginal seas, which entrains surface water to the deep basins.

[11] The mean ages show the same main features as the tracer concentrations (Figure 2) reflecting the direct dependency of the two parameters. The westward flow of the LIW at 150–400 m, with a renewal timescale of 10–20 yr (determined using a series of tracer experiments based on an eddy-permitting general circulation model of the Mediterranean [*Stratford and Williams*, 1997]), cannot be resolved with these data. In contrast, one can clearly see water at depth with mean ages of 50–60 yr and an old layer between the very young near-surface water and the deep water. The separation of the eastern and the western basins of the Mediterranean Sea at the Strait of Sicily, causes the EMDW

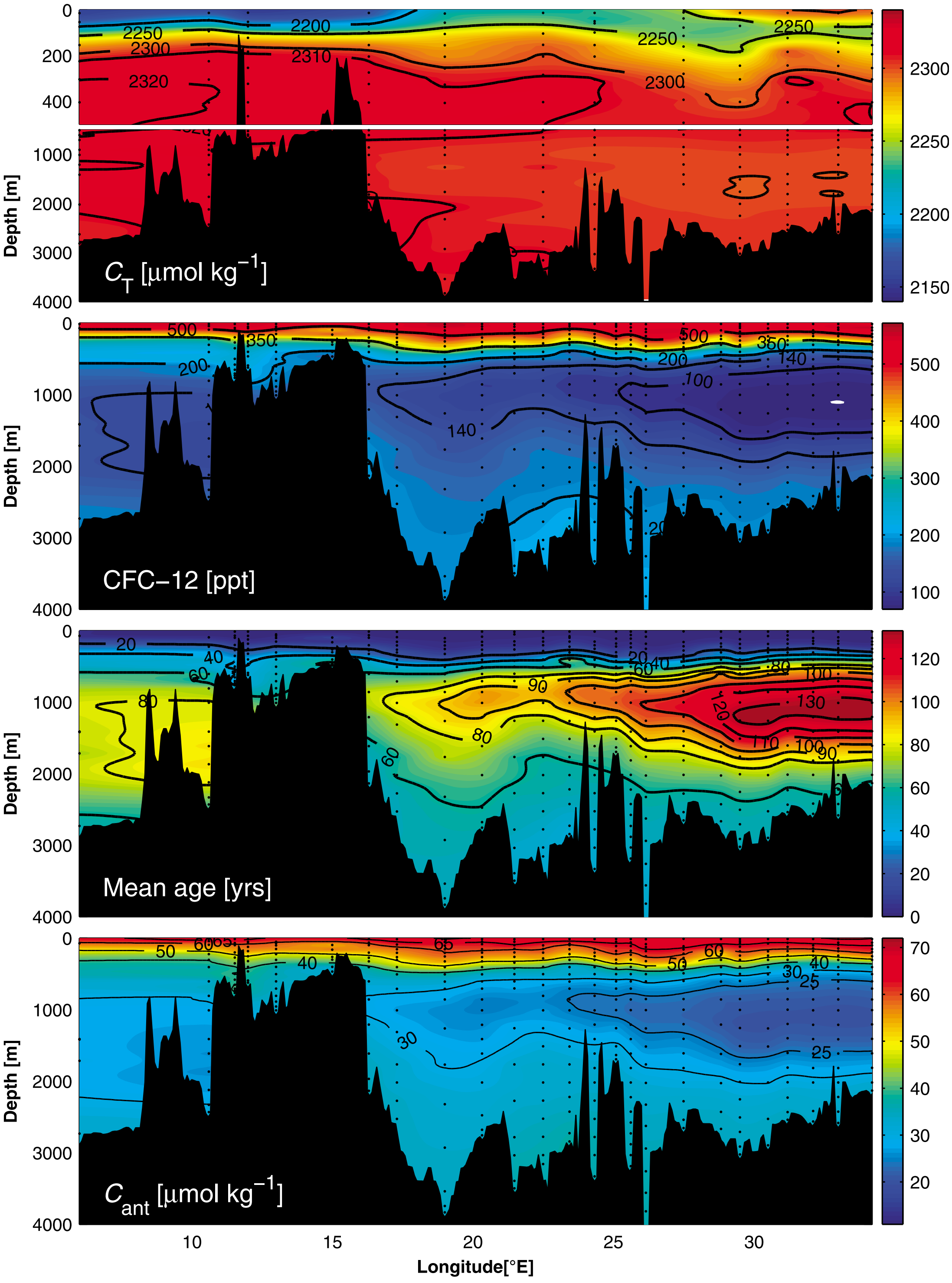

Figure 2. Section plots of the four parameters C_T, CFC-12, mean age, and C_{ant}. The stations used for the section are shown in Figure 1.

to be retained in the eastern basin, where it slowly upwells with a speed of ~35 m yr^{-1} [*Steinfeldt*, 2004] and hence a region of relatively old water with mean ages of more than 130 years can be found around 1200 m.

[12] According to the tracer concentration and the mean age, anthropogenic CO$_2$ has penetrated the entire water column. The upper 500 m are very high in C_{ant} with a maximum concentrations of 70 μmol kg^{-1} (error range: 67–73 μmol kg^{-1}), the EMDW contains ~34 μmol kg^{-1} (error range: 29–39 μmol kg^{-1}) and throughout the basin concentrations always exceed 20 μmol kg^{-1}, even in the easternmost part with the oldest water (Figure 2). Other studies

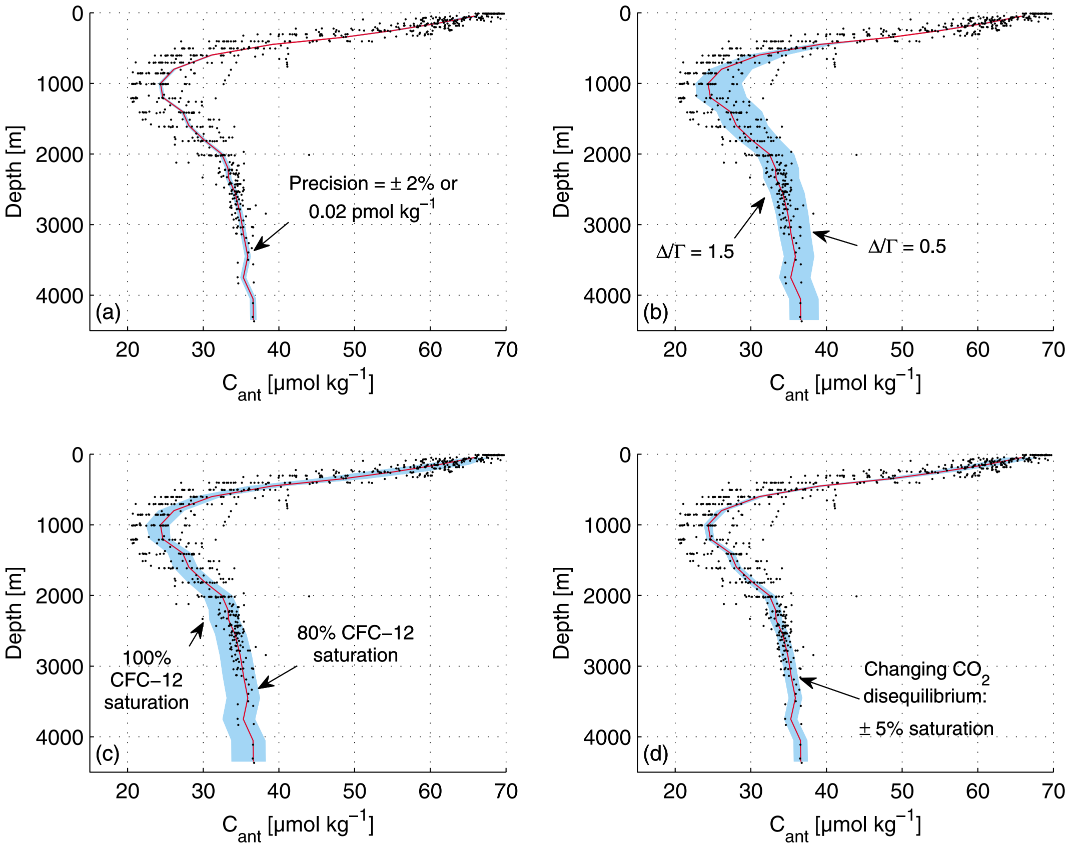

Figure 3. All estimated C_{ant} concentrations (black dots) together with the mean C_{ant} depth profile (red line). Additionally, the error ranges resulting from the maximum and minimum values of several assumptions are plotted (blue shading): (a) uncertainty resulting from analytical precision of ±2% or ±0.02 pmol kg^{-1}, whichever is greater; (b) uncertainty resulting from the maximum and minimum Δ/Γ ratios of 1.5 and 0.5; (c) uncertainty due to the CFC-12 surface water saturation limits of 100% and 80%; (d) uncertainty resulting from a changing CO_2 disequilibrium starting with 100% in the year 1900, linearly decreasing and increasing, respectively, by 5% until the year 2000.

of the global oceans show such high concentrations being restricted to depths <2000 m [*Sabine et al.*, 2004; *Touratier et al.*, 2005, 2007; *Tanhua et al.*, 2008]. Consequently, the Mediterranean Sea water column stores large amounts of anthropogenic CO_2, which can be explained by its high potential to take up C_{ant} coupled with fast deep water formation in autumn and winter. This is discussed further in section 5.1. Recently published C_{ant} estimates, using the TrOCA method in the Mediterranean Sea show much higher concentrations in the surface water of up to 135 μmol kg^{-1} [*Rivaro et al.*, 2010]. This implies a pCO_2 increase of about 200 ppm since preindustrial times, which seems impossible. Also in deeper layers C_{ant} concentrations from *Rivaro et al.* [2010] tend to be higher than our estimates, but increased C_{ant} concentrations in the relatively young WMDW and the EMDW are not seen.

3.2. Anthropogenic CO_2 Inventories

[13] Anthropogenic CO_2 concentrations were integrated vertically over 50 m layers and linearly interpolated between layers where measurements were missing. The resulting column inventories of C_{ant} (Figure 1) are high relative to those estimated for the remainder of the World Ocean. For example the maximum observed column inventory was 154 mol m^{-2} (error range: 132–179 mol m^{-2}) (integrated over a depth of 4300 m), which is considerably higher than the maximum column inventories of 90 mol m^{-2} (integrated over ~5000 m) estimated with the TTD method from the GLODAP v1.1 data set in the North Atlantic [*Waugh et al.*, 2006]. However, the mean sampling year for the GLODAP data set is 1994, so the time difference to the data presented here is 7 yr. Assuming linear propagation of C_{ant} over time into the water column, the percentage C_{ant} increase in the atmosphere over this time period can be subtracted from the C_{ant} estimates in the water, resulting in time-corrected column inventories for the Mediterranean Sea for the year 1994. The maximum Mediterranean inventory of C_{ant} would have been 133 mol m^{-2} (error range: 114–154 mol m^{-2}) in the year 1994, which remains ~45% higher than the maximum column inventories estimated by *Waugh et al.* [2006] for the global ocean.

[14] In the open ocean, anthropogenic CO_2 concentrations decrease rapidly with depth so that only the upper ocean contributes to the C_{ant} column inventory (nearly 50% of the column inventory is contained within the upper 400 m of the water column [*Sabine et al.*, 2004; *Waugh et al.*, 2006]). In

Table 1. Water Volume, Mean Depth, Anthropogenic CO_2 Inventory and Mass/Volume Ratio of the Eastern Basin and the Entire Mediterranean Sea in the Year 2001 and Adjusted to the Year 1994 for Comparison With the World Ocean in the Year 1994 [*Waugh et al.*, 2006]

	Volume (10^6 km^3)	Mean Depth (m)	C_{ant} (Error Range) (Pg C)	C_{ant}/Volume (Pg C/10^6 km^3)
Eastern Basin	2.22	1680	1.0 (0.7–1.2)	0.44
Mediterranean Sea	3.75	1500	1.7 (1.3–2.1)	0.46
Mediterranean Sea^{1994}	3.75	1500	1.5 (1.1–1.8)	0.4
Atlantic/Indic/Pacific^{1994}	1332.5	4000	134 (94–121)	0.1

contrast, Mediterranean C_{ant} profiles are characterized by a thick layer of minimum C_{ant} concentrations between 500 and 2000 m with elevated concentrations both above and below, so deep and bottom water also contributes significantly to column inventories. See, for example, the mean C_{ant} depth profile shown in Figure 3.

[15] Based on our data, we have estimated the anthropogenic CO_2 inventory of the entire Mediterranean Sea with the corresponding uncertainty, although we note that only a few stations were occupied outside the eastern basin. The C_{ant} concentrations were averaged over 50 m layers and multiplied by the layer volume, which was calculated from a 5 min Terrain Base bathymetry (2-Minute Gridded Global Relief Data (ETOPO2v2), June 2006). Adding up these layer inventories then gave the total inventory. Our data suggest that the Adriatic Sea and the Aegean Sea have differing C_{ant} profile characteristics, likely related to the direct influence of the deep water formation and the shallow depths. This is discussed further in section 4 and section 5.1. Therefore the C_{ant} inventory for these two basins were determined separately using two stations in the southern Aegean Sea, assuming that these stations reflect the properties of the two basins better than the midbasin profiles. As a result we obtain a total inventory of 1.7 Pg (error range: 1.3–2.1 Pg) of anthropogenic carbon for the Mediterranean Sea in the year 2001 (Table 1). The inventory for the eastern basin only is 1.0 Pg (error range: 0.7–1.2 Pg) of anthropogenic carbon. *Waugh et al.* [2006] estimated a total anthropogenic carbon inventory for the Atlantic, Pacific, and Indian Ocean of 134 Pg C in 1994. Hence, compared to the World Ocean, the Mediterranean Sea only contains 0.3% of the water volume but 1.1% of the C_{ant} (after adjustment of the Mediterranean inventory to the year 1994). The relative fraction (mass/volume) in the Mediterranean Sea is therefore remarkably high compared to the global mean.

3.3. Inorganic Carbon Exchange Through the Strait of Gibraltar

[16] The C_T and the C_{ant} fluxes through the Strait of Gibraltar were estimated on assumption of a two-layer system of inflowing Atlantic surface water and outflowing LIW in the Strait. These fluxes should, however, be viewed with caution, as they do not arise from direct measurements within the Strait and because they are explicitly dependent on the water mass exchange.

[17] We assume that the 100 m depth horizon in the Strait of Gibraltar corresponds to the border between the inflow and the outflow [*Lafuente et al.*, 2002]. For the flux calculations, mean C_T and C_{ant} concentrations in the respective water masses from our three westernmost stations were used (without those located in the Tyrrhenian Sea). Only the C_T concentrations of the inflowing Atlantic surface water were taken from data collected west of Gibraltar [*Aït-Ameur and Goyet*, 2006]. The water volume transports and the respective C_T and C_{ant} fluxes are summarized in Table 2. We estimate a net flux of 38 Tg C yr^{-1} (error range: 30–47 Tg C yr^{-1}) into the Atlantic Ocean, which agrees with previously estimated fluxes [*Dafner et al.*, 2001; *Aït-Ameur and Goyet*, 2006; *de la Paz et al.*, 2008; *Huertas et al.*, 2009]. However, the net flux of anthropogenic CO_2 is in the opposite direction, 3.5 Tg C yr^{-1} (error range: −1.8–9.2 Tg C yr^{-1}), into the Mediterranean Sea and matches a recently published estimate, based on the ΔC^* method (4.2 Tg C yr^{-1} [*Huertas et al.*, 2009]). As noted earlier, C_{ant} concentrations estimated with the TrOCA method [*Touratier and Goyet*, 2004] were much higher at depth. *Aït-Ameur and Goyet* [2006] assessed the total C_{ant} flux entering the Atlantic at intermediate depths through the Strait of Gibraltar with the TrOCA method and their result is one order of magnitude higher than the estimates based on the TTD and ΔC^* methods. As a result, the *Aït-Ameur and Goyet* [2006] estimate gave a net flux of C_{ant} out of the Mediterranean Sea. This seems implausible, because as long as atmospheric CO_2 concentrations increase, the inflowing surface waters from the Atlantic should always have higher C_{ant} concentrations than deeper outflowing waters, which have not been in contact with the atmosphere for several years. Therefore it appears that the TrOCA method is not well suited for C_{ant} estimation in the Mediterranean Sea.

[18] In order to assess how much anthropogenic CO_2 has been taken up within the Mediterranean basin via air-sea exchange, we estimated the total C_{ant} flux into the Mediterranean Sea through the Strait of Gibraltar since preindustrial times and compared this to our estimate of the total C_{ant} inventory. We assumed a linear relationship between the C_{ant} increase in the atmosphere and the C_{ant} uptake by the Mediterranean Sea. This in turn results in a linear relationship between the C_{ant} increase in the atmosphere and the increase of the net C_{ant} transport through the Strait of Gibraltar (assuming steady state). The historical atmosphere CO_2 mixing ratios were taken from the Law Dome and the

Table 2. Carbon Fluxes Through the Strait of Gibraltar[a]

	Water Volume (Sv)	C_T (Error Range) (Tg C yr^{-1})	C_{ant} (Error Range) (Tg C yr^{-1})
Atlantic inflow	+0.89[b]	+722[c] (721–723)	+21.6[d] (19.3–24.3)
Mediterranean outflow	−0.85[b]	−761[e] (753–768)	−18.1[f] (15.1–21.2)
Net flux	+0.04	−38 (30–47)	+3.5 (−1.8–9.2)

[a] Positive values denote Fluxes into the Mediterranean Sea.

[b] *Huertas et al.* [2009].

[c] Averaged C_T concentrations in the upper 100 m west of Gibraltar from *Aït-Ameur and Goyet* [2006].

[d] Averaged C_{ant} concentrations in the upper 100 m of the three most western stations from this work.

[e] C_T concentrations of the three most western stations from this work, averaged between depths of 100 and 300 m.

[f] C_{ant} concentrations of the three most western stations from this work, averaged between depths of 100 and 300 m.

Mauna Loa data sets. From 1850 to 2001 a total anthropogenic input of 157 Tg C (error range: −85–415 Tg C) through the Strait of Gibraltar was determined. This accounts for almost 10% of the total C_{ant} inventory of the Mediterranean Sea, which means that ~90% must have been taken up directly from the atmosphere within the basin. This percentage seems reasonable, taking into account that the mean residence time of the water in the Mediterranean Sea is about 150 years. *Huertas et al.* [2009] estimated a contemporary uptake of anthropogenic CO_2 from the atmosphere of 25 ± 3.4 Tg C yr^{-1} in the Mediterranean Sea. Again, we assumed a linear relationship between the C_{ant} increase in the atmosphere and the increase in the uptake from the atmosphere by the ocean. With the estimate of 25 Tg C yr^{-1} [*Huertas et al.*, 2009], the total C_{ant} uptake from the atmosphere since 1850 then sums up to 1 ± 0.1 Pg C, which is around 60% of our total C_{ant} inventory estimate of the Mediterranean Sea. Considering the different methods, assumptions, and uncertainties, the results appear to be internally consistent.

4. Error Estimation

[19] In addition to the analytical error of ±2% or ±0.02 pmol kg^{-1} in the CFC-12 measurements, the assumptions made for the subsequent calculations of C_{ant} concentrations, inventories, and fluxes lead to further uncertainties in the results which we consider to be systematic errors. To provide an estimate for these uncertainties, all calculations were rerun as follows with realistic maximum and minimum values for each of the assumptions used: (1) a time-dependent CFC-12 saturation in surface waters that implies undersaturation during the period of exponential CFC-12 increase in the atmosphere (starting with 86%) and 100% saturation since 1999, (2) a Δ/Γ ratio of 1 in the TTD calculations, and (3) a constant air-sea pCO_2 disequilibrium over time for the TTD approach.

[20] For the error estimation the maximum saturation of CFC-12 in surface waters was assumed to be 100% and the minimum saturation 80%. Maximum and minimum Δ/Γ ratios in the TTD calculations were set to 1.5 and 0.5, respectively. We used the simplest assumption for the air-sea pCO_2 disequilibrium over time and assumed that natural sources and sinks of CO_2 have remained constant. Increasing CO_2 concentrations in the atmosphere then only shift them to a higher level by the additional anthropogenic pCO_2 uptake. However, changes in temperature, biology, and biogeochemistry can lead to enhancement or weakening of the natural background sources and sinks. For instance, *Louanchi et al.* [2009] modelled the transformation of the Mediterranean Sea from a net source of 0.62 Tg C yr^{-1} in the 1960 s to a net sink of −1.98 Tg C yr^{-1} in the 1990s. As these changes are hard to predict and are mostly unknown, we do not account for them in detail in our error estimation. The three time-series stations European Station for Time-series in the Ocean, Hawaii Ocean Time-Series, and Bermuda Atlantic Time-series Study, all located in the northern subtropics, show a pCO_2 increases indistinguishable from the atmospheric pCO_2 increase [*Bindoff et al.*, 2007]. Following this assumes that in general the C_{ant} uptake by the Mediterranean Sea has tracked the CO_2 increase in the atmosphere and we apply a ±5% change over time in the CO_2 disequilibrium for our error estimation. We assume a linear variation of anthropogenic CO_2 saturation starting with 100% in the year 1900 down to 95% and up to 110% in the year 2000, respectively.

[21] To compare the effect of these uncertainties, each is plotted with the mean midbasin C_{ant} depth profile (Figure 3). Figure 4a shows the minimum and maximum errors of the column inventories, which result from the combined uncertainties. In Figure 4b we see the mean C_{ant} profile with the standard deviation, which comprises the regional differences and the analytical error. Most regional variation occurs at depths between ~600 and 1200 m. The crosses in Figure 4b are data from the two stations on the southern Aegean shelf with a maximum depth of about 1000 m (Figure 1) and the circled dots are C_{ant} concentrations from stations in the shallow area around the Strait of Sicily. This leads us to assume that shallow regions in the Mediterranean Sea, in general, show more variability in terms of anthropogenic CO_2. Together with the systematic errors we can calculate a total error (Figure 4b). To account for the mapping error in our total C_{ant} inventory estimate and in the flux calculations through the Strait of Gibraltar we use the basin-wide standard deviation together with the systematic errors and propagate the resulting total error (Figure 4b) with all inventory and flux calculations.

5. Discussion

5.1. Anthropogenic CO_2 in the Mediterranean Basin

[22] The fast overturning circulation in the Mediterranean Sea has led to an overall invasion of the anthropogenic tracer CFC-12 as well as anthropogenic CO_2 in the basin. Our results show that the Mediterranean Sea has taken up a large amount of C_{ant} on both a per-volume and a per-area basis, compared to estimates of the global oceans. Surface pCO_2 has been calculated from our A_T and C_T measurements and shows values of 400 ppm and higher throughout the basin, suggesting a net CO_2 flux to the atmosphere. Underway pCO_2 measurements in June 2005 (personal communication, Tobias Steinhoff) were consistent with this high surface pCO_2. With increasing atmospheric CO_2 concentrations as a result of human activity, the sea-to-air flux decreases, so a net uptake of C_{ant} takes place. The reason why the per-area-uptake is higher than in other oceanic regions seems to be due to the fast deep water formation processes in the Mediterranean Sea combined with surface water having a relatively low Revelle factor. A low Revelle factor implies that, for a given change in atmospheric CO_2, the anthropogenic CO_2 concentration in equilibrated surface water will be higher than in waters with a high Revelle factor. Due to the strong temperature dependency of the Revelle factor, lowest values between 8 and 9 are found in the tropics [*Sabine et al.*, 2004], whereas in Antarctic waters, values are as high as 15 and in the North Atlantic about 13. In addition high alkalinity has a lowering effect on the Revelle factor. Hence, Mediterranean water has a Revelle factor between 9 and 10 and therewith a relatively high uptake capacity for C_{ant}.

[23] No samples were collected within the areas of deep water formation, neither in the western nor in the eastern basins. However, the two stations located in the southern part of the Aegean Sea (Figure 1) clearly differ from all

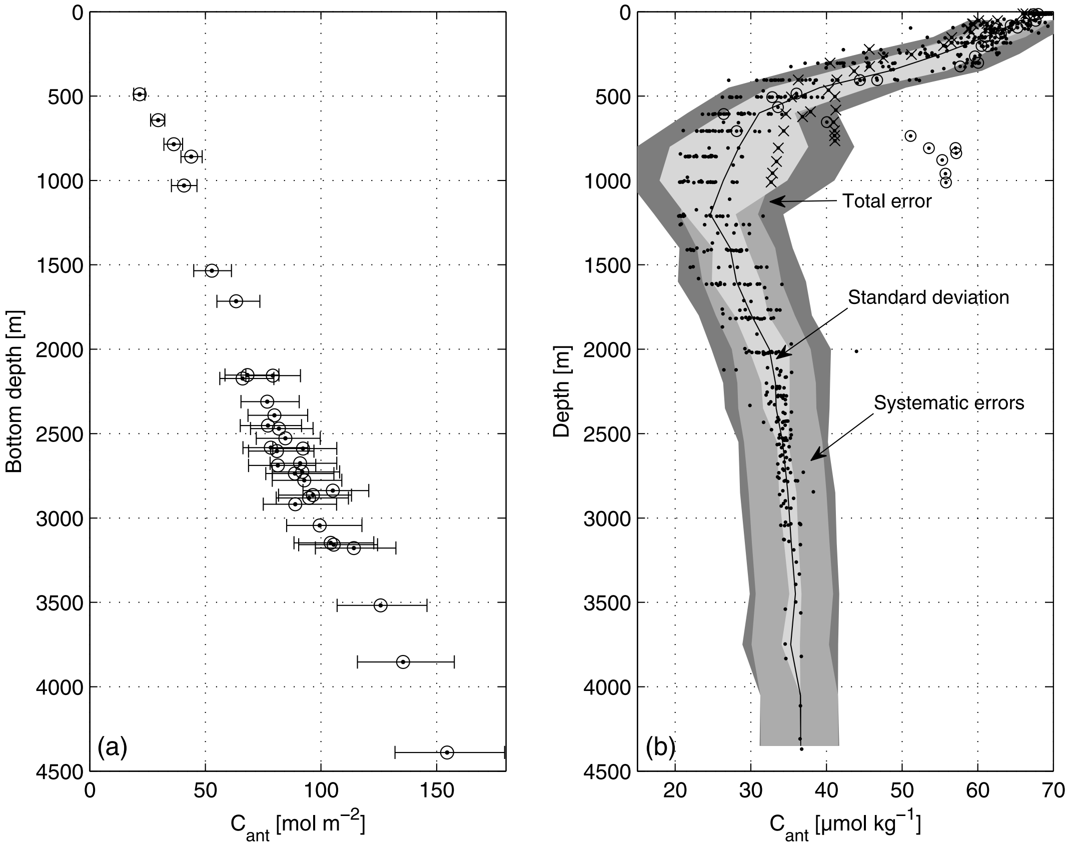

Figure 4. (a) The column inventories in mol m^{-2} with estimated error limits plotted versus the bottom depth. (b) All estimated C_{ant} concentrations and the mean C_{ant} depth profile are plotted together with its standard deviation, which includes the analytical error and the spatial variations (light gray shading), the systematic errors (gray shading), and the resulting total error (dark gray shading). The crosses are data from two stations on the southern Aegean shelf with a maximum depth of about 1000 m (Figure 1), and the encircled dots are C_{ant} concentrations from stations in the shallow area around the Strait of Sicily. The basinwide standard deviation plus the systematic errors were used to calculate the error bounds of the C_{ant} inventory in the Mediterranean Sea and of the fluxes through the Strait of Gibraltar.

other stations and may reflect the properties of that basin. Assuming that these stations are representative for both the Aegean and the Adriatic, we used them to calculate a C_{ant} inventory for these marginal seas. The resulting C_{ant} per volume ratio of 0.63 Pg C/10^6 km^3 is high compared to the remainder of the Mediterranean Sea (0.46 Pg C/10^6 km^3) and to the World Ocean (0.1 Pg C/10^6 km^3), suggesting that these areas might play a major role for the uptake of C_{ant}. In Figure 5, station 534 (Aegean Shelf station) is compared to the closely located station 533 (deep basin station) illustrating the differences in terms of C_{ant} and mean age. Our hypothesis is that in the Aegean and the Adriatic Seas waters with high uptake capacity, which are preconditioned for deep water formation, quickly cool in winter and transfer anthropogenic CO$_2$ into the deep basin. This scenario could also hold for the Gulf of Lyon.

[24] The C_{ant} estimate for the Aegean and the Adriatic Seas has major uncertainties, both because of the lack of data and by reason of the change in the deep water formation rate in the eastern Mediterranean Sea in the late 1980 s. The so-called Eastern Mediterranean Transient, identified by *Roether et al.* [1996], describes the transition from a

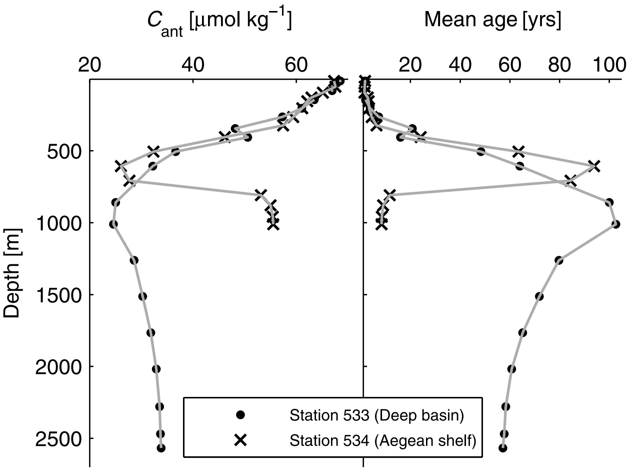

Figure 5. Comparison of the vertical profiles of C_{ant} and mean age at two closely located stations. At station 533 the water depth is more than 2500 m, whereas station 534 is located on the shallower Aegean shelf.

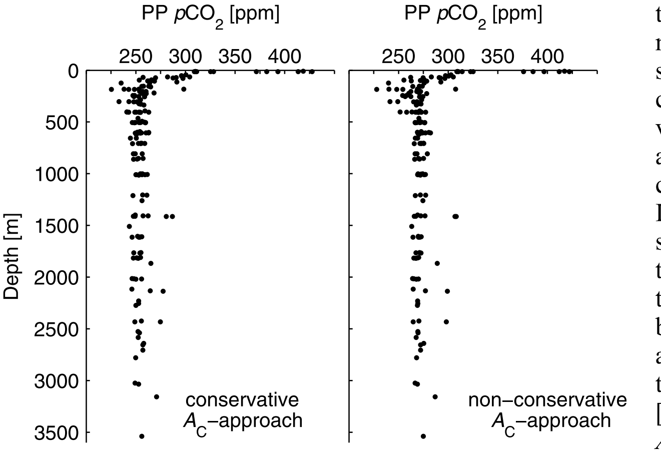

Figure 6. Scatterplot of the preformed preindustrial pCO_2 estimates, determined with (left) the conservative A_C approach and (right) the nonconservative A_C approach.

system with a single source of deep water in the Adriatic to one with an additional source in the Aegean Sea. This additional source only contributes to the deep water formation since about 1990 but with a threefold higher production rate [*Roether et al.*, 1996]. Further studies in 1997 and 1999 [*Theocharis et al.*, 2002] showed that thermohaline deep water formation was still changing at that time and that the eastern Mediterranean Sea was therefore in a transient state. A problem related to this is, that steady state is assumed for the TTD calculations and this assumption must be considered to be of doubtful validity in the year 2001. Thus, future measurements with a second tracer are advised to reduce this uncertainty.

5.2. Preformed Preindustrial pCO_2

[25] There are several methods to estimate the C_{ant} concentration of ocean waters and they are all based on assumptions and have associated uncertainties. In order to cross-check the C_{ant} estimates presented here, obtained with the TTD method, a back-calculation technique was also applied to the carbon and carbon-related data taken during the cruise (C_T, A_T, oxygen, nutrients). For all stations, where C_T had been measured, the preformed preindustrial (PP) pCO_2 was determined. "Preformed" refers to the properties of a water mass at the time when it was last in contact with the atmosphere. Back-calculation approaches attempt to correct properties for all changes that have occurred since the time that a water parcel lost contact with the sea surface. If anthropogenic effects (e.g., elevated atmospheric pCO_2) have influenced the properties, additional correction for these changes result in the "preformed preindustrial" conditions. Accordingly, for each water sample of our profiled stations, the PP pCO_2 is an estimate for the partial pressure of CO_2 the same water mass would have had when it was last at the ocean surface before the period of significant anthropogenic influence.

[26] Two approaches were followed to calculate the PP pCO_2. First, C_T was simply corrected for respiration using the apparent oxygen utilization (AOU) and a C:$-O_2$ Redfield ratio of 0.76 [*Körtzinger et al.*, 2001]. It was assumed that the carbonate alkalinity A_C is conservative, that is, there is no carbonate dissolution, because Mediterranean waters are supersaturated throughout the water column with respect to calcite and aragonite [*Schneider et al.*, 2007] (the "conservative A_C approach"). Second, variation of A_C was allowed and C_T was corrected for respiration and for changes due to carbonate dissolution (the "nonconservative A_C approach"). In both approaches the TTD-based estimate of C_{ant} was subtracted, resulting in an estimate of PP C_T. To calculate the PP pCO_2 from PP C_T in the conservative A_C approach the measured alkalinity was corrected for NO_3^- release by biological remineralization. In the nonconservative A_C approach the salinity derived alkalinity was determined from the surface relationship $A_T = 73.7S - 285.7$ μmol kg^{-1} [*Schneider et al.*, 2007]. In both cases it was assumed that A_T has not changed from its preindustrial values. The PP pCO_2 was calculated with the software program CO2SYS [*Lewis and Wallace*, 1998] using the carbonic acid dissociation constants (K_1 and K_2) from *Mehrbach et al.* [1973] as refitted by *Dickson and Millero* [1987] and the dissociation constant for HSO_4^- from *Dickson* [1990]. In Figure 6 the PP pCO_2 of the two approaches is plotted versus depth. Both profiles do not show much variation with depth, indicating that, on the whole, the estimates for C_{ant} and respiration, which both have very different and varying depth profiles, are reliable.

[27] With the nonconservative A_C approach the PP pCO_2 is scattered around 270 ppm, implying that surface waters were almost in equilibrium with atmospheric CO_2 concentrations in the preindustrial period. Looking at the corresponding alkalinities in Figure 7, it becomes apparent that in this case there must be a significant alkalinity addition by carbonate dissolution, especially below 500 m. However, the calcite and aragonite saturation state of the Mediterranean Sea is high throughout the water column, hence carbonate dissolution seems unlikely. Furthermore, a gradual increase of alkalinity with depth would be expected but is not seen.

[28] The conservative A_C approach results in a lower PP pCO_2 around ~250 ppm, implying that surface waters, which feed the deep waters, were undersaturated with respect to CO_2 during the preindustrial period. If this approach were valid, the surface A_T-S correlation used in the nonconservative A_C approach would not apply to the waters that supply the deep waters, and an explanation for the low pCO_2 of ~250 ppm is needed. We note that in the eastern basin, the water below 500 m has its origin in the deep water formation areas of the Adriatic and, since the late 1980s, also of the Aegean Sea. An exchange with the western basin is inhibited by the shallow Strait of Sicily. Hence the preformed surface characteristics of this water body are set in the Adriatic and the Aegean Seas. Compared to surface waters in midbasin, from which the A_T-S relationship was determined, a steeper A_T-S correlation might be expected in these areas, because they are highly influenced by the inflow of rivers and the Black Sea, both carrying high alkalinities [*Schneider et al.*, 2007]. Using such a relationship to determine the preformed alkalinities would shift them closer to the values used in the conservative A_C approach. During deep water formation in autumn and winter, cold winds rapidly cool the high salinity surface waters in the marginal seas and cause pCO_2 to decrease. This very dense water probably

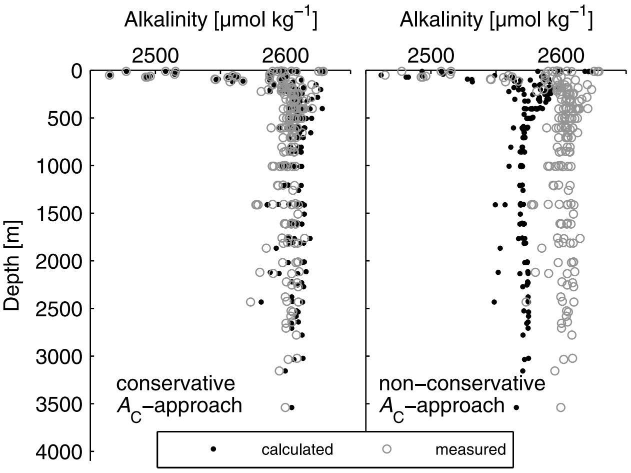

Figure 7. Depth profiles of measured total alkalinity (gray circles) and calculated preformed alkalinity (black dots). (left) The preformed alkalinity was determined from the measured alkalinity by correction for NO_3^- release by biological remineralization, like in the conservative A_C approach. (right) The salinity derived alkalinity, determined from the surface A_T-S relationship, like in the nonconservative A_C approach.

sinks before equilibrium with the atmosphere is reached and a PP $p\mathrm{CO}_2$ of less than 280 ppm could be expected. $p\mathrm{CO}_2$ measurements in the Aegean Sea in February 2006 support this, since the surface waters were undersaturated relative to the contemporary atmosphere [*Krasakopoulou et al.*, 2009]. For these reasons, the conservative A_C approach is favored over the the nonconservative A_C approach and the resulting estimates of preindustrial preformed $p\mathrm{CO}_2$ appear to be reasonable, which in turn suggests that our TTD-based estimates of C_{ant} are accurate.

6. Conclusions

[29] The results presented here show that substantial anthropogenic carbon is present throughout the water column over the entire Mediterranean Sea. The column inventories with a maximum of 154 mol m^{-2} (error range: 132–179 mol m^{-2}) are high compared to those in other areas of the World Ocean. The total inventory of 1.7 Pg of anthropogenic carbon has an error range of at least 1.3–2.1 Pg C. We estimate that there is a net flux of anthropogenic carbon through the Strait of Gibraltar into the Mediterranean Sea of 3.5 Tg C yr^{-1} (error range: −1.8–9.2 Tg C yr^{-1}) but that about 90% of the total C_{ant} inventory in the basin has been taken up directly from the atmosphere via gas exchange. Nevertheless, the Mediterranean is a source of anthropogenic CO_2 for intermediate depths in the Atlantic Ocean, since the dense water formed in the Mediterranean Sea spills out of the Strait of Gibraltar and transports C_{ant} to depth and, as noted by *Álvarez et al.* [2005], this entrains additional C_{ant} from central Atlantic waters. To reduce the mapping error associated with the basinwide extrapolation and the flux estimates, tracer measurements in the areas where no samples have been taken are needed, especially in the marginal seas, in the western basin and in the Strait of Gibraltar. Measurements of a second tracer (e.g., SF_6) are important in order to constrain the Δ/Γ ratio and therewith to reduce the uncertainty in the TTD method. Furthermore, knowledge about the saturation state of CFC-12 in areas where the water subducts (Gulf of Lyon, Adriatic Sea, Aegean Sea, Levantine basin) would help to reduce the errors in the age calculations. The effect of changing deep water mass formation over the past 20 years implies that a repeat survey of C_{ant} in the basin is required to validate assumptions of the TTD approach. Despite the uncertainties and assumptions the results of the back-calculated PP $p\mathrm{CO}_2$ with the conservative A_C approach suggest that the TTD method gives a reasonable estimate for the C_{ant} concentrations. Further measurements of alkalinity in the marginal seas are necessary, however, to confirm the hypothesis that the surface relationship between salinity and alkalinity is steeper in the deep water formation areas than in midbasin and the implication that no carbonate dissolution takes place in the Mediterranean Sea.

[30] **Acknowledgments.** We thank Birgit Klein, Peter Streu, and Tobias Steinhoff for collection and measurement of the samples. Thanks also to the crew of R/V Meteor for their assistance and to Wolfgang Roether, the chief scientist of the cruise. Funding for this work was provided by the CarboOcean IP of the European Comission (grant 511176-2) and by the Deutsche Forschungsgemeinschaft (DFG).

References

Aït-Ameur, N., and C. Goyet (2006), Distribution and transport of natural and anthropogenic CO_2 in the Gulf of Cádiz, *Deep Sea Res., Part II*, *53*, 1329–1343.

Álvarez, M., F. Pérez, D. Shoosmith, and H. Bryden (2005), Unaccounted role of Mediterranean Water in the drawdown of anthropogenic carbon, *J. Geophys. Res.*, *110*, C09S03, doi:10.1029/2004JC002633.

Alvarez, M., et al. (2009), Estimating the storage of anthropogenic carbon in the subtropical Indian Ocean: A comparison of five different approaches, *Biogeosciences*, *6*, 681–703.

Besiktepe, S., H. Sur, E. Ozsoy, M. Latif, T. Oguz, and U. Unluata (1994), The circulation and hydrography of the Marmara Sea, *Prog. Oceanogr.*, *34*, 285–334.

Bindoff, N., et al. (2007), Observations: Oceanic climate change and sea level, in *Climate Change* 2007*: The Physical Science Basis. Contribution of Working Group I to the Fourth Assessment Report of the Intergovernmental Panel on Climate Change*, edited by S. Solomon et al., chap. 5, Cambridge University Press, Cambridge, United Kingdom and New York, NY.

Brewer, P. (1978), Direct observation of the oceanic CO_2 increase, *Geophys. Res. Lett.*, *5*(12), 997–1000.

Bryden, H., J. Candela, and T. Kinder (1994), Exchange through the Strait of Gibraltar, *Progr. Oceanogr.*, *33*, 201–248.

Bulsiewicz, K., H. Rose, O. Klatt, A. Putzka, and W. Roether (1998), A capillary-column chromatographic system for efficient chlorofluorocarbon measurement in ocean waters, *J. Geophys. Res.*, *103*(C8), 15,959–15,970.

Chen, C., and F. Millero (1979), Gradual increase of oceanic carbon dioxide, *Nature*, *277*, 205–206.

Copin-Montégut, C. (1993), Alkalinity and carbon budgets in the Mediterranean Sea, *Global Biogeochem. Cycles*, *7*, 915–925.

Dafner, E., R. Sampere, and H. Bryden (2001), Total organic carbon distribution and budget through the Strait of Gibraltar in April 1998, *Mar. Chem.*, *73*, 233–252.

de la Paz, M., B. Debelius, D. Macias, A. Vazquez, A. Gomez-Parra, and J. M. Forja (2008), Tidal-induced inorganic carbon dynamics in the Strait of Gibraltar, *Cont. Shelf Res.*, *28*, 1827–1837.

Dickson, A. (1990), Standard potential of the reaction $AgCl(s) + 1/2\,H_2\,(g) = Ag(s) + HCl(aq)$ and the standard acidity constant of the ion HSO_4^- in synthetic sea water from 273.15 K to 318.15 K, *J. Chem. Thermodyn.*, *22*, 113–127.

Dickson, A., and F. Millero (1987), A comparison of the equilibrium-constants for the dissociation of carbonic-acid in seawater media, *Deep Sea Res., Part I*, *34*, 1733–1743.

Friis, K., A. Körtzinger, J. Pätsch, and D. Wallace (2005), On the temporal increase of anthropogenic CO2 in the subpolar North Atlantic, *Deep Sea Res., Part I*, *52*, 681–698.

Gascard, J. (1978), Mediterranean deep water formation baroclinic instability and oceanic eddies, *Oceanol. Acta*, *1*, 315–330.

Gruber, N., J. Sarmiento, and T. Stocker (1996), An improved method for detecting anthropogenic CO_2 in the oceans, *Global Biogeochem. Cycles*, *10*, 809–837.

Hall, T., and R. Plumb (1994), Age as a diagnostic of stratospheric transport, *J. Geophys. Res.-Atmospheres*, *99*(D1), 1059–1070.

Huertas, I. E., A. F. Ríos, J. García-Lafuente, A. Makaoui, S. Rodríguez-Gálvez, A. Sánchez-Román, A. Orbi, J. Ruíz, and F. F. Pérez (2009), Anthropogenic and natural CO_2 exchange through the Strait of Gibraltar, *Biogeosciences*, *6*, 647–662.

Körtzinger, A., J. Hedges, and P. Quay (2001), Redfield ratios revisited: Removing the biasing effect of anthropogenic CO_2, *Limnol. Oceanogr.*, *46*, 964–970.

Krasakopoulou, E., S. Rapsomanikis, A. Papadopoulos, and E. Papathanassiou (2009), Partial pressure and air-sea CO_2 flux in the Aegean Sea during February 2006, *Cont. Shelf Res.*, *29*, 1477–1488.

Lafuente, J., E. Fanjul, J. Vargas, and A. Ratsimandresy (2002), Subinertial variability in the flow through the Strait of Gibraltar, *J. Geophys. Res.*, *107*(C10), 3168, doi:10.1029/2001JC001104.

Lewis, E., and D. Wallace (1998), *Program Developed for CO_2 System Calculations*, ORNL/CDIAC-105, Carbon Dioxide Information Analysis Center, Oak Ridge National Laboratory, U.S. Department of Energy, Oak Ridge, Tennessee.

Louanchi, F., M. Boudjakdji, and L. Nacef (2009), Decadal changes in surface carbon dioxide and related variables in the Mediterranean Sea as inferred from a coupled data-diagnostic model approach, *ICES J. Mar. Sci.*, *66*, 1538–1546.

Mehrbach, C., C. Culberso, J. Hawley, and R. Pytkowic (1973), Measurement of apparent dissociation constants of carbonic acid in seawater at atmospheric pressure, *Limnol. Oceanogr.*, *18*, 897–907.

Menard, H., and S. Smith (1966), Hypsometry of ocean basin provinces, *J. Geophys. Res.*, *71*, 4305–4325.

O'Neil Baringer, M., and J. Price (1997), Mixing and Spreading of the Mediterranean Outflow, *J. Phys. Oceanogr.*, *27*, 1654–1677.

Ovchinnikov, I. (1984), Intermediate water formation in the Mediterranean Sea, *Oceanology*, *24*, 217–225.

Pollak, M. (1951), The sources of the deep water of the Mediterranean Sea, *J. Mar. Res.*, *10*, 128–151.

Reid, J. (1979), Contribution of the Mediterranean Sea outflow to the Norwegian Greenland Sea, *Deep Sea Res., Part I*, *26*, 1199–1223.

Rivaro, P., R. Messa, S. Massolo, and R. Frache (2010), Distributions of carbonate properties along the water column in the Mediterranean Sea: Spatial and temporal variations, *Mar. Chem.*, *121*, 236–245.

Roether, W., B. Manca, B. Klein, D. Bregant, D. Georgopoulos, V. Beitzel, V. Kovacevic, and A. Luchetta (1996), Recent changes in eastern Mediterranean deep waters, *Science*, *271*, 333–335.

Sabine, C., et al. (2004), The oceanic sink for anthropogenic CO_2, *Science*, *305*, 367–371.

Santana-Casiano, J., M. Gonzalez-Davila, and L. Laglera (2002), The carbon dioxide system in the Strait of Gibraltar, *Deep Sea Res., Part II*, *49*, 4145–4161.

Schneider, A., D. W. R. Wallace, and A. Körtzinger (2007), Alkalinity of the Mediterranean Sea, *Geophys. Res. Lett.*, *34*, L15608, doi:10.1029/2006GL028842.

Serra, N., and I. Ambar (2002), Eddy generation in the Mediterranean undercurrent, *Deep Sea Res., Part II*, *49*, 4225–4243.

Steinfeldt, R. (2004), Ages and age spectra of Eastern Mediterranean deep water, *J. Mar. Syst.*, *48*, 67–81.

Stratford, K., and R. Williams (1997), A tracer study of the formation, dispersal, and renewal of Levantine Intermediate Water, *J. Geophys. Res.*, *102*(C6), 12,539–12,549.

Stratford, K., R. Williams, and P. Drakopoulos (1998), Estimating climatological age from a model-derived oxygen-age relationship in the Mediterranean, *J. Mar. Syst.*, *18*, 215–226.

Tanhua, T., A. Körtzinger, K. Friis, D. Waugh, and D. Wallace (2007), An estimate of anthropogenic CO_2 inventory from decadal changes in oceanic carbon content, *Proc. Natl. Acad. Sci. U. S. A.*, *104*, 3037–3042.

Tanhua, T., D. W. Waugh, and D. W. R. Wallace (2008), Use of SF_6 to estimate anthropogenic CO_2 in the upper ocean, *J. Geophys. Res.*, *113*, C04037, doi:10.1029/2007JC004416.

Tanhua, T., E. P. Jones, E. Jeansson, S. Jutterström, W. M. Smethie Jr., D. W. R. Wallace, and L. G. Anderson (2009), Ventilation of the Arctic Ocean: Mean ages and inventories of anthropogenic CO_2 and CFC-11, *J. Geophys. Res.*, *114*, C01002, doi:10.1029/2008JC004868.

Theocharis, A., B. Klein, K. Nittis, and W. Roether (2002), Evolution and status of the Eastern Mediterranean Transient (1997–1999), *J. Mar. Syst.*, *33*, 91–116.

Tixeront, J. (1969), Le Bilan Hydrologique de la Mer Noire et de la Mer Méditerranée, *Bull. Int. Assoc. Sci. Hydrol.*, *14*, 61–69.

Touratier, F., and C. Goyet (2004), Applying the new TrOCA approach to assess the distribution of anthropogenic CO_2 in the Atlantic Ocean, *J. Mar. Syst.*, *46*, 181–197.

Touratier, F., C. Goyet, C. Coatanoan, and C. Andrie (2005), Assessments of anthropogenic CO_2 distribution in the tropical Atlantic Ocean, *Deep Sea Res. Part I*, *52*, 2275–2284.

Touratier, F., L. Azouzi, and C. Goyet (2007), CFC-11, $\Delta^{14}C$ and ^3H tracers as a means to assess anthropogenic CO_2 concentrations in the ocean, *Tellus, Ser. B*, *59*, 318–325.

Vazquez-Rodriguez, M., et al. (2009), Anthropogenic carbon distributions in the Atlantic Ocean: data-based estimates from the Arctic to the Antarctic, *Biogeosciences*, *6*, 439–451.

Walker, S., R. Weiss, and P. Salameh (2000), Reconstructed histories of the annual mean atmospheric mole fractions for the halocarbons CFC-11, CFC-12, CFC-113, and carbontetrachloride, *J. Geophys. Res.*, *105* (C6), 14,285–14,296.

Wallace, D. (1995), Monitoring global ocean carbon inventories, OOSDP Background Report. Texas A&M University, College Station, Tex.

Warner, M., and R. Weiss (1985), Solubilities of Chlorofluorocarbon-11 and Chlorofluorocarbon-12 in water and seawater, *Deep Sea Res., Part I*, *32*, 1485–1497.

Waugh, D., T. Haine, and T. Hall (2004), Transport times and anthropogenic carbon in the subpolar North Atlantic Ocean, *Deep-Sea Res., Part I*, *51*, 1475–1491.

Waugh, D. W., T. M. Hall, B. I. McNeil, R. Key, and R. J. Matear (2006), Anthropogenic CO_2 in the oceans estimated using transit time distributions, *Tellus, Ser. B*, *58*, 376–389.

Weiss, R. F., and B. A. Price (1980), Nitrous oxide solubility in water and seawater, *Mar. Chem.*, *8*, 347–359.

A. Körtzinger, A. Schneider, T. Tanhua, and D. W. R. Wallace, Leibniz-Institut für Meereswissenschaften an der Universität Kiel (IFM-GEOMAR), Düsternbrooker Weg 20, D-24105 Kiel, Germany. (aschneider@ifm-geomar.de)

5 An evaluation of tracer measurements and anthropogenic carbon in the equatorial and the tropical North Atlantic

An evaluation of tracer measurements and anthropogenic carbon in the equatorial and the tropical North Atlantic

The basis of this work are combined dichlorodifluoromethane and sulfur hexafluoride measurements from four cruises to the tropical Atlantic between 2006 and 2009. Anthropogenic carbon concentrations are estimated using the transit time distribution method. The ratio of mean age and width, which is one assumption in the transit time distribution approach, has been determined to be 0.5 for the upper 1500 m in the tropical region. At depth anthropogenic carbon concentrations $>3\ \mu\mathrm{mol\,kg^{-1}}$ are found down to 5000 m. In the upper Labrador Sea Water, at around 1800 m, increased anthropogenic carbon concentrations of 5 - 10 $\mu\mathrm{mol\,kg^{-1}}$ are found. Comparison with tracer data from a N-S section crossing the equator along 23°W, that had been in 1999, revealed a anthropogenic carbon increase of 5 - 10 $\mu\mathrm{mol\,kg^{-1}}$ for the upper 700 m and no or little change at around 1000 m. The equatorial belt (5°S - 5°N) shows increased anthropogenic carbon concentrations compared to the area north of it (5° - 15°N). Mean column inventories in the upper 1000 m are 4 $\mu\mathrm{mol\,kg^{-1}}$ higher and the total anthropogenic carbon inventory is increased by 35%. This trend has not been described in the past.

1 Introduction

The atmospheric carbon dioxide (CO_2) increase of more than 100 ppt since the late 18th century is exceptional in earth history and has been clearly ascribed to anthropogenic emissions. About 50% of the anthropogenic CO_2 (C_{ant}) has been taken up by the ocean and the biosphere [*Denman et al.*, 2007], which delayed the warming effect in the atmosphere. Quantifying the oceanic uptake is difficult as C_{ant} cannot be distinguished from the natural CO_2 background. Different methods have been developed to estimate the oceans C_{ant} inventory and regions of increased uptake have been identified. In this context, the upwelling regions in the tropical Atlantic Ocean might play a considerable role for the C_{ant} uptake because in upwelling regions older water, that has been traveling in the ocean interior for several years, comes up to the surface. Due to remineralization of organic matter this water has increased inorganic carbon concentrations and thus is a source of CO_2 for the atmosphere. However, at the same time it is a sink for anthropogenic CO_2 because the magnitude of the CO_2 source has decreased, due to higher atmospheric CO_2 concentrations compared to conditions in the upwelling zone during preindustrial times.

The tropical Atlantic Ocean is affected by a multitude of zonal currents. Induced by the trade winds a westward surface water current, the Equatorial Current (EC), is found at the equator and is accompanied by poleward Ekman transport north and south of the equator. This leads to upwelling along the equator associated with lower water temperatures. The so called 'cold tongue' develops in northern summer, when the trade winds are strongest. The poleward flowing surface waters loose contact with the atmosphere when they reach the subduction zones of the Subtropical Gyres and return back to the equator at depths around 300 - 500 m [*Schott et al.*, 2004]. These shallow overturning circulations are named the Subtropical Cells (STC). The southern STC is intensified due to the Meridional Overturning Circulation, which transports warm water towards the north in the North Brazilian Undercurrent. Below the westward flowing EC, the Equatorial Undercurrent flows in opposite direction, as well as the North and the South Equatorial Undercurrents at around 5°N and 5°S, respectively. A cyclonic circulation in the shadow zone south and southeast of the northern Subtropical Gyre causes the permanent, quasi-stationary Guinea Dome [*Siedler et al.*, 1992], which is mainly fed by the North Equatorial Undercurrent [*Schott et al.*, 2004]. Ekman upwelling occurs both, in the Guinea Dome and along the coast. Similar features are also found in the southern hemisphere.

The intermediate and deep zonal currents in the equatorial region are influenced by currents from the northern and the southern hemisphere. These are the North Atlantic Deep Water (NADW) coming from the north as part of the Deep Western Boundary Current and the Antarctic Intermediate Water (AAIW) coming from the south along the South American continent. At low latitudes both water masses are partly deflected towards the east and can be detected along the equator. The NADW is separated into the upper and the lower NADW, which both show increased chlorofluorocarbon (CFC) concentrations [*Weiss et al.*, 1985; *Rhein et al.*, 1995; *Rhein and Stramma*, 2005]. The upper NADW is also named upper Labrador Sea Water (LSW).

The water, that comes up to the surface in the equatorial upwelling region, is a mixture of the water masses participating in the Subtropical Cells. Of major interest for the C_{ant} uptake is the contribution of water that has not been in contact with the atmosphere since CO_2 concentrations started to increase. This could be the case for AAIW, that has been circulated around the southern Subtropical Gyre before entering the equatorial region [*Warner and Weiss*, 1992; *Stramma and Schott*, 1999] and for Indian Central Water brought into the Atlantic Ocean by the Agulhas Current [*Tomczak and Godfrey*, 1994].

On several recent cruises to the tropical Atlantic, dichlorodifluoromethane (CFC-12) and sulfur hexafluoride (SF_6) concentrations were determined. With the help of these tracer measurements the mean ages of the different water masses in the eastern tropical Atlantic are calculated and differences in age distribution and C_{ant} concentration between the Guinea Dome area and the equatorial band are highlighted. Further, the column inventories of anthropogenic carbon of all sampled stations are determined and estimates for the total C_{ant} inventory of the equatorial and the Guinea Dome regions are given.

2 Methodology

2.1 Water samples

Between 2006 and 2009 four cruises were undertaken to the tropical Atlantic. Three cruises with the R/V Meteor (M68/2 in 2006 and M80/1 and M80/2 in 2009) and one cruise with the R/V Maria S. Merian (MSM10/1 in 2008). The stations of the four cruises that were sampled for tracers are shown in figure 1. Cruises MSM10/1 and M80/2 were part of a tracer release experiment. Following the tracer release in 2007, the tracer concentration and distribution has been surveyed once a year to study circulation and upwelling processes in the area. This explains the unique cruise tracks and the high sampling density. Altogether almost 6000 CFC-12 and 1200 SF_6 samples were taken. Generally, the upper 1000 - 1500 m of the water column were sampled, with some additional deep stations. Most samples were measured onboard and only a subset of about 100 samples were flame sealed and taken back for shore-based analysis.

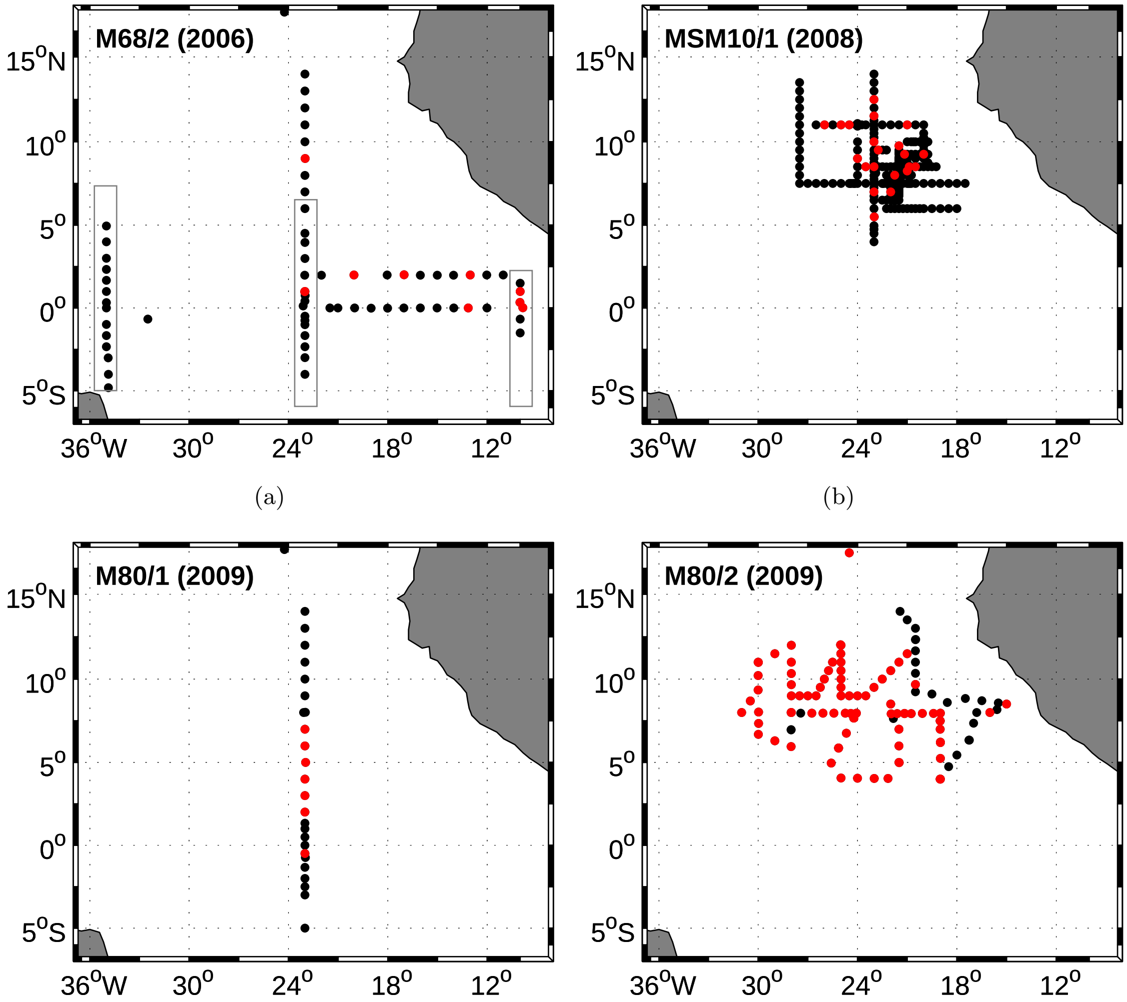

(a) (b) (c) (d)

Figure 1: Sampled stations of all cruises to the tropical Atlantic. Red dots indicate the stations where SF_6 was measured additionally to CFC-12. On map (a) three sections that were sampled for trichlorofluoromethane (CFC-11) in the year 1999 are highlighted in gray [*Touratier et al.*, 2005]
.

Two slightly different purge and trap systems, both followed by gas chromatography, were used for the tracer analysis. The first one (system A) is a system similar to that described by *Bullister and Weiss* [1988] and is not suitable for measuring SF_6, because cooling of the trap is achieved with Peltier elements reaching minimum temperatures at -45 to -50°C. For quantitative detection of SF_6 temperatures of about -60°C are necessary. Samples for system A are collected in glass syringes and are measured directly onboard. The second system (system B) uses liquid nitrogen for cooling of the trap to -60°C and thus CFC-12 and SF_6 can be trapped simultaneously. Samples are collected in glass ampoules and can be measured directly onboard or be flame sealed for later analysis. The precolumn of system B is a 30 cm 1/8 ″ stainless steel tubing packed with Porasil C. The main column is a 2 m 1/8 ″ stainless steel tubing packed with 180 cm Carbograph and 20 cm molecular sieve 5Å. During one cruise (MSM10/1 in 2008) capillary columns instead of packed columns were used for the gas chromatographic separation (system B*). The precolumn used for system B* is a 1/8 ″ stainless steel tubing packed with 50 cm Porasil C and 50 cm molecular sieve 5Å. The main column is a combination of two capillary columns arranged in series. The first one is a 75 m DB 624 and the second one a 30 m RT-molecular sieve 5Å.

The precision of the CFC-12 measurements for the different cruises using system A was in the range of ±1 to 1.9 % or ±6 to 10.8 fmol kg^{-1}, whichever was greater. For system B the precision ranged from ±3.8 to 6 % or ±40 to 50 fmol kg^{-1}. The precision of the SF$_6$ measurements could only be determined for two cruises. For M80/2 it was ±10 % or ±0.05 fmol kg^{-1}, whichever was greater and for MSM10/1 (system B*) the SF$_6$ precision was ±2.2 %.

For direct comparison with the atmospheric mixing ratios, the measured tracer concentrations are converted into equivalent mixing ratios, which are calculated as:

$$\text{Equivalent mixing ratio} = \frac{c}{F(T,S)\cdot(P_{\text{atm}} - P_{\text{H}_2\text{O}}(T,S))},$$

where c is either the CFC-12 or the SF$_6$ concentration in pmol kg^{-1}, $F(T,S)$ is the temperature and salinity dependent solubility function for each of the gases in mol kg^{-1} atm^{-1} [*Warner and Weiss*, 1985; *Bullister et al.*, 2002], P_{atm} is the mean atmospheric pressure in atm and $P_{\text{H}_2\text{O}}(T,S)$ is the temperature and salinity dependent partial pressure of water vapor [*Weiss and Price*, 1980].

2.2 Anthropogenic carbon calculation

Using the Transient Time Distribution (TTD) method, the mean age and the anthropogenic carbon concentration can be estimated. The TTD method assumes that a water parcel consists of waters with varying time histories. Instead of a single age, each water parcel has an age or transit time distribution. Using the measured transient tracer concentration together with its atmospheric time history, the TTD and mean age can be determined for each water sample. The interior concentration $c(t)$ of the tracer at time t is given by [*Hall and Plumb*, 1994]:

$$c(t) = \int_0^\infty c_0(t-t')\cdot G(t')dt',$$

where $c_0(t-t')$ is the surface water tracer concentration in the year $t-t'$. $G(t')$ is the TTD, which can be approximated for steady transport by an inverse Gaussian function [*Waugh et al.*, 2004], that is:

$$G(t') = \sqrt{\frac{\Gamma^3}{4\pi\Delta^2 t'^3}}\cdot\exp\left(\frac{-\Gamma\,(t'-\Gamma)^2}{4\Delta^2 t'}\right),$$

where Γ is the mean transit time ('mean age') and Δ defines the width of the TTD.

Further, in combination with the atmospheric histories of CO$_2$ and a regional alkalinity-salinity correlation, the anthropogenic carbon content can then be estimated as follows:

$$C_{\text{ant}}(t) = \int_0^\infty C_{\text{ant},0}(t-t')\cdot G(t')dt',$$

where t is the sampling year.

For the TTD calculations 100% saturation has been assumed for surface waters with respect to SF_6 and a time dependent saturation, as estimated by *Tanhua et al.* [2008] has been used for CFC-12. The atmospheric time history of SF_6 was taken from *Maiss and Brenninkmeijer* [1998] combined with measurements made since 1995 by the National Oceanic & Atmospheric Administration [*NOAA/ESRL*, 2011]. For CFC-12 the atmospheric time history from *Walker et al.* [2000] was used and continued from 1998 onwards with measurements from the National Oceanic & Atmospheric Administration [*NOAA/ESRL*, 2011]. Given that waters in the equatorial Atlantic have their origin in both hemispheres, a global mean was used for the atmospheric time histories of both tracers. The past CO_2 concentrations in the atmosphere are merged from reconstructions from the Law Dome ice core [*Etheridge et al.*, 1996] and since 1959 from direct measurements at the Mauna Loa, Hawaii [*Tans*, 2011]. A constant CO_2 disequilibrium has been assumed between ocean surface waters and the atmosphere. The alkalinity-salinity relationship in the tropical region, used to convert the anthropogenic part of the atmospheric carbon mixing ratios (in ppt) into dissolved anthropogenic carbon concentrations (in $\mu\text{mol kg}^{-1}$), was determined from total alkalinity (A_T) and salinity measurements during the M68/2 and M80/1 cruises ($A_\mathrm{T} = 66.7 \cdot S - 45.9\ \mu\text{mol kg}^{-1}$).

The ratio of the constants Δ and Γ in the inverse Gaussian function is a measure for mixing. A larger ratio implies stronger mixing. For ocean interior waters it has been shown, that the usage of a ${}^{\Delta}/_{\Gamma}$ ratio of 1 is appropriate [*Waugh et al.*, 2004]. Whether this ratio is applicable for the upper 1500 m of the tropical Atlantic has not been tested. However, on the basis of two transient tracers with differing atmospheric time histories, e.g. CFC-12 and SF_6, the appropriate ${}^{\Delta}/_{\Gamma}$ ratio can be approximated.

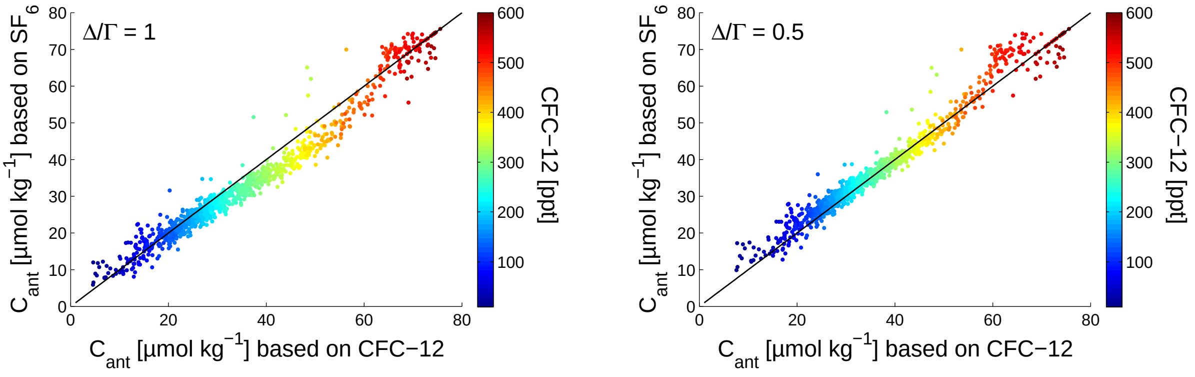

(a)

(b)

Figure 2: The SF_6 based C_ant estimates are plotted against the CFC-12 based C_ant estimates. Colour coded are the CFC-12 concentrations in ppt. The black line indicates a one to one relation. (a) ${}^{\Delta}/_{\Gamma} = 1$ has been used to calculate C_ant. (b) ${}^{\Delta}/_{\Gamma} = 0.5$ has been used to calculate C_ant.

To do so, the C_ant concentrations are determined initially based on CFC-12 measurements and a second time based on SF_6 measurements using the same ${}^{\Delta}/_{\Gamma}$ ratio. As indicator for the appropriate ${}^{\Delta}/_{\Gamma}$ ratio, the resulting C_ant estimates from all cruises are plotted against each other (Fig. 2). Panel (a) shows the C_ant concentrations estimated with a ${}^{\Delta}/_{\Gamma}$ ratio of 1 and panel (b) with a ${}^{\Delta}/_{\Gamma}$ ratio of 0.5. When using the appropriate ${}^{\Delta}/_{\Gamma}$ ratio a one to one relation would be expected (black lines). Colour coded are the CFC-12 concentrations in ppt. The increasing scatter at low CFC-12 concentrations is suggestive of a blank problem especially in the SF_6 measurements, because these concentrations are close to the detection limit. The Δ/Γ of 1 in panel (a) does not fit the observations well. The value of 0.5 in panel (b), instead, gives a much more consistent agreement between the tracers. At high CFC-12 concentrations (younger waters) a deviation of the data from the one to one line is apparent. This deviation is presumably caused by the decreasing gradient in the atmospheric CFC-12 concentrations, which is reflected in the water concentrations in figure 3(a) and which makes it difficult to determine the appropriate age and corresponding C_{ant} concentration. *Tanhua et al.* [2008] found, that for waters exceeding ~450 ppt, the uncertainty in the CFC-12 based C_{ant} estimates increases. This limit seems to be in agreement with our data, as the data points greater than 450 ppt in CFC-12 are the ones varying from the linear relationship. From figure 2 it becomes clear that a Δ/Γ ratio of 1 is not applicable for the upper 1500 m in the tropical Atlantic. Instead, less mixing is assumed and a Δ/Γ of 0.5 is used to calculate the mean age and the anthropogenic carbon concentrations.

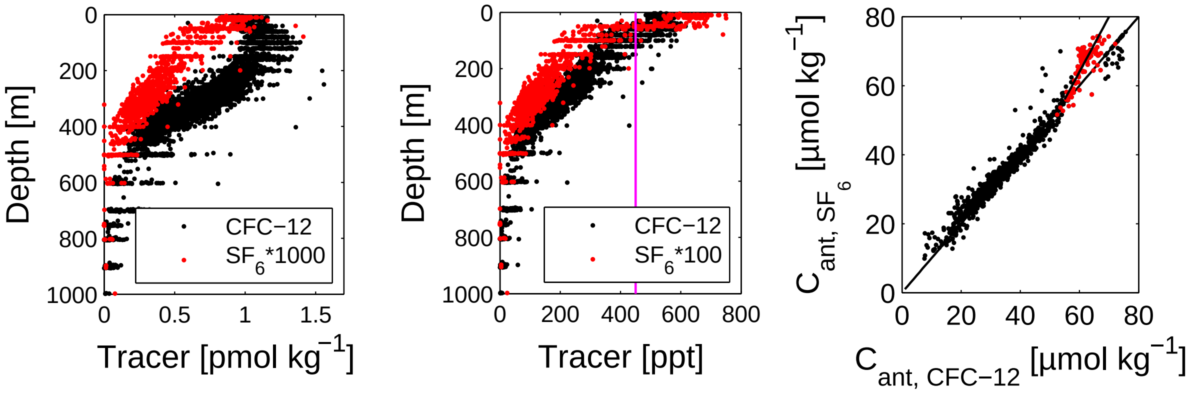

(a) (b) (c)

Figure 3: (a) and (b) show depth profiles of the CFC-12 (black) and SF_6 (red) measurements from all cruises to the tropical Atlantic. (a) The tracer concentrations in pmol kg^{-1}, where the SF_6 values are multiplied by 1000. (b) The tracer equivalent mixing ratios in ppt, where the SF_6 values are multiplied by 100. The magenta line indicates the CFC-12 border of 450 ppt. (c) The SF_6 based C_{ant} estimates plotted against the CFC-12 based C_{ant} estimates. Data points with CFC-12 concentrations between 450 and 540 ppt are highlighted in red and the transfer function is illustrated.

Figures 3(a) and (b) show the depth profiles of CFC-12 and SF_6 in μmol kg^{-1} and in ppt. In the upper 100 to 200 m, where CFC-12 samples exceed 450 ppt, indicated by the magenta line, a pronounced vertical gradient can only be seen in the SF_6 data. This is due to the hardly changing atmospheric CFC-12 concentrations in the last two decades. All samples with CFC-12 concentrations greater than 540 ppt are therefore assumed to be recently ventilated and the tracer age is set to zero, which means that the C_{ant} concentrations are only influenced by the carbonate system parameters. For samples with CFC-12 concentrations between 450 and 540 ppt, the SF_6 measurements are used to calculate the C_{ant} concentrations, as they give more reliable results. When no SF_6 measurements were available, a transfer function was applied to the CFC-12 based C_{ant} estimates. This function ($y = 1.3 \cdot x - 14$) was determined by linear correlation between all existing pairs of SF_6 based and CFC-12 based C_{ant} estimates for samples with CFC-12 concentrations between 450 and 540 ppt (Fig. 3(c)). This function would adjust the data to match the one to one relationship in figures 2 and 3(c).

3 Results and Discussion

3.1 Hydrography and vertical profiles

The main water masses in the region can be identified with the help of a temperature-salinity (T-S) diagram, shown together with the isopycnals in figure 4. The upper LSW and the AAIW have a potential density (σ_Θ) of 27.75 $\mathrm{kg\,m^{-3}}$ and 27.3 $\mathrm{kg\,m^{-3}}$, respectively. Both are clearly defined in the equatorial band (5°S - 5°N), highlighted in red. The Central Water (CW) with a core density of 26.5 $\mathrm{kg\,m^{-3}}$ extends almost linear across the T-S diagram. South of 15°N the origin of the CW lies mainly in the South Atlantic and *Stramma and Schott* [1999] described the South Atlantic Central Water (SACW) as a straight line between the T-S points 5°C, 34.3 and 20°C, 36.0. This is the same T-S curve as of the Indian and the Western South Pacific Central Waters [*Tomczak and Godfrey*, 1994]. According to *Tomczak and Godfrey* [1994] part of the SACW is, in fact, Indian Central Water. The T-S line of North Atlantic Central Water (NACW) is found at higher salinities. The reason why samples in the T-S diagram north of 5°N have higher salinities is that SACW mixes with NACW in this area. The 25.8 $\mathrm{kg\,m^{-3}}$ isopycnal represents the lower boundary of the Tropical Surface Water. Especially in the area

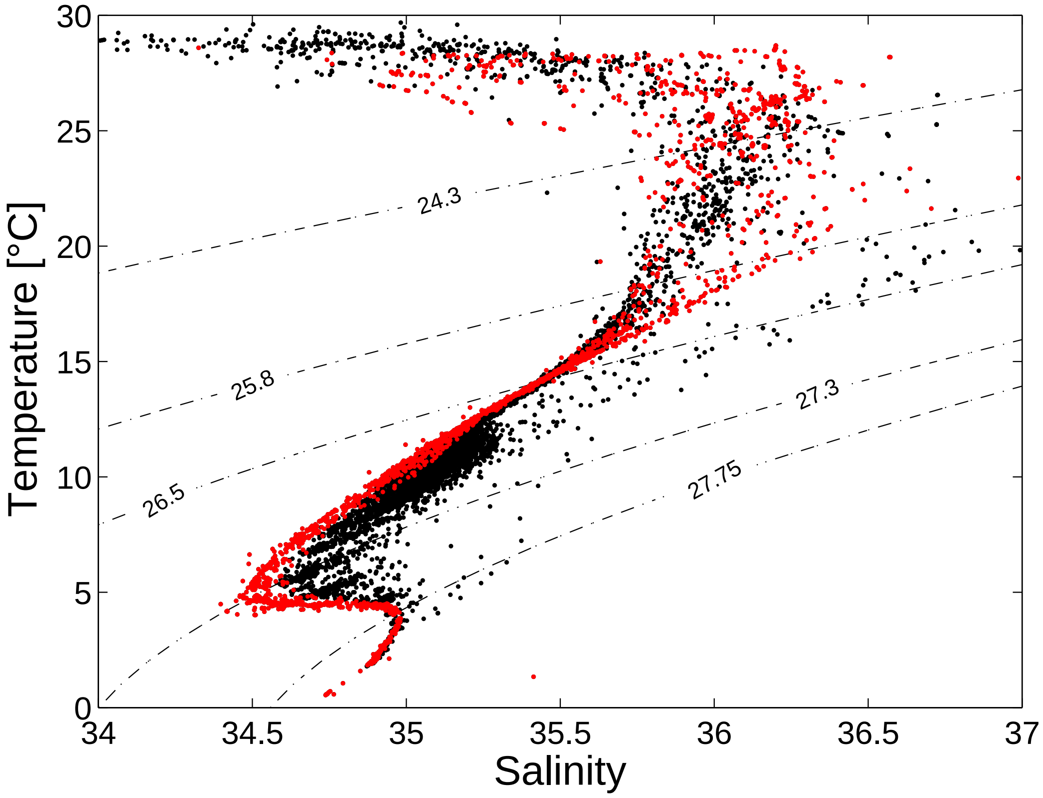

Figure 4: T-S diagram of all sampled stations in the tropical Atlantic. Some characteristic water masses described in the text can be identified with the help of isopycnals. Red dots indicate the stations located in the equatorial region between 5°N and°S.

of the Intertropical Convergence Zone (ITCZ) (located at around 10°N in northern fall), the warm surface waters are characterized by relatively low salinities due to precipitation. These decreasing salinities are more pronounced in the samples north of 5°N (Fig. 4, black dots).

Figure 5 shows the depth profiles of oxygen, mean age and anthropogenic carbon over the entire water column. The vertical oxygen distribution (a) illustrates the pronounced oxygen minimum zone found between 400 and 500 m. Lowest oxygen concentrations are about 40 μmol kg^{-1} and are far from being suboxic (oxygen concentrations of <4.5 μmol kg^{-1} are defined as suboxic [*Warren*, 1994; *Morrison et al.*, 1999]). Comparing the oxygen profile with the profile of the mean age (b) demonstrates that no age maximum is present at the depth of the oxygen minimum. Hence, the low oxygen concentrations seem to be the consequence of enhanced remineralization combined with increasing water age. The C_{ant} concentrations (Fig. 5(c)) are highest at the surface and decrease from maximum values of 75 μmol kg^{-1} down to about 5 μmol kg^{-1} at 1000 m depth. A relative C_{ant} maximum around 1800 m represents the upper LSW and at depths around 3700 and 4000 m a further maximum is found in the lower NADW.

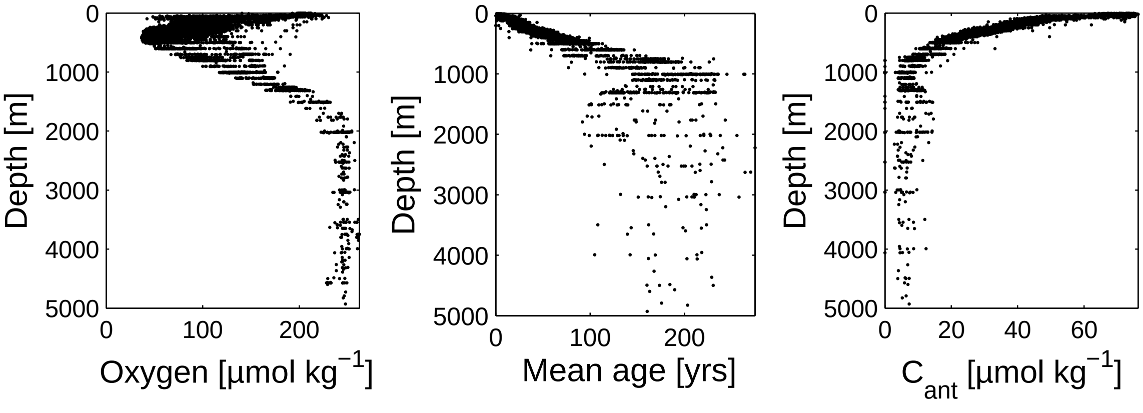

(a) (b) (c)

Figure 5: Depth profiles over the entire water column of (a) oxygen, (b) mean age and (c) anthropogenic carbon. All samples from the cruises to the tropical Atlantic between 2006 and 2009 are shown.

A comparison of the tracer measurements and the C_{ant} estimates with data from *Touratier et al.* [2005] exhibits the same characteristics in the water column. Figures 6(a) and (c) show CFC-11 measurements made on three N-S sections between 6°S and 6°N (see figure 1(a)) in 1999 [*Touratier et al.*, 2005] and the CFC-12 measurements on the same sections from this work, respectively. CFC-11 is more soluble in sea water than CFC-12, which has lead to higher equilibrium concentrations of CFC-11 in surface water (Fig. 7(a)). However, the relation between the equilibrium concentrations is not constant because of the varying atmospheric histories of CFC-11 and CFC-12 (Fig. 7(b)). Consequently, CFC-11 concentrations are about twice as high in middle-aged waters and the CFC-11 to CFC-12 ratio decreases in older waters and somewhat in younger waters of the upper water column. Figure 6(b) shows the C_{ant} concentrations computed from the so called 'Tracer combining Oxygen, inorganic Carbon and total Alkalinity approach' (TrOCA) [*Touratier and Goyet*, 2004], using measurements of oxygen, dissolved inorganic carbon and total alkalinity from the cruise in 1999. In figure 6(d) the C_{ant} estimates are calculated with the TTD method, using the shown CFC-12 concentrations. Like in the tracer profiles, the maxima in the upper LSW and the lower NADW can be clearly identified in both C_{ant} estimates. The mean C_{ant} concentrations based on the TrOCA method are about 5 - 10 μmol kg^{-1} higher than the estimates based on the TTD method (especially below 1000 m), and show much more scatter. The scatter could originate from regional variations given that considerable scatter is also seen in the CFC-11 data. However, these regional variations would presumably be present in the CFC-12 measurements, which were sampled on the identical sections. Nevertheless, both approaches show that the entire water column has been penetrated by C_{ant}.

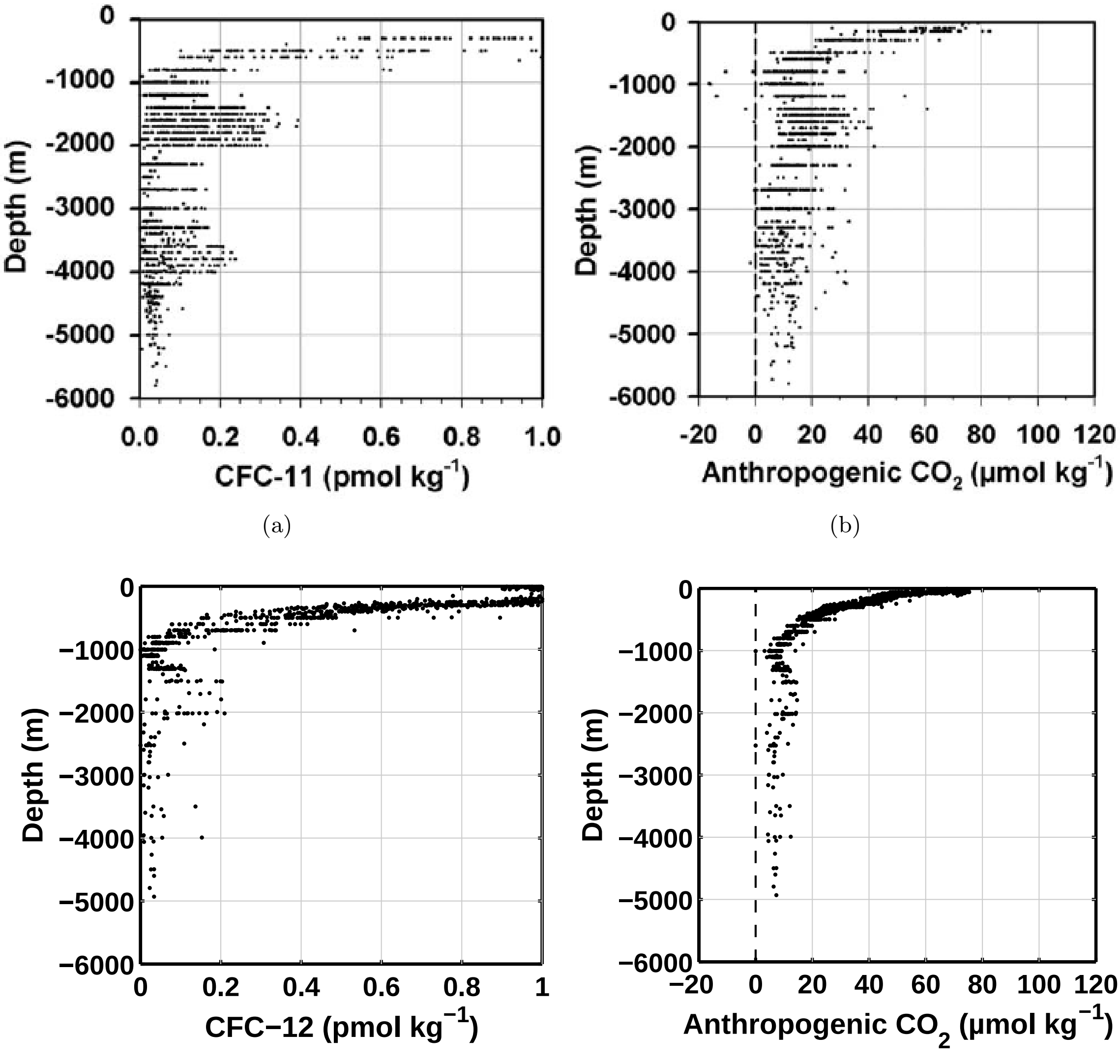

(a) (b)

(c) (d)

Figure 6: The upper two panels show results from a cruise in 1999 to the tropical Atlantic [*Touratier et al.*, 2005] and are compared to data in the bottom two panels from the cruises, which are subject of this work. (a) CFC-11 concentrations measured in 1999. (b) Anthropogenic carbon estimates based on the TrOCA approach. (c) CFC-12 concentrations from measurements made between 2006 and 2009. (d) C_{ant} estimates based on the TTD method.

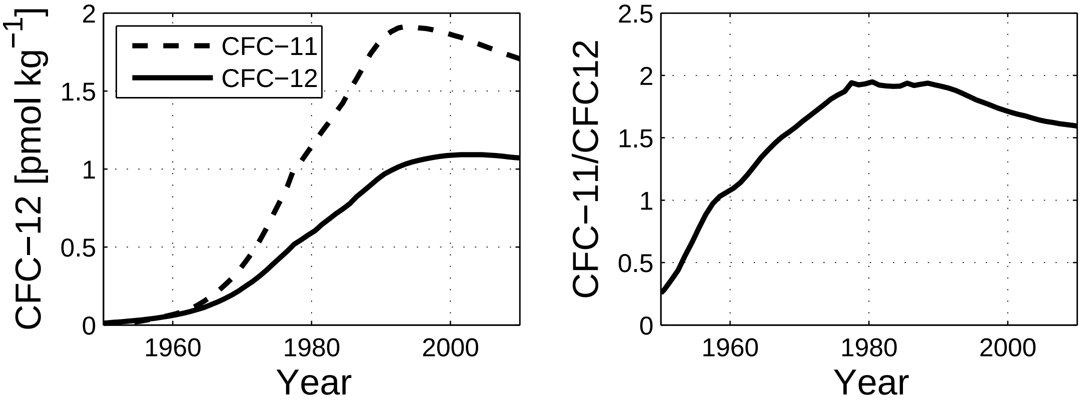

(a) (b)

Figure 7: (a) Estimated surface water equilibrium concentrations of CFC-11 and CFC-12 in pmol kg^{-1} at a temperature of 25°C over the past 60 years. (b) Ratio of the equilibrium concentrations over the past 60 years.

3.2 Hydrographic sections

During the four cruises, which form the basis for this work, a considerable number of stations has been occupied on a N-S section along 23°W and crossing the equator. All measurements in the upper 1500 m around 23°W from the four cruises have been combined to create the section plot of anthropogenic CO_2 in figure 8(a). The fact that stations were sampled at the same latitudes on repeated cruises, the uncertainty in the measurements and temporal variation of the tracer concentrations (samples taken between 2006 to 2009) lead to occasional sharp breaks appearing in the contour plot.

Highest C_{ant} concentrations are found in surface waters decreasing rapidly with depth. Mixed layer concentrations north of 6°N are about 10 μmol kg^{-1} lower than south of 6°N. This can be attributed to increased precipitation in the vicinity of the ITCZ, leading to dilution and a related change in the Revelle factor. As in the C_{ant} depth profile, on the 23°W section a C_{ant} minimum is observed around 1000 m. These depths are occupied by AAIW and Upper Circumpolar Water (a water mass located below the AAIW) [*Oudot et al.*, 1999]. In the northern hemisphere, concentrations below 10 μmol kg^{-1} seem to be extended over a wider depth range. Below 1000 m C_{ant} increases again due to the upper LSW, which brings younger water in the area.

The CFC-11 measurements made on the 23°W section in 1999 [*Touratier et al.*, 2005] were now used to calculate C_{ant} concentrations with the TTD method in the same way as described for CFC-12 data. In figure 8(b) the C_{ant} concentration on the 23°W section in the year 1999 is plotted and reveals the same distribution pattern as in the years 2006 to 2009 (Fig. 8(a)). To illustrate the change in anthropogenic carbon during the 7 - 10 year period (mean 8.5 years), the concentrations were subtracted from each other. The resulting difference (ΔC_{ant}) is attributed to an increase in anthropogenic carbon. The ΔC_{ant} section is shown in figure 8(c). In the upper 700 m a general C_{ant} increase can be observed. The distribution is very patchy with ΔC_{ant} values between 5 - 15 μmol kg^{-1}, which could be caused by the zonal currents in the equatorial region. At the equator at around 200 m depth the Equatorial Undercurrent is visible with very low change in C_{ant} of less than 5 μmol kg^{-1}. North and south of it, small ΔC_{ant} could represent

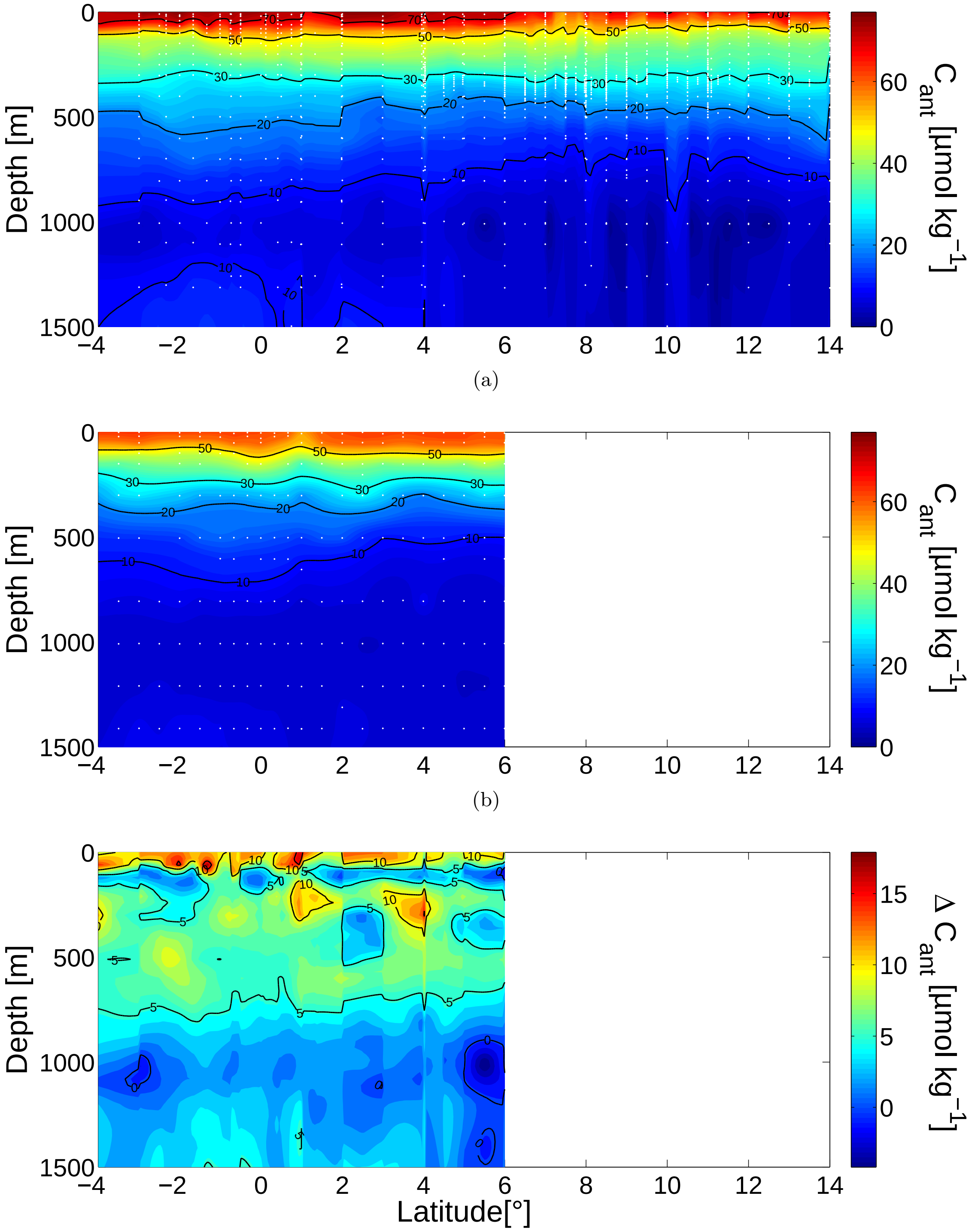

(a)

(b)

(c)

Figure 8: Section plot of C_{ant} concentrations at 23°W. (a) TTD based C_{ant} estimates using CFC-12 and SF_6 measurements from 2006 - 2009. (b) TTD based C_{ant} estimates using CFC-11 measurements from 1999. (c) The difference (ΔC_{ant}) between the two estimates.

the North and the South Equatorial Undercurrents, respectively.

The mean annual $p\mathrm{CO_2}$ increase in surface waters has been estimated to be 1.5 μatm [*Takahashi et al.*, 2009]. This corresponds to an increase in dissolved inorganic carbon of ~8 $\mu\mathrm{mol\,kg^{-1}}$ for a time period of 8.5 years. Between the years 1983 and 1993 a mean annual $p\mathrm{CO_2}$ increase of about 2.3 μatm was found in the eastern equatorial Atlantic [*Oudot et al.*, 1995], which would correspond to an increase of dissolved inorganic carbon of ~12 $\mu\mathrm{mol\,kg^{-1}}$ in 8.5 years. Hence, the high ΔC_{ant} values of up to 15 $\mu\mathrm{mol\,kg^{-1}}$ in the mixed layer (Fig. 8) might be a slight overestimation caused by low-biased C_{ant} estimates in surface waters based on CFC-11 data. In the AAIW at around 1000 m depth the average ΔC_{ant} is zero. In the upper LSW again an increase is observed. On a repeatedly sampled meridional Atlantic section A16 from Iceland to 56°S, decadal C_{ant} changes between 0 and 8 $\mu\mathrm{mol\,kg^{-1}}$ were found in the upper 1000 m of the low latitudes [*Wanninkhof et al.*, 2010]. Below that depth there was almost no change. The authors used an eMLR approach along density surfaces between cruises in 1989/1993 and 2003/2005, resulting in a rather smooth ΔC_{ant} distribution, which is in general agreement with the findings presented here. The patchiness in our data could be attributed to changes in oceanographic features with vertical structure, such as eddies, Rossby waves and movement of fronts, features normally 'neutralized' by the eMLR approach.

3.3 Density surfaces

The high vertical and horizontal sampling density between 15 - 30°W and 5 - 15°N (the area where the tracer had been released and referred to as 'patch' in the following) allows a detailed investigation of the area in comparison with the equatorial region. The mean age distribution and the anthropogenic carbon concentration on different depth horizons are examined in order to find regional differences and to possibly identify ventilation pathways of the oxygen minimum zone. Four characteristic isopycnals were chosen. The potential density of 26.5 $\mathrm{kg\,m^{-3}}$ (100 - 200 m) is the core of the Central Water and the lower Equatorial Undercurrent. The core of the oxygen minimum zone (~400 m) is found at $\sigma_\Theta = 27.1\ \mathrm{kg\,m^{-3}}$, which is also the border between the CW and the AAIW. The AAIW (~800 m) has a potential density of 27.3 $\mathrm{kg\,m^{-3}}$. As additional layer, $\sigma_\Theta = 26.85\ \mathrm{kg\,m^{-3}}$ was chosen. This was the density where the tracer had been released and thus the sample density has been extremely high at that depth during the tracer hunt cruises.

In figure 9 the mean age and the C_{ant} concentrations are shown on the isopycnal layers. The CW exhibits low mean ages (15 - 30 yrs) and high C_{ant} concentrations (around 45 $\mu\mathrm{mol\,kg^{-1}}$). In the northern parts, the CW is older and carries lower C_{ant} concentrations. As the Cape Verde Frontal Zone at around 15°N separates the NACW and the SACW [e.g., *Siedler and Onken*, 1996], these higher mean ages could be due to the fact that the tropical Central Water mainly consists of northward spreading SACW. At $\sigma_\Theta = 26.85\ \mathrm{kg\,m^{-3}}$ differences within the patch that seemed homogeneous in the CW layer, are noticeable. Older waters are found in the southeastern part (difference of up to 15 years) with corresponding lower C_{ant} concentrations, which could be caused by varying contributions (vertically and seasonally) of the North Equatorial Undercurrent and the North Equatorial Countercurrent in the area. Using CTD (Conductivity, Temperature, Depth sensor) hydrography data, ADCP (Acoustic Doppler Current Profiler) velocities and Argo float trajectories, *Stramma et al.* [2008] found that the ventilation of the oxygen minimum zone in the area south and east of the Cape Verde Islands is weaker at 300 to 600 m depth than at 150 to 300 m depth. The northwestern part of the patch and the equatorial region exhibit similar ages and C_{ant} concentrations. Stronger differences between the equatorial and the northern region become visible with increasing depth (Fig. 9(e) - (h)). Younger waters

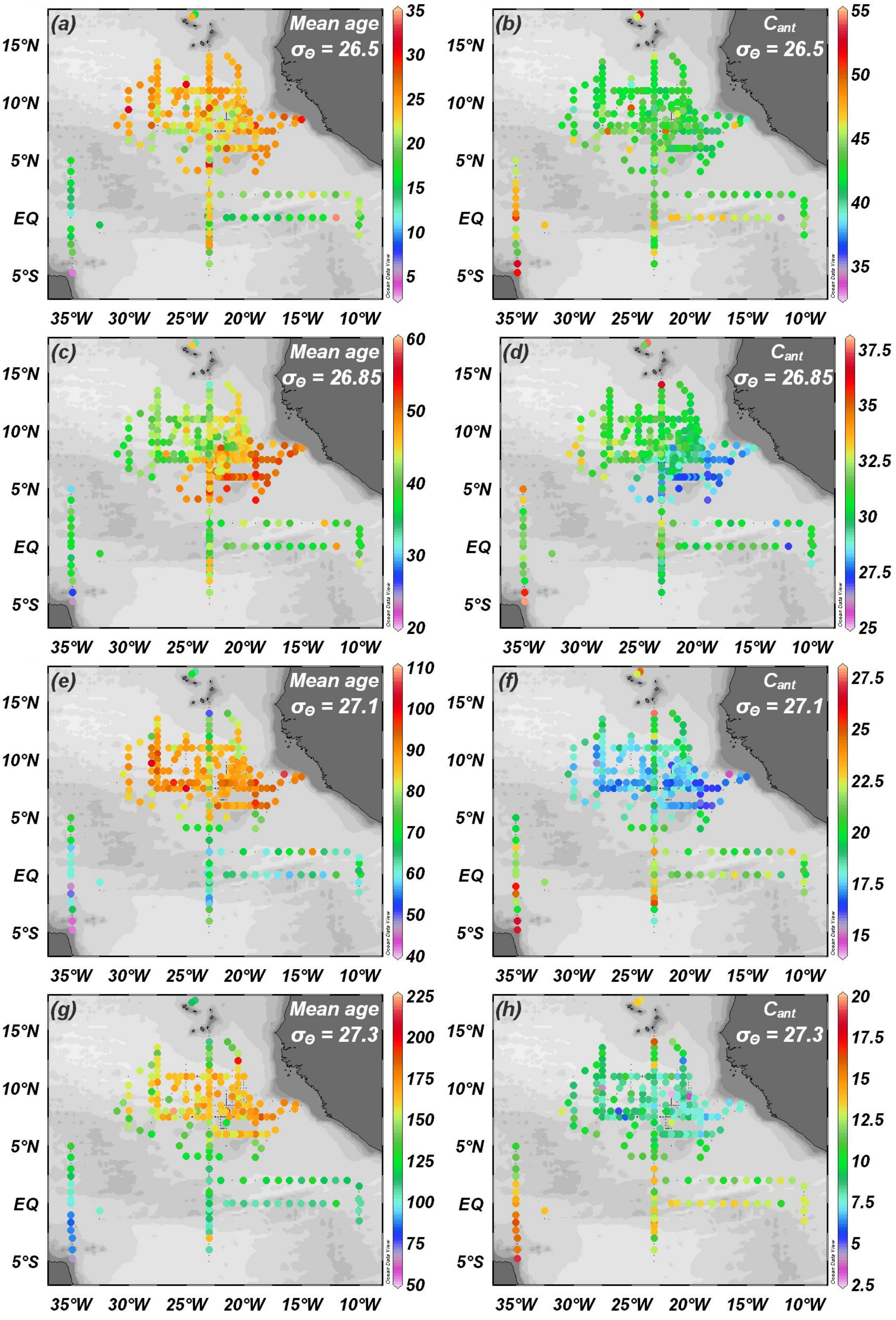
(a) Mean age σΘ = 26.5
(b) Cant σΘ = 26.5
(c) Mean age σΘ = 26.85
(d) Cant σΘ = 26.85
(e) Mean age σΘ = 27.1
(f) Cant σΘ = 27.1
(g) Mean age σΘ = 27.3
(h) Cant σΘ = 27.3
15°N
10°N
5°N
EQ
5°S
35°W
30°W
25°W
20°W
15°W
10°W
35 30 25 20 15 10 5
55 50 45 40 35
60 50 40 30 20
37.5 35 32.5 30 27.5 25
110 100 90 80 70 60 50 40
27.5 25 22.5 20 17.5 15
225 200 175 150 125 100 75 50
20 17.5 15 12.5 10 7.5 5 2.5
Ocean Data View

Figure 9: Mean age [yrs] and C_{ant} concentrations [μmol kg^{-1}] at characteristic potential densities (σ_Θ [kg m^{-3}]). (a) and (b) Central Water, (c) and (d) Tracer release, (e) and (f) Oxygen minimum zone, (g) and (h) Antarctic Intermediate Water.

are found in the oxygen minimum zone layer ($\sigma_\Theta = 27.1\,\mathrm{kg\,m^{-3}}$) and also in the AAIW layer ($\sigma_\Theta = 27.3\,\mathrm{kg\,m^{-3}}$) of the equatorial band. North of 15°N the water ages also seem to be younger than in the patch, but there are too few data to confirm this. In the AAIW layer very young waters are found close to the Brasilian coast, south of the equator. This is supposed to be the water coming from the south, moving towards the east at the equator. Along the equator, mean ages and C_{ant} concentration show a uniform distribution at all depths. Overall, figure 9 shows that water ages vary considerably on the isopycnals, which seems to be the main reason for the different C_{ant} concentrations.

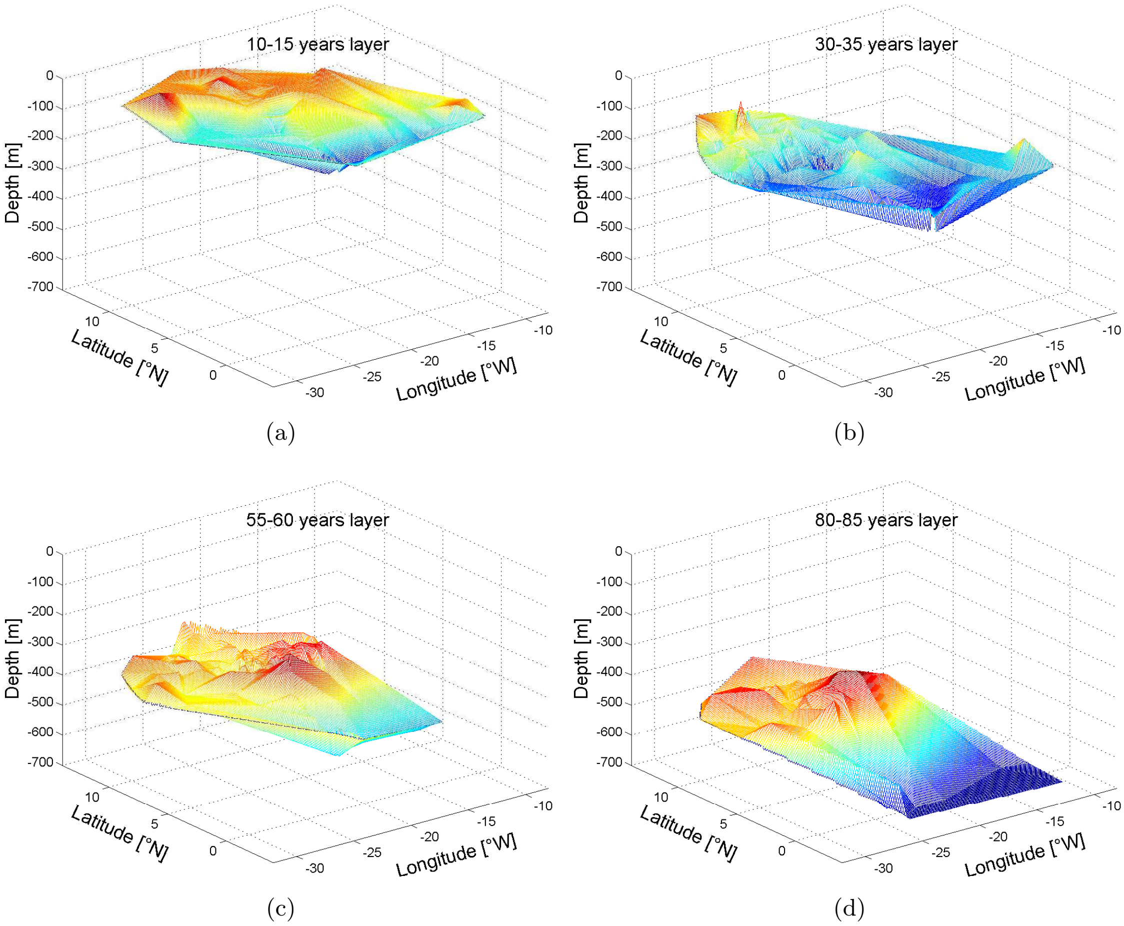

(a)

(b)

(c)

(d)

Figure 10: Four isochrones (layers of the same mean age) are plotted against water depth in the sampling area. The colour code illustrates the relative depth variations for each isochrone.

Figure 10 visualizes four different layers of the same mean age (isochrones) in a space spanned by longitude, latitude and depth. For the sake of clarity, the four isochrones are plotted in four separate panels. In addition, the relative depth variations are indicated by the color code. (Samples on the 34°W section have been left out.) The isochrones are (a) 10 - 15 years, (b) 30 - 35 years, (c) 55 - 60 years and (d) 80 - 85 years. In general, an elevation (decline) on an isochrone could be an evidence for upwelling (downwelling) or for the lateral inflow of older (younger) water. A defined elevation would also be expected in a region of reduced ventilation, where the water recirculates and the age increases. Here, in all four panels, a deepening of the isochrones towards the equator is apparent, which could be attributed to the strong zonal currents. Apart from that, panel (a) shows a rather homogeneous pattern. The panels (b) and particularly (c) reveal two clear elevations centered at 5°N/22°W and 6°N/17°W, which are located in the area of the Guinea Dome and thus can be attributed to the upward displacement of the isopycnals in the dome. *Siedler et al.* [1992] localized the upper thermocline center of the dome at about 9°N/25°W in summer but mentioned that these positions are not well defined as they also found a double-cell structure. In the 80 - 85 years layer the Guinea Dome region is more homogeneous and the decline towards the equator is most pronounced.

Both, the Guinea Dome and the Equator are known as areas of regional upwelling. The well-established upward displacement of isopycnals in the Guinea Dome region can be identified in the isochrones as uplifting of older water (Fig. 10). In the equatorial region the upwelling is rather a diffusive process that cannot be seen in the mean age distribution, due to the much stronger influence of the zonal currents.

3.4 Inventories

3.4.1 Column inventories

Column inventories demonstrate regional differences in the amount of C_{ant} stored in the water column per square meter, depending also on the water depth. Figure 11 shows the column inventories of the upper 1000 m of the tropical Atlantic. Below 1000 m the sample density is too poor to calculate distinct column inventories for each station. From 5°S to 5°N the C_{ant} inventories are about $4\,\text{mol}\,\text{m}^{-2}$ higher than north of 5°N. Next to the map in figure 11 the depth profiles of the C_{ant} concentrations north and south of 5°N are plotted and demonstrate the difference between the two regions. North of 5°N C_{ant} concentrations are high in a thin surface layer and then rapidly decrease. In the equatorial band a more moderate decrease is apparent, which leads to overall higher column inventories.

A column inventory over the entire water column has been estimated with mean C_{ant} values below 1000 m, due to the sampling sparseness at depth. On average the entire column inventories are $48\,\text{mol}\,\text{m}^{-2}$ with a maximum of $55\,\text{mol}\,\text{m}^{-2}$ and a minimum of $42\,\text{mol}\,\text{m}^{-2}$. The column inventories estimated by *Gruber* [1998] (based on the ΔC^{*} method) for the latitude belt from the equator to 10°N in the year 1982 gave a mean value of $29\,\text{mol}\,\text{m}^{-2}$. The global C_{ant} column inventory maps by *Waugh et al.* [2006] (based on the TTD method) and by *Sabine et al.* [2004] (based on the ΔC^{*} method) for a mean sampling year of 1994, show column inventories of about $40\,\text{mol}\,\text{m}^{-2}$ and $38\,\text{mol}\,\text{m}^{-2}$, respectively, for the equatorial region. Considering the time difference of 25 years (1982 - 2007) and 13 years (1994 - 2007) between these estimates and the present work, the findings seem in good agreement.The percentaged atmospheric C_{ant} increase between the sampling years is comparable to the increase in the respective C_{ant} column inventories. However, a clear trend of higher C_{ant} inventories at the equator is not evident in the previous estimates.

3.4.2 Total inventory

A total C_{ant} inventory has been calculated for the area between 8 and 36°W and 4.5°S and 15°N. The size of the area is $6 \cdot 10^{6}\,\text{km}^{2}$ and a total water volume of $25 \cdot 10^{6}\,\text{km}^{3}$ is involved. The total inventory has been determined to be 3.4 Pg of anthropogenic carbon. At depth, where no data of C_{ant} are available, a concentration of $5\,\mu\text{mol}\,\text{kg}^{-1}$ was assumed. This is the mean value of all samples at depths between 2700 m and 3200 m and below 4100 m, where no direct influence of the upper LSW and the lower NADW is evident. In the year 1982 *Gruber* [1998] already found anthropogenic carbon all the way to the bottom in some regions of the

Atlantic Ocean. Between 40 and 50°N levels at depth were $>5\ \mu\text{mol kg}^{-1}$. Further south, levels decreased to almost zero below 2000 m, although below 4000 m a weak C_{ant} signal associated with Antarctic Bottom Water flowing north was visible [*Wallace*, 2001]. According to *Waugh et al.* [2006] 50% of the C_{ant} content is generally found in the upper 500 m and 75% in the upper 1500 m. In our estimates for the tropical Atlantic, the percentages found are lower (40% and 60%), because the entire water column is influenced by anthropogenic input and additionally the NADW at the equator contributes to increased C_{ant} values at depth.

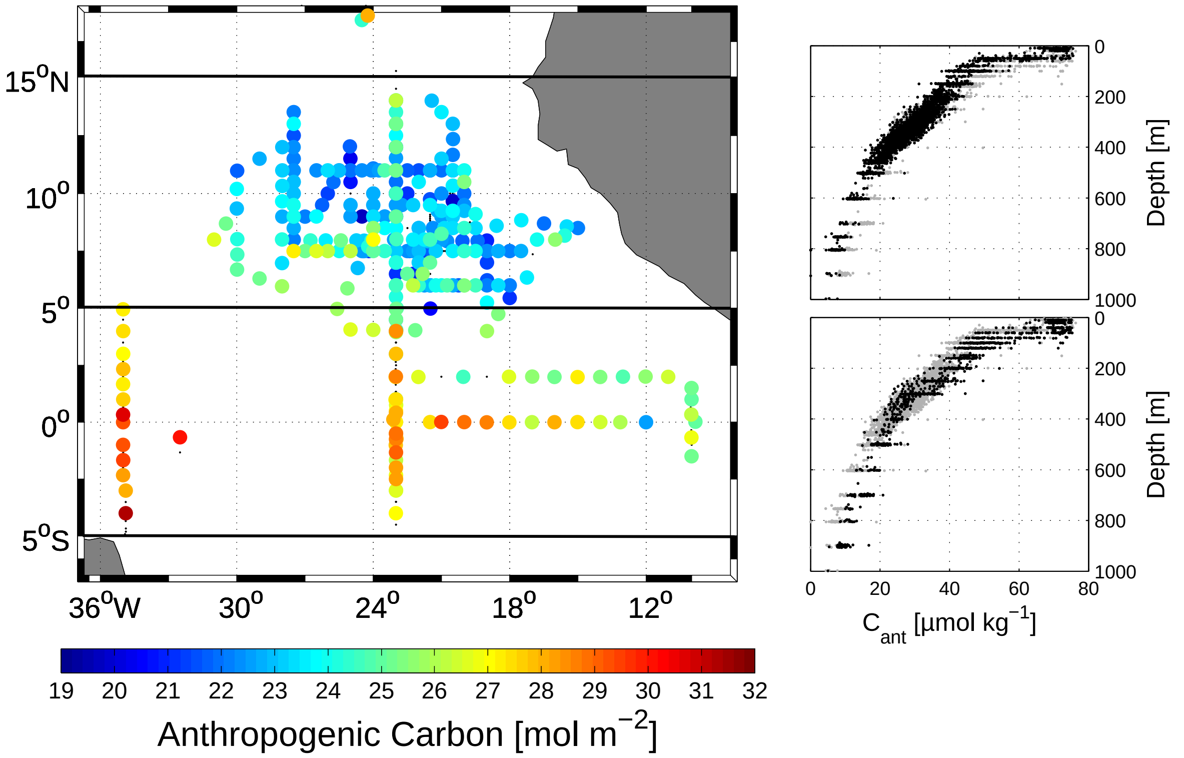

Figure 11: Column inventories of the upper 1000 m for all sampled stations. On the right hand side the C_{ant} depth profiles for the areas from 5°S to 5°N and from 5 to 15°N are shown.

By reason of the differences in water mass ages and the associated C_{ant} concentrations and column inventories, the study area is partitioned into two regions of same size. One spanning 4.5° north and south of the equator and the second one from 4.5 to 15°N, each with an area of $2.8 \cdot 10^6\ \text{km}^2$. The zonal extension was 11 - 36°W for both. For these two regions the total C_{ant} inventory turned out to be 1.4 Pg C in the northern part and 1.9 Pg C in the southern part. *Gruber* [1998] estimated an Atlantic C_{ant} inventory from the equator to 10°N of 2.3 Pg C in the year 1982. For the same area our C_{ant} estimates gave an inventory of 3.4 Pg C. Using the estimate by *Gruber* [1998] and extending it to the year 2007 by assuming the same relative C_{ant} increase in the ocean as in the atmosphere, would result in an inventory of 3.9 Pg of anthropogenic carbon in 2007.

4 Conclusions

The CFC-12 and SF_6 measurements from four cruises presented here provide an extensive and reliable dataset of the mean age and C_{ant} distribution in the tropical Atlantic Ocean. The

SF_6 measurements were used to a) improve the mean age estimates of waters with CFC-12 concentrations exceeding 450 ppt and b) to constrain a value of 0.5 for the Δ to Γ ratio, which is required for the TTD approach.

A comparison of the CFC-12 data with CFC-11 data collected on a cruise to the tropical Atlantic in 1999 [*Touratier et al.*, 2005] reveals identical characteristics in the depth profiles. The C_{ant} estimates based on the TrOCA method from that cruise in 1999 [*Touratier et al.*, 2005] also show the same main features in the water column but they exceed the C_{ant} concentrations estimated here with the TTD method by 5 - 10 $\mu\mathrm{mol\,kg^{-1}}$ and show much more scatter. The CFC-11 measurements in 1999 on a N-S section crossing the equator at 23°W from *Touratier et al.* [2005] were used to estimate C_{ant} concentrations with the TTD approach. The results are subtracted from the C_{ant} concentrations estimated on the same section as part of the present work and reveal an increase of 5 - 10 $\mu\mathrm{mol\,kg^{-1}}$ anthropogenic carbon in the upper 700 m for a period of 8 years. No or only little C_{ant} increase is observed in the AAIW, whereas the upper LSW again shows an increased positive change.

An analysis of mean age and C_{ant} distribution on isopycnals highlights differences between the equatorial belt and the area north of it: a) The mean age on an isopycnal decreases towards the south and the Guinea Dome area exhibits a pronounced local increase in mean age. b) The C_{ant} concentrations are increased in the equatorial region. On average, the column inventories in the upper 1000 m are 4 $\mathrm{mol\,m^{-2}}$ higher in the area from 5°S to 5°N than between 5° and 15°N. The total inventory in the equatorial belt is 35% higher. Existing estimates of C_{ant} inventories in the tropical Atlantic are unfortunately based on older samples (1982 [*Gruber*, 1998] and 1994 [*Waugh et al.*, 2006]) and thus a direct comparison to our results is difficult. However, by applying a linear scaling factor to the inventory estimates (based on the atmospheric C_{ant} increase between the different sampling years) reasonable agreement is found.

References

Bullister, J., and R. Weiss, Determination of CCl_3F and CCl_2F_2 in seawater and air, *Deep Sea Research Part A. Oceanographic Research Papers*, *35*, 839 – 853, 1988.

Bullister, J., D. Wisegarver, and F. Menzia, The solubility of sulfur hexafluoride in water and seawater, *Deep-Sea Research Part I-Oceanographic Research Papers*, *49*, 175–187, 2002.

Denman, K., et al., Couplings between changes in the climate system and biogeochemistry, in *Climate Change 2007: The Physical Science Basis. Contribution of Working Group I to the Fourth Assessment Report of the Intergovernmental Panel on Climate Change*, edited by S. Solomon, D. Qin, M. Manning, Z. Chen, M. Marquis, K. B. Averyt, T. M., and H. Miller, Cambridge University Press, Cambridge, United Kingdom and New York, NY, USA, 2007.

Etheridge, D., L. Steele, R. Langenfelds, R. Francey, J. Barnola, and V. Morgan, Natural and anthropogenic changes in atmospheric CO_2 over the last 1000 years from air in Antarctic ice and firn, *Journal of Geophysical Research-Atmospheres*, *101*, 4115–4128, 1996.

Gruber, N., Anthropogenic CO_2 in the Atlantic Ocean, *Global Biogeochemical Cycles*, *12*, 165–191, 1998.

Hall, T., and R. Plumb, Age as a diagnostic of stratospheric transport, *Journal of Geophysical Research-Atmospheres*, *99*, 1059–1070, 1994.

Maiss, M., and C. Brenninkmeijer, Atmospheric SF_6: Trends, sources, and prospects, *Environmental Science & Technology*, *32*, 3077–3086, 1998.

Morrison, J., et al., The oxygen minimum zone in the Arabian Sea during 1995, *Deep Sea Research Part II: Topical Studies in Oceanography*, *46*, 1903–1931, 1999.

NOAA/ESRL, *Halocarbons & other Atmospheric Trace Species Group (HATS)*, 2011, [http://www.esrl.noaa.gov/gmd/hats/index.html].

Oudot, C., J. Ternon, and J. Lecomte, Measurements of atmospheric and oceanic CO_2 in the Tropical Atlantic - 10 years after the 1982-1984 FOCAL cruises, *Tellus Series B-Chemical and Physical Meteorology*, *47*, 70–85, 1995.

Oudot, C., J. Ternon, C. Andrie, E. Braga, and P. Morin, On the crossing of the equator by intermediate water masses in the western Atlantic Ocean: Identification and pathways of Antarctic Intermediate Water and Upper Circumpolar Water, *Journal of Geophysical Research-Ocenas*, *104*, 20,911–20,926, 1999.

Rhein, M., and L. Stramma, Seasonal variability in the Deep Western Boundary Current around the Eastern tip of Brazil, *Deep-Sea Research Part I-Oceanographic Research Papers*, *52*, 1414–1428, 2005.

Rhein, M., L. Stramma, and U. Send, The Atlantic Deep Western Boundary Current - Water masses and transports near the equator, *Journal of Geophysical Research-Oceans*, *100*, 2441–2457, 1995.

Sabine, C., et al., The oceanic sink for anthropogenic CO_2, *Science*, *305*, 367–371, 2004.

Schott, F., J. Junior McCreary, and G. Johnson, Shallow overturning circulations of the tropical-subtropical oceans, in *Earth's Climate : the Ocean-Atmosphere Interaction*, edited by Chunzai Wang and Shang-Ping Xie and James A. Carton, Geophysical Monograph, pp. 261–304, AGU, Washington, DC, USA, 2004.

Siedler, G., and R. Onken, Eastern recirculation, in *The Warmwatersphere of the North Atlantic Ocean*, edited by W. Krauß, vol. Ch.11, pp. 339–364, Gebrüder Borntraeger, Berlin, Stuttgart, 1996.

Siedler, G., N. Zangenberg, and R. Onken, Seasonal changes in the Tropical Atlantic Circulation - Observation and simulation of the Guinea Dome, *Journal of Geophysical Research-Oceans*, *97*, 703–715, 1992.

Stramma, L., and F. Schott, The mean flow field of the tropical Atlantic Ocean, *Deep-Sea Research Part II-Topical Studies in Oceanography*, *46*, 279–303, 1999.

Stramma, L., P. Brandt, J. Schafstall, F. Schott, J. Fischer, and A. Körtzinger, Oxygen minimum zone in the North Atlantic south and east of the Cape Verde Islands, *Journal of Geophysical Research-Oceans*, *113*, 2008.

Takahashi, T., et al., Climatological mean and decadal change in surface ocean pCO_2, and net sea-air CO_2 flux over the global oceans, *Deep-Sea Research Part II-Topical Studies in Oceanography*, *56*, 554–577, 2009.

Tanhua, T., D. W. Waugh, and D. W. R. Wallace, Use of SF_6 to estimate anthropogenic CO_2 in the upper ocean, *Journal of Geophysical Research-Oceans*, *113*, 2008.

Tans, P., *Trends in Atmospheric Carbon Dioxide (NOAA/ESRL)*, 2011, [http://www.esrl.noaa.gov/gmd/ccgg/trends/].

Tomczak, M., and J. Godfrey, *Regional Oceanography: An Introduction*, Elsevier, 1994.

Touratier, F., and C. Goyet, Applying the new TrOCA approach to assess the distribution of anthropogenic CO_2 in the Atlantic Ocean, *Journal of Marine Systems*, *46*, 181–197, 2004.

Touratier, F., C. Goyet, C. Coatanoan, and C. Andrie, Assessments of anthropogenic CO_2 distribution in the tropical Atlantic Ocean, *Deep-Sea Research Part I-Oceanographic Research Papers*, *52*, 2275–2284, 2005.

Walker, S., R. Weiss, and P. Salameh, Reconstructed histories of the annual mean atmospheric mole fractions for the halocarbons CFC-11, CFC-12, CFC-113, and carbontetrachloride, *Journal of Geophysical Research-Oceans*, *105*, 14,285–14,296, 2000.

Wallace, D., Storage and Transport of Excess CO_2 in the Oceans: the JGOFS/WOCE Global CO_2 Survey, in *Ocean Circulation and Climate*, edited by John Church and Gerold Siedler and John Gould, pp. 489–521, Academic Press, London, San Diego, 2001.

Wanninkhof, R., S. C. Doney, J. L. Bullister, N. M. Levine, M. Warner, and N. Gruber, Detecting anthropogenic CO_2 changes in the interior Atlantic Ocean between 1989 and 2005, *Journal of Geophysical Research-Oceans*, *115*, 2010.

Warner, M., and R. Weiss, Solubilities of Chlorofluorocarbon-11 and Chlorofluorocarbon-12 in water and seawater, *Deep-Sea Research Part A-Oceanographic Research Papers*, *32*, 1485–1497, 1985.

Warner, M., and R. Weiss, Chlorofluoromethanes in South-Atlantic Antarctic Intermediate Water, *Deep-Sea Research Part A-Oceanographic Research Papers*, *39*, 2053–2075, 1992.

Warren, B., Context of the suboxic layer in the Arabian Sea, *Journal of Earth System Science*, *103*, 301–314, 1994, 10.1007/BF02839540.

Waugh, D., T. Haine, and T. Hall, Transport times and anthropogenic carbon in the subpolar North Atlantic Ocean, *Deep-Sea Research Part I-Oceanographic Research Papers*, *51*, 1475–1491, 2004.

Waugh, D. W., T. M. Hall, B. I. McNeil, R. Key, and R. J. Matear, Anthropogenic CO_2 in the oceans estimated using transit time distributions, *Tellus Series B-Chemical and Physical Meteorology*, *58*, 376–389, 2006.

Weiss, R. F., and B. A. Price, Nitrous oxide solubility in water and seawater, *Marine Chemistry*, *8*, 347–359, 1980.

Weiss, R. F., J. L. Bullister, R. H. Gammon, and M. J. Warner, Atmospheric chlorofluoromethanes in the deep equatorial Atlantic, *Nature*, *314*, 608–610, 1985.

6 Conclusions and Outlook

Mediterranean Sea:

- The negative intercept of the alkalinity-salinity regression in Mediterranean waters is a result of strong evaporation in the basin combined with alkalinity inputs by rivers and the Black Sea at the high salinity end of the correlation.
- Sources of alkalinity for the Mediterranean Sea are rivers and the Black Sea in roughly equal proportion. The main sink of alkalinity appears to be sedimentation of carbonates and to one third the exchange with the Atlantic Ocean through the Strait of Gibraltar.
- Mediterranean waters are supersaturated throughout with respect to calcite and aragonite. Hence, the excess alkalinity at depth can not be a result of carbonate dissolution but of the high alkalinity signal from rivers and the Black Sea. In the intermediate and deep water formation areas these high alkalinity waters are probably transfered to depth whereas the surface waters are mainly affected by low alkalinity water from the Atlantic.
- The residence time of water in the Mediterranean Sea has been estimated to be 150 years. Consequently the mean ages found in the basin are low (maximum mean age is less than 140 years) and the entire water column has been affected by anthropogenic emissions.
- The $p\mathrm{CO}_2$ of water subducting in the deep water formation areas is assumed to be undersaturated with respect to atmospheric CO_2 mixing ratios.
- The maximum C_{ant} column inventories are about 45% higher than in the North Atlantic deep water formation area and the total C_{ant} inventory of 1.7 Pg makes 1.1% of the global estimate, while the water volume represents only 0.3%. A low Revelle factor combined with deep water formation has been hypothesized to be the reason for the high C_{ant} concentrations and inventories in the Mediterranean basin.
- A net export of 38 $\mathrm{Tg\,C\,yr^{-1}}$ into the Atlantic Ocean has been estimated at the Strait of Gibraltar. The net flux of anthropogenic carbon is in opposite direction into the Mediterranean Sea and amounts to 3.5 $\mathrm{Tg\,C\,yr^{-1}}$. However, more than 90% of the total C_{ant} have been taken up directly from the atmosphere within the basin.

Tropical Atlantic:

- C_{ant} estimates using CFC-12 measurements and the TTD method are effectively improved with additional SF_6 measurements. Firstly, for samples exceeding CFC-12 concentrations of 450 ppt (young waters), the SF_6 measurements produce more reliable age estimates, because in contrast to hardly changing atmospheric CFC-12 concentrations in the past 20 years, atmospheric SF_6 concentrations continue to increase. And secondly, with the help of SF_6 the appropriate value for the Δ to Γ ratio, which is required for the TTD calculations, has been determined to be 0.5 in the upper 1500 m of the tropical Atlantic.

- The C_{ant} increase in the tropical Atlantic between 1999 and 2006 - 2009 is more than 10 μmol kg^{-1} in the mixed layer and between 5 and 10 μmol kg^{-1} in the water column down to 700 m depth. Around 1000 m (Antarctic Intermediate Water and Upper Circumpolar Water) there is no discernible change in C_{ant}. Below that depth, in the upper Labrador Sea Water, again an increase of 0 - 5 μmol kg^{-1} is observed.

- The equatorial band from 5°S to 5°N is characterized by younger waters with increased C_{ant} concentrations compared to waters on the same isopycnals in the area north of 5°N. The column inventories of the upper 1000 m in the equatorial band are 4 mol m^{-2} higher (+18%) than between 5°N and 15°N. The total inventory is increased by 35%, which is the result of the additional contribution of Labrador Sea Water and lower North Atlantic Deep Water carrying increased C_{ant} concentrations at depth.

- An upward displacement of isochrones (layers of the same age) is apparent in the Guinea Dome and has been attributed to upwelling of older water or to decreased ventilation in the area.

The presented work reveals that the C_{ant} concentrations and inventories in marginal seas or in certain other regions can vary substantially from mean global estimates. *Lee et al.* [2011] also found increased C_{ant} storage capacity in four marginal seas with overturning circulation (including the Mediterranean Sea) compared to the global ocean. Thus, measurements in such regions help to improve estimates for the total anthropogenic carbon that has been taken up by the ocean since preindustrial times. Further, it is important to understand the behavior of C_{ant} uptake and how it changes over time in order to predict future changes in global oceanic uptake associated with increasing atmospheric CO_2 concentrations and with changes in the biogeochemistry caused by global warming, climate change and also human-induced perturbations (e.g. nutrient inputs, river discharge and carbonate chemistry). This information could be provided by investigation of marginal seas with and without overturning circulation and by combining different methods to determine C_{ant}. The SF_6 measurements are a potential tool for age calculations of younger water masses and thus for identifying changes in water movement and circulation in the upper ocean. However, it is necessary to improve its analysis in order to improve the precision and the accuracy of the SF_6 concentrations. Knowledge of the carbonate system parameters in the mixed layer and their change over time, as well as the saturation of the tracers in the surface ocean will improve the assumptions of the TTD method and thereby the C_{ant} estimates.

Purpose of a recent cruise to the Mediterranean Sea is the repeated sampling of the basin complementary to the measurement made in 2001. The tracers SF_6 and CFC-12 plus the carbonate system parameters were determined, which will allow to constrain the appropriate Δ to Γ ratio for the Mediterranean Sea and thus to reduce the uncertainties in the C_{ant} estimates. Some additional stations in the deep water formation area of the Adriatic Sea will provide data to test the hypothesis of greatly increased surface alkalinity in this region and its transfer to depth, as well as the CO_2 undersaturation of the subducting waters. The repeated measurements with a time difference of 10 years to the previous cruise allows the determination of a decadal C_{ant} increase in two different ways. On the one hand by using the eMLR approach and on the other hand by subtraction of the C_{ant} estimates of both cruises based on the TTD method.

Acknowledgements

I would like to thank Prof. Dr. Douglas Wallace and Prof. Dr. Arne Körtzinger for making this thesis possible. Even if Doug's schedule did not allow for much time, his scientific input always took me a big step forward. Special thanks go to Arne, who was always willing to discuss several problems with me - sometimes over and over again.

Thanks to Toste who introduced me to the TTD method, provided several Matlab scripts to get started with my work and who gave a lot of input to the analytical work in the laboratory and at sea.

I am very grateful to Tina for sharing her enormous experience in the laboratory and for being that patient with me.

Funding for this work was provided by the CarboOcean IP of the European Comission (grant 511176-2) and by the Deutsche Forschungsgemeinschaft (DFG).

There are several other people I would like to thank:

Tobi, for discussing more than 5 years about CO_2, the carbonate system and life and for answering all my questions concerning Matlab and chemistry. Thanks for making my last cruise unforgettable and for all the laughters in all situations (tsunami, telephone, disputation) and for the sometimes very hard trainings.

Alina, for endless discussions about the wondrously TTD.

Hermann and Birgit, for being wonderful colleagues and supporting my work whenever they could.

Moritz, for always supporting me in every sense and for prove-reading part of the thesis.

My father Eckart, for prove-reading part of the thesis.

My brother Jan, for also prove-reading part of the thesis and for sharing his PhD experience with me plus the habit to do everything at the very last moment.

My flatmate Julia, for sharing time and wine in our kitchen and talking about all our sorrows.

Katha, for talking about everything but science until the early morning hours.

My parents for believing in me.

Chloe for sending chocolate.

And last but not least my volleyball team, for tolerating my moods in the hot phase and providing a survival pack.

Bibliography

Andrié, C., Chlorofluoromethanes in the deep equatorial Atlantic revisited, in *The South Atlantic: present and past circulation*, pp. 273–288, Springer, 1996.

Andrié, C., M. Rhein, S. Freudenthal, and O. Plahn, CFC time series in the deep water masses of the western tropical Atlantic, 1990-1999, *Deep-Sea Research Part I-Oceanographic Research Papers*, *49*, 281–304, 2002.

Barnola, J. M., D. Raynaud, Y. S. Korotkevich, and C. Lorius, Vostok ice core provides 160,000-year record of atmospheric CO_2, *Nature*, *329*, 408–414, 1987.

Beining, P., and W. Roether, Temporal evolution of CFC-11 and CFC-12 concentrations in the ocean interior, *Journal of Geophysical Research-Oceans*, *101*, 16,455–16,464, 1996.

Bethoux, J., B. Gentili, P. Morin, E. Nicolas, C. Pierre, and D. Ruiz-Pino, The Mediterranean Sea: a miniature ocean for climatic and environmental studies and a key for the climatic functioning of the North Atlantic, *Progress in Oceanography*, *44*, 131–146, 1999.

Brewer, P., Direct observation of the oceanic CO_2 increase, *Geophysical Research Letters*, *5*, 997–1000, 1978.

Broecker, W., S. Sutherland, W. Smethie, T. Peng, and G. Ostlund, Oceanic radiocarbon - separation of the natural and bomb components, *Global Biogeochemical Cycles*, *9*, 263–288, 1995.

Bullister, J., *Atmospheric CFC, CCl_4, and SF_6 History Update*, 2010, [http://cdiac.ornl.gov/oceans/new_atmCFC.html].

Bullister, J., and R. Weiss, Determination of CCl_3F and CCl_2F_2 in seawater and air, *Deep Sea Research Part A. Oceanographic Research Papers*, *35*, 839 – 853, 1988.

Bulsiewicz, K., H. Rose, O. Klatt, A. Putzka, and W. Roether, A capillary-column chromatographic system for efficient chlorofiuorocarbon measurement in ocean waters, *Jounal of Geophysical Research*, *103*, 15,959–15,970, 1998.

Carpenter, J., New measurements of oxygen solubility in pure and natural water, *Limnology and Oceanography*, *11*, 264–277, 1965.

Chen, C., and F. Millero, Gradual increase of oceanic carbon dioxide, *Nature*, *277*, 205–206, 1979.

Chester, R., *Marine Geochemistry*, Wiley-Blackwell, 2003.

Civitarese, G., M. Gacic, M. Lipizer, and G. L. E. Borzelli, On the impact of the Bimodal Oscillating System (BiOS) on the biogeochemistry and biology of the Adriatic and Ionian Seas (Eastern Mediterranean), *Biogeosciences*, *7*, 3987–3997, 2010.

Deleersnijder, E., J. Campin, and E. Delhez, The concept of age in marine modelling I. Theory and preliminary model results, *Journal of Marine Systems*, *28*, 229–267, 2001.

Delhez, E., J. Campin, A. Hirst, and E. Deleersnijder, Toward a general theory of the age in ocean modelling, *Ocean Modelling*, *1*, 17 – 27, 1999.

Dickson, A., An exact definition of total alkalinity and a procedure for the estimation of alkalinity and total inorganic carbon from titration data, *Deep-Sea Research Part A-Oceanographic Research Papers*, *28*, 609 – 623, 1981.

Doney, S. C., V. J. Fabry, R. A. Feely, and J. A. Kleypas, Ocean Acidification: The other CO_2 problem, *Annual Review of Marine Science*, *1*, 169–192, 2009.

Etheridge, D., L. Steele, R. Langenfelds, R. Francey, J. Barnola, and V. Morgan, Natural and anthropogenic changes in atmospheric CO_2 over the last 1000 years from air in Antarctic ice and firn, *Journal of Geophysical Research-Atmospheres*, *101*, 4115–4128, 1996.

Forster, P., et al., Changes in atmospheric constituents and in radiative forcing, in *Climate Change 2007: The Physical Science Basis. Contribution of Working Group I to the Fourth Assessment Report of the Intergovernmental Panel on Climate Change*, edited by S. Solomon, D. Qin, M. Manning, Z. Chen, M. Marquis, K. B. Averyt, T. M., and H. Miller, Cambridge University Press, Cambridge, United Kingdom and New York, NY, USA, 2007.

Friedrichs, M., M. McCarntey, and M. Hall, Hemispheric-Asymmetry of Deep-Water Transport Modes in the Western Atlantic, *Journal of Geophysical Research-Oceans*, *99*, 25,165–25,179, 1994.

Friis, K., A review of marine anthropogenic CO_2 definitions: introducing a thermodynamic approach based on observations, *Tellus Series B-Chemical and Physical Meteorology*, *58*, 2–15, 2006.

Friis, K., A. Körtzinger, J. Pätsch, and D. Wallace, On the temporal increase of anthropogenic CO_2 in the subpolar North Atlantic, *Deep-Sea Research Part I-Oceanographic Research Papers*, *52*, 681–698, 2005.

Gascard, J., Mediterranean deep water formation baroclinic instability and oceanic eddies, *Oceanologica Acta*, *1*, 315–330, 1978.

Goyet, C., C. Coatanoan, G. Eischeid, T. Amaoka, K. Okuda, R. Healy, and S. Tsunogai, Spatial variation of total CO_2 and total alkalinity in the northern Indian Ocean: A novel approach for the quantification of anthropogenic CO_2 in seawater, *Journal of Marine Research*, *57*, 135–163, 1999.

Grodsky, S., and J. Carton, Surface drifter pathways originating in the equatorial Atlantic cold tongue, *Geophysical Research Letters*, *29*, 2002.

Gruber, N., J. Sarmiento, and T. Stocker, An improved method for detecting anthropogenic CO_2 in the oceans, *Global Biogeochemical Cycles*, *10*, 809–837, 1996.

Haine, T., and T. Hall, A generalized transport theory: Water-mass composition and age, *Journal of Physical Oceanography*, *32*, 1932–1946, 2002.

Haine, T., and K. Richards, The influence of the seasonal mixed-layer on oceanic uptake of CFCs, *Journal of Geophysical Research-Oceans*, *100*, 10,727–10,744, 1995.

Hall, T., and R. Plumb, Age as a diagnostic of stratospheric transport, *Journal of Geophysical Research-Atmospheres*, *99*, 1059–1070, 1994.

Johns, W., T. Lee, R. Beardsley, J. Candela, R. Limeburner, and B. Castro, Annual cycle and variability of the North Brazil Current, *Journal of Physical Oceanography*, *28*, 103–128, 1998.

Johnson, K., W. KD, D. Butler, W. Johnson, and C. Wong, Coulometric total carbon-dioxide analysis for marine studies - Maximizing the performance of an automated gas extraction system and coulometric detector, *Marine Chemistry*, *44*, 167–187, 1993.

Josey, S., D. Oakley, and R. Pascal, On estimating the atmospheric longwave flux at the ocean surface from ship meteorological reports, *Journal of Geophysical Research-Oceans*, *102*, 27,961–27,972, 1997.

Key, R., et al., A global ocean carbon climatology: Results from Global Data Analysis Project (GLODAP), *Global Biogeochemical Cycles*, *18*, 2004.

Klein, B., W. Roether, B. Manca, D. Bregant, V. Beitzel, V. Kovacevic, and A. Luchetta, The large deep water transient in the Eastern Mediterranean, *Deep-Sea Research Part I-Oceanographic Research Papers*, *46*, 371–414, 1999.

Körtzinger, A., P. Quay, and R. Sonnerup, Relationship between anthropogenic CO_2 and the ^{13}C Suess effect in the North Atlantic Ocean, *Global Biogeochemical Cycles*, *17*, 2003.

Kress, N., and B. Herut, Spatial and seasonal evolution of dissolved oxygen and nutrients in the Southern Levantine Basin (Eastern Mediterranean Sea): chemical characterization of the water masses and inferences on the N : P ratios, *Deep-Sea Research Part I-Oceanographic Research Papers*, *48*, 2347–2372, 2001.

Krom, M., N. Kress, S. Brenner, and L. Gordon, Phosphorus Limitation of Primary Productivity in the Eastern Mediterranean Sea, *Limnology and Oceanography*, *36*, 424–432, 1991.

Lascaratos, A., W. Roether, K. Nittis, and B. Klein, Recent changes in deep water formation and spreading in the eastern Mediterranean Sea: a review, *Progress in Oceanography*, *44*, 5–36, 1999.

Lee, K., C. L. Sabine, T. Tanhua, T.-W. Kim, R. A. Feely, and H.-C. Kim, Roles of marginal seas in absorbing and storing fossil fuel CO2, *Energy & Environmental Science*, *4*, 1133–1146, 2011.

Lo Monaco, C., N. Metzl, A. Poisson, C. Brunet, and B. Schauer, Anthropogenic CO_2 in the Southern Ocean: Distribution and inventory at the Indian-Atlantic boundary (World Ocean Circulation Experiment line I6), *Journal of Geophysical Research-Oceans*, *110*, 2005.

Luyten, J., and H. Stommel, Gyres Driven by Combined Wind and Buoyancy Flux, *Journal of Physical Oceanography*, *16*, 1551–1560, 1986.

Mintrop, L., F. Perez, M. Gonzalez-Davila, M. Santana-Casiano, and A. Körtzinger, Alkalinity determination by potentiometry: Intercalibration using three different methods, *Ciencias Marinas*, *26*, 23–37, 2000.

Molinari, R., S. Garzoli, E. Katz, D. Harrison, P. Richardson, and G. Reverdin, A synthesis of the first GARP Global Experiment (FGGE) in the equatorial Atlantic Ocean, *Progress In Oceanography*, *16*, 91 – 112, 1986.

Ovchinnikov, I., Intermediate water formation in the Mediterranean Sea, *Oceanology*, *24*, 217–225, 1984.

Pearson, P., and M. Palmer, Atmospheric carbon dioxide concentrations over the past 60 million years, *Nature*, *406*, 695–699, 2000.

Perez, F., M. Alvarez, and A. Rios, Improvements on the back-calculation technique for estimating anthropogenic CO_2, *Deep-Sea Research Part I-Oceanographic Research Papers*, *49*, 859–875, 2002.

Petit, J., et al., Climate and atmospheric history of the past 420,000 years from the Vostok ice core, Antarctica, *Nature*, *399*, 429–436, 1999.

Pilson, M., *An Introduction to the Chemistry of the Sea*, Prentice-Hall, 1998.

Pollak, M., The sources of the deep water of the Mediterranean Sea, *Journal of Marine Research*, *10*, 128–151, 1951.

Quay, P., B. Tilbrook, and C. Wong, Oceanic uptake of fossil-fuel CO_2: ^{13}C evidence, *Science*, *256*, 74–79, 1992.

Revelle, R., and H. Suess, Carbon dioxide exchange between atmosphere and ocean and the question of an increase of atmospheric CO_2 during the past decades, *Tellus*, *9*, 18–27, 1957.

Rhein, M., and L. Stramma, Seasonal variability in the Deep Western Boundary Current around the Eastern tip of Brazil, *Deep-Sea Research Part I-Oceanographic Research Papers*, *52*, 1414–1428, 2005.

Rhein, M., L. Stramma, and U. Send, The Atlantic Deep Western Boundary Current - Water masses and transports near the equator, *Journal of Geophysical Research-Oceans*, *100*, 2441–2457, 1995.

Roether, W., and R. Schlitzer, Eastern Mediterranean deep water renewal on the basis of chlorofluoromethane and tritium data, *Dynamics of Atmospheres and Oceans*, *15*, 333 – 354, 1991, The Mediterranean Sea.

Roether, W., B. Manca, B. Klein, D. Bregant, D. Georgopoulos, V. Beitzel, V. Kovacevic, and A. Luchetta, Recent changes in eastern Mediterranean deep waters, *Science*, *271*, 333–335, 1996.

Sabine, C., et al., The oceanic sink for anthropogenic CO_2, *Science*, *305*, 367–371, 2004.

Schlitzer, R., W. Roether, H. Oster, H. Junghans, M. Hausmann, H. Johannsen, and A. Michelato, Chlorofluoromethane and oxygen in the Eastern Mediterranean, *Deep Sea Research Part A. Oceanographic Research Papers*, *38*, 1531 – 1551, 1991.

Schott, F., J. Fischer, and L. Stramma, Transports and Pathways of the Upper-Layer Circulation in the Western Tropical Atlantic, *Journal of Physical Oceanography*, *28*, 1904–1928, 1998.

Schott, F., M. Dengler, P. Brandt, K. Affler, J. Fischer, B. Bourles, Y. Gouriou, R. Molinari, and M. Rhein, The zonal currents and transports at 35°W in the tropical Atlantic, *Geophysical Research Letters*, *30*, 1349–1352, 2003.

Schott, F., J. Junior McCreary, and G. Johnson, Shallow overturning circulations of the tropical-subtropical oceans, in *Earth's Climate : the Ocean-Atmosphere Interaction*, edited by Chunzai Wang and Shang-Ping Xie and James A. Carton, Geophysical Monograph, pp. 261–304, AGU, Washington, DC, USA, 2004.

Shiller, A., Calculating the Oceanic CO_2 Increase: A Need for Caution, *Journal of Geophysical Research-Oceans*, *86*, 11,083–11,088, 1981.

Siedler, G., N. Zangenberg, and R. Onken, Seasonal changes in the Tropical Atlantic Circulation - Observation and simulation of the Guinea Dome, *Journal of Geophysical Research-Oceans*, *97*, 703–715, 1992.

Steinfeldt, R., Ages and age spectra of Eastern Mediterranean deep water, *Journal of Marine Systems*, *48*, 67–81, 2004.

Stramma, L., and F. Schott, The mean flow field of the tropical Atlantic Ocean, *Deep-Sea Research Part II-Topical Studies in Oceanography*, *46*, 279–303, 1999.

Stratford, K., and R. Williams, A tracer study of the formation, dispersal, and renewal of Levantine Intermediate Water, *Journal of Geophysical Research-Oceans*, *102*, 12,539–12,549, 1997.

Stratford, K., R. Williams, and P. Drakopoulos, Estimating climatological age from a model-derived oxygen-age relationship in the Mediterranean, *Journal of Marine Systems*, *18*, 215–226, 1998.

Takahashi, T., et al., Climatological mean and decadal change in surface ocean pCO_2, and net sea-air CO_2 flux over the global oceans, *Deep-Sea Research Part II-Topical Studies in Oceanography*, *56*, 554–577, 2009.

Tans, P., *Trends in Atmospheric Carbon Dioxide (NOAA/ESRL)*, 2011, [http://www.esrl.noaa.gov/gmd/ccgg/trends/].

Theocharis, A., K. Nittis, K. Kontoyiannis, E. Papageorgiou, and E. Balopoulos, Climatic changes in the Aegean Sea influence the Eastern Mediterranean thermohaline circulation (1986-1997), *Geophysical Research Letters*, *26*, 1617–1620, 1999.

Touratier, F., and C. Goyet, Applying the new TrOCA approach to assess the distribution of anthropogenic CO_2 in the Atlantic Ocean, *Journal of Marine Systems*, *46*, 181–197, 2004.

Touratier, F., L. Azouzi, and C. Goyet, CFC-11, $\Delta^{14}C$ and ^{3}H tracers as a means to assess anthropogenic CO_2 concentrations in the ocean, *Tellus Series B-Chemical and Physical Meteorology*, *59*, 318–325, 2007.

Wallace, D., Monitoring global ocean carbon inventories, OOSDP Background Report. Texas A&M University, College Station, Texas, USA, 1995.

Waugh, D., T. Haine, and T. Hall, Transport times and anthropogenic carbon in the subpolar North Atlantic Ocean, *Deep-Sea Research Part I-Oceanographic Research Papers*, *51*, 1475–1491, 2004.

Wolf-Gladrow, D. A., R. E. Zeebe, C. Klaas, A. Körtzinger, and A. G. Dickson, Total alkalinity: The explicit conservative expression and its application to biogeochemical processes, *Marine Chemistry*, *106*, 287–300, 2007.

Zeebe, R., and D. Wolf-Gladrow, *CO_2 in seawater: Equilibrium, kinetics, isotopes*, Elsevier, 2001.

Abbreviations

A_{adj}	Salinity adjusted total alkalinity
AA-II	AutoAnalyzer II
AD	Angola Dome
AABW	Antarctic Bottom Water
AAIW	Antarctic Intermediate Water
ADCP	Acoustic Doppler Current Profiler
AOU	Apparent oxygen utilization
A_{C}	Carbonate alkalinity
A_{T}	Total alkalinity
$A_{\mathrm{T}}^{\mathrm{Ex}}$	Excess alkalinity
AW	Atlantic Water
BiOS	Bimodal Oscillating System
c	Centi $(1 \cdot 10^{-2})$
C	Carbon
C_{ant}	Anthropogenic carbon
C_{bio}	Change in C_{T} due to biological production and respiration
C_{carb}	Change in C_{T} due to calcium carbonate production and dissolution
CO_2	Carbon dioxide
CDIAC	Carbon Dioxide Information Analysis Center
CFC	Clorofluorocarbon
CFC-11	Trichlorofluoromethane
CFC-12	Dichlorodifluoromethane
CFC-113	Trichlorotrifluoroethane
C_{T}	Total dissolved inorganic carbon (also: DIC)
C_{T}^{0}	Preformed carbon
CTD	Conductivity, temperature, depth sensor
CRM	Certified Reference Material
CW	Central Water
Δ	'Width' of the TTD
ΔC^*	A back-calculation technique to estimate C_{ant}
DFG	Deutsche Forschungsgemeinschaft
DIC	Total dissolved inorganic carbon (also: C_{T})
EC	Equatorial Current
ECD	Electron Capture Detector
EIC	Equatorial Intermediate Current
EMDW	Eastern Mediterranean Deep Water
eMLR	Extended Multiple Linear Regression
EUC	Equatorial Undercurrent

f	Femto $(1 \cdot 10^{-15})$
GC	Gas chromatograph
GD	Guinea Dome
GLODAP	Global Ocean Data Analysis Project
GWP	Global Warming Potential
Γ	'Mean age' of the TTD
ITCZ	Intertropical Convergence Zone
k	Kilo $(1 \cdot 10^{3})$
K_1	First dissociation constant of carbonic acid
K_2	Second dissociation constant of carbonic acid
K_{sp}	Solubility constant of calcite or aragonite
LIW	Levantine Intermediate Water
LSW	Labrador Sea Water
m	Milli $(1 \cdot 10^{-3})$
μ	Mycro $(1 \cdot 10^{-6})$
M51/2	Meteor cruise 51/2
M68/2	Meteor cruise 68/2
M80/1	Meteor cruise 80/1
M80/2	Meteor cruise 80/2
MAW	Modified Atlantic Water
MLR	Multiple Linear Regression
MOC	Meridional Overturning Circulation
MOW	Mediterranean Overflow Water
MSM10/1	Maria S. Merian cruise 10/1
NACW	North Atlantic Central Water
NADW	North Atlantic Deep Water
NBC	North Brazilian Current
NBUC	North Brazilian Undercurrent
NEC	North Equatorial Current
NECC	North Equatorial Coutercurrent
NEUC	North Equatorial Undercurrent
NICC	North Intermediate Counterurrent
Ω	Saturation state of carbonate
p	Pico $(1 \cdot 10^{-12})$
pH	Negative common logarithm of the hydrogen ion concentration (-log $[\mathrm{H}^+]$)
pK_1	Negative common logarithm of the first dissociation constant of carbonic acid
pK_2	Negative common logarithm of the second dissociation constant of carbonic acid
P	Peta $(1 \cdot 10^{15})$
P	Pressure
P_{atm}	Atmospheric pressure
$P_{\mathrm{H_2O}}(T,S)$	T and S dependent partial pressure of water vapor
$p\mathrm{CO}_2$	Partial pressure of carbon dioxide
PP	Preformed preindustrial
ppm	Parts per million
ppt	Parts per trillion
PT1/PT2	Purge and Trap system 1 and 2
R/V	Research Vessel
S	Salinity

S_{ref}	Reference salinity
SACW	South Atlantic Central Water
SEC	South Equatorial Current
SEUC	South Equatorial Undercurrent
SF_6	Sulfur hexafluoride
SICC	South Intermediate Counterurrent
SIO	Scripps Institution of Oceanography
SST	Sea Surface Temperature
STC	Subtropical Cell
Sv	Severdrup ($1\ \mathrm{Sv} = 1 \cdot 10^6\ \mathrm{m}^3\,\mathrm{s}^{-1}$)
σ_Θ	Potential density
T	Tera ($1 \cdot 10^{12}$)
T	Temperature
TrOCA	Tracer combining Oxygen, inorganic Carbon and total Alkalinity
TTD	Transit time distribution
τ	Residence time
WMDW	Western Mediterranean Deep Water
WOCE	World Ocean Circulation Experiment

Eidesstattliche Versicherung

Ich versichere an Eides statt, dass ich die von mir vorgelegte Dissertation - abgesehen von der Beratung durch meinen Betreuer - selbstständig und ohne unerlaubte Hilfe angefertigt habe und alle benutzten Quellen und Hilfsmittel vollständig angegeben habe. Die Zusammenarbeit mit anderen Wissenschaftlern habe ich kenntlich gemacht. Die Arbeit ist unter Einhaltung der Regeln guter wissenschaftlicher Praxis der Deutschen Forschungsgemeinschaft entstanden. Ferner habe ich weder diese noch eine ähnliche Arbeit an einer anderen Abteilung oder Hochschule im Rahmen eines Prüfungsverfahrens vorgelegt, veröffentlicht oder zur Veröffentlichung vorgelegt.

Kiel, 04. Mai 2011 ....
Anke Schneider

Curriculum Vitae

Anke Schneider
born 16. January 1978 in Lich
German

Presentations:

Schneider, A. (September 2010). DISCO symposium, Honolulu, Hawaii, USA (oral): Tracers and anthropogenic carbon in the ocean.

Schneider, A., T. Tanhua, A. Körtzinger und D.W.R. Wallace (October 2009). CARBOOCEAN final meeting, Bergen, Norway (oral): Surprisingly high anthropogenic CO_2 in the eastern Mediterranean.

Schneider, A., D.W.R. Wallace, T. Tanhua, B. Klein und W. Roether (April 2008). EGU General Assembly, Wien, Austria (poster): Anthropogenic carbon in the Mediterranean Sea.

Publications:

Schneider, A., T. Tanhua, A. Körtzinger und D.W.R. Wallace (**2010**). High anthropogenic carbon content in the eastern Mediterranean. *Journal of Geophysical Research - Oceans*, 115 (C12), doi: 10.1029/2010JC006171.

Schneider, A., A. Körtzinger und D.W.R. Wallace (**2007**). Alkalinity of the Mediterranean Sea. *Geophysical Research Letters*, 34 (15), doi: 10.1029/2006GL028842.

Research cruises:

2009	Meteor 80/1, Tropical Atlantic
2008	MS Merian 10/1, Tropical Atlantic
2007	Heincke 273, Baltic Sea
2006	Meteor 68/2, Equatorial Atlantic

Awards and Scholarships:

July 2008	Second poster prize for the poster: "Anthropogenic carbon in the Mediterranean Sea" presented at the summer school "Observing and Understanding Earth" in Konstanz, Germany
04/04 - 12/04	Scholarship from the DAAD: "Stipendium zum Anfertigen von Abschlussarbeiten"

Summer Schools:

July 2008	Zukunftskolleg Summer School "Observing and Understanding Earth", Konstanz, Germany.
October 2007	Third international SOLAS Summer School, Cargèse, Corsica, France.

Education:

since 08/05	Postgraduate studies at the Leibniz-Institute of Marine Sciences (IFM-GEOMAR) at the University of Kiel
04/04 - 12/04	Stay abroad as part of the diploma thesis, Southern Cross University, Lismore, Australia
10/99 - 01/05	Undergraduate studies of Marine Environmental Sciences at the Carl von Ossietzky University of Oldenburg (Degree: Diplom)
10/98 - 09/99	Undergraduate studies of Agricultural Sciences at the Justus-Liebig-University of Giessen
09/95 - 08/98	Secondary school, Liebiggymnasium in Giessen
08/94 - 08/95	Stay abroad as part of an exchange programme AFS (American Field Service), Mexico City, Mexico
08/90 - 07/94	Secondary school, Liebiggymnasium in Giessen
08/84 - 07/90	Primary school, Pestalozzischule in Giessen

Languages:

German	native language
English	very good
Spanish	good
French	basic